ELECTRON TUNNELING AND HOPPING THROUGH PROTEINS

Thesis by

Crystal Shih

In Partial Fulfillment of the Requirements for

the Degree of Doctor of Philosophy

California Institute of Technology

Pasadena, California

2008

(Defended May 5, 2008)

A C K N O W L E D G M E N T S

I've loved science ever since I was in the third grade, but as I also "loved" New Kids on the Block, my opinion was not really to be trusted. However unwise I was in some choices, I had fantastic teachers, among them Karen Wickersham, Heston Bates, and Ross Graham, to take my interest and root it in science.

My interest in chemistry intensified when I arrived at college and had the fortune of having the irrepressible Phil Miller as my TA for organic chemistry. Phil inspired me to change my major from biology to chemistry, and I will always be grateful to him for his advice.

I joined Greg Fu's lab in spring of 2002. Greg is not only a brilliant teacher, but also a considerate advisor; I've really appreciated his guidance and support. My mentor in the group, Brian Hodous, provided a good deal of laboratory common sense and technique, as well as hours of smiles and entertainment. I am indebted to Ryo Shintani; not only did he help me with my experiments and Japanese homework countless times, but he's also continued to provide me with friendship, inspiration, and very solid advice whenever I've needed it.

However brief my experience was in Dave MacMillan's lab, I want to thank Roxanne Kunz, Alan Northrup, and Joel Austin for making it fun and educational. I don't think I'll ever come across a baymate as fun, clever, or driven as Ian Mangion.

And now, I'm at the meat of the order: Harry Gray, Jay Winkler, and my friends in the Gray Group. Harry's positive attitude, insights, and generosity have carried me through confusing results and dry spells. He's changed my perception of academics, fed

my Dodger addiction, and taught me the importance of keeping steady, holding my head high, and "not peaking too soon". Jay Winkler dragged me into the rocky world of MATLAB, and I am very thankful for his guidance. I've appreciated his patience and support while I was learning the ropes, as well as our enlightening discussions.

I've interacted with a number of interesting and fun people in the Gray group, and I appreciate their being here to make life different and exciting every day. Brian Leigh's hours of instruction have been invaluable over the course of my grad school career; his generosity, patience, and sense of humor have been indispensable to my sanity at especially rough patches. Yen Hoang Le Nguyen's zeal for life kept me inspired, and her discussions about all things, from knitting to my currently non-working reaction, always kept me on my intellectual toes. Jillian Dempsey's been a fantastic roommate, officemate, co-TA, and friend, always ready with a smile and good advice. Gretchen Keller's positive attitude makes her such a great person to be around; planning parties with her has been fun. A conversation with the cheerful, sweet, and enthusiastic Heather Williamson unfailingly gives me an extra shot of motivation when my energy starts to flag. I love Nicole Bouley's energetic enthusiasm for life (and Jane Austen)!! Keiko Yokoyama's smiles and steady company unfailingly cheer me up when I'm frustrated, and I adore her taste in fine art. Lionel Cheruzel's witty mind, incredible work ethic, and modesty are to be marveled at. Too bad he's French. ;) I'd especially like to thank him for reading through a portion of my thesis. Kyle Lancaster is a talented mixer; "Equilibrium" got me through props, and I enjoy his interesting taste in music. Alec Durrell is fun and funny company during exhausting and annoying temperature studies. When I joined the lab, Mayra Sheikh, a very talented undergrad, had more experience in

the Gray group than I, and I really enjoyed learning from and joking with her. My own SURF of two years, Deepak Mishra, has been fun to collaborate with, (being the triple threat of motivated, intelligent, *and* independent!) despite his inherent flaw of being a chemical engineering major.

I'd argue that no other class in the Gray Group takes as much pride and love in each other as mine. As my first party co-coordinator, as well as one of the Nanosecond-I GLAs, Don Walker has had the burden of dealing with me at my most anal and most stressed out, and he's unfailingly calmed me down with his relaxed and steady attitude. While she's extremely intelligent, I still think Melanie Pribisko Yen's got to be more than 75% heart, because I haven't seen anyone so strong, courageous, and generous. I'm especially grateful for her friendship this last year, what with our picosecond trial by fire and long march to graduation. As well as being my permanent officemate, Bert Lai is the second little brother I never had. He's been a constant source of comfort when things go south, and he's one of the best wingmen to have when flying high.

I would not have been able to do half the experiments or studies I'd wanted to do without Yuling Sheng's assistance, advice, and friendship. She's made working with protein *fun*, a development I'd never expected! I am especially thankful to her for taking on the burden of carrying out mutations and expressing the bulk of the proteins.

I am also extremely thankful to Angel Di Bilio, for his advice on labeling and purification protocols, as well as his unique and helpful prespective.

Outside of lab, I've met a number of really great people at Caltech. Steven Baldwin's a great guy to go to Dodger games with, and one of only two people I'd ever trust with My Scorebook. Baseball aside, he's a great friend, and I'm thankful to have

him here to support me with an insightful scientific discussion, a margarita, or a much-needed trip to Borders.

Through first year classes, candidacy, bad lab days, laser time, and tons of travel, Anna Folinsky, Jennifer Roizen, and I have kept to our Thursday Lunch routine, at times also entertaining illustrious guests such as the Pasadena PD (uninvited) and Brian Stoltz (very welcome). I not only learned a lot about Jewish culture, but I also discovered a lot about myself in our varied and interesting discussions. I am especially grateful to Anna for her unique personality, interesting opinions, and fierce support. Anna tells it like it IS!!! I'd also like to thank our occasional guests, Jennifer Stockdill and Erin Koos for their fun opinions and warm hearts.

Finally, a number of people outside of my Caltech life have ensured that beyond having just *having* a life, I'm having an absolutely *fantastic* one. First, the Los Angeles Dodgers are great to watch when you've just messed up a whole crop of labeled protein and have no idea what to with your latest laser data. The Jane Austen Society of North America has a fantastic contingent here in Southern California, and I've especially loved participating in the Pasadena reading group for the fun non-scientific discussion. The PCG have nurtured my love for writing, and I'm glad to have their encouragement in all things, from my writer's block to my next laser study. They kept me fantastic company while I was marching away on the thesis, and I am grateful to them for their support, and for remembering flippy. I'd also like to thank my many friends at DWG. Their encouragement and perspective has been invaluable. Having Jennifer Santucci and Victoria Young only a drive away, and always up for an adventure, has done much to give me peace of mind when I most needed it. Alyson Lee has been a constant

inspiration to me and I've appreciated our many discussions, as well as her unflagging support. Amy Ishizawar should get thousands of pounds of mochi, because she's been absolutely indispensable (not findispensable!) in keeping me laughing and sane throughout grad school, and especially through this last push towards graduation.

Margaret Douglass, ever in Europe, but ever on-line and supportive, is always ready to pitch an article on elephants to me when I need a break (and even when I don't need one). Our trip through Austria will always be one of the best trips I've ever had in my life. The Next Fifth East crew from college has been extremely generous in accommodating my circumstances and schedule when planning get-togethers. I am especially grateful to Flora Lee, Roland Burton, and Corinna Sherman for taking time out of their busy schedules to check in and/or visit.

"My boyfriend, the doctor" Jeffery Byers had me at the words "ligand field splitting". An honest opinion when I didn't want but needed it, a fountain of chemical and baseball knowledge, a partner-in-crime to escape campus with, he is the best friend I've ever had, and I am extremely grateful to him for his support over the years.

Finally, I'd like to thank my family for their love and generosity. My cat Lina always knows when I need a good cuddle. My brother Terry has always inspired me to push harder and question everything, and his unflappable strength is very easy to lean on when things get difficult. I am especially grateful to him for his visits out to see me, as he is quite busy himself. My parents have done more for me and my brother than I think *can* be done, and I hope they know how grateful I am to have such intelligent, interesting, loving, and compassionate people as my care-takers and role models. It is to them I dedicate this thesis.

This thesis is dedicated to my Mom and Dad,

for being the best inspiration a person could have.

THESIS ABSTRACT

Long-range electron tunneling is a central component of processes that are essential for biological function. While many studies have been made to understand electron transfer in proteins, biologically efficient electron transfer at distances exceeding 25 Å remains unobserved in these experiments and hence unresolved. It is proposed that long-range electron transfer is in actuality multistep electron tunneling. What is reported in this thesis is the design, synthesis, and study of many protein systems for the purpose of studying multistep electron tunneling in azurin.

In each system, a histidine has been introduced on the protein for attachment of a high-potential ruthenium or rhenium sensitizer ($[Ru(trpy)(tfmbpy)]^{2+}$ or $[Re(dmp)(CO)_3]^{+}$); a nitrotyrosine, tryptophan, or tyrosine is placed between the two metal centers on the tunneling pathway. The electron transfer is triggered with the excitation of the metal label with laser light, and the kinetics are monitored, for the most part, by time-resolved UV-VIS spectroscopy.

The first system to empirically demonstrate multistep electron tunneling in proteins was discovered; ultrafast electron transfer is observed between the copper and rhenium centers in the Re124/W122 system; the system was structurally characterized and studied by time-resolved UV-VIS and IR spectroscopies. A two-step tunneling model is proposed; the data sets for the different methods utilized are all in excellent agreement with the model.

Systematic perturbations were made to the working hopping system. It was discovered that nitrotyrosine can participate as an intermediate, but studies to

demonstrate its participation in multistep tunneling are not yet fully realized. A second hopping system was discovered in the development of the Re126/W122 system.

TABLE OF CONTENTS

LIST OF TABLES, FIGURES, AND SCHEMES

Chapter One: Background & Research Plan

Chapter Two: Preparation & Characterization of Ru^{2+}- and Re^{+}-modified *Pseudomonas aeruginosa* Azurins

Chapter Three: Dramatic Acceleration of Electron Flow through Proteins

Chapter Four: Controlling Electron Hopping

Chapter Five: Studying Hopping in Another Pathway of Azurin

Chapter Six: Future Directions

CHAPTER ONE

Background & Research Plan

1.1 STATEMENT OF INTENT

Long-range electron transfer is a central component of processes that are essential for biological function. While many studies have been made to understand electron transfer in proteins, biologically efficient electron transfer at distances exceeding 25 Å remains unobserved in these experiments, and hence unresolved. It is proposed that long-range electron transfer is in actuality multistep electron tunneling. What is reported in this thesis is the design and synthesis of many protein systems for the purpose of studying multistep electron tunneling in azurin, two of which conclusively demonstrate the postulated phenomenon. This chapter gives a brief summary of current electron transfer theory, an overview of the metal-modified metalloprotein program, and outlines the various aspects of the research plan taken in this project.

1.2 ELECTRON TRANSFER IN PROTEINS

Electron Transfer Theory

Though not understood, the importance of electron transfer reactions in proteins has always been noted: in 1941, Szent-Györgyi observed that "electrons wander directly from enzyme to enzyme" in redox enzymes that were immobilized in membranes.[1] This electron "wandering" was much debated; popular models included electron "packets" traveling through a semiconductive of the protein medium,[1] as well as conformational

changes bringing electron donors and acceptors in close contact for the reaction to occur.[2] In 1974, Hopfield proposed that the electrons tunneled through the protein medium the same way that particles could tunnel through energy barriers.[3] It is now accepted that electrons tunnel through a protein medium that is highly tuned to facilitate the efficient transfer of electrons. But what makes an electron transfer efficient?

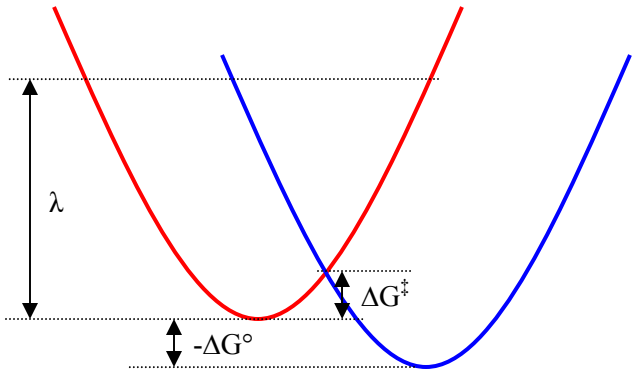

Figure 1.1. Potential energy curves. Representation of reactant (red) and product (blue) potential energy curves, with activation barrier ($\Delta G^{\ddagger}$), driving force ($-\Delta G^{\circ}$), and reorganization energy (λ) noted

A central tenet of electron transfer theory is the Franck-Condon principle, which states that because electrons move much faster than nuclei, the nuclei remain fixed during the actual reaction; therefore, the transition state of the reaction must be in a nuclear-configuration space where the reactant and product states are degenerate (in **Figure 1.1**, where the two energy curves intersect).[4,5] And so, the kinetics of the reaction are dependent on the activation barrier ($\Delta G^{\ddagger}$). According to Marcus theory, the activation barrier for adiabatic electron transfer reactions depends on the driving force ($-\Delta G^{\circ}$) and reorganization energy (λ).[6] The driving force is the difference between the reduction potentials of the electron donor (D) and acceptor (A). The reorganization energy

comprises inner-sphere (ligand) and outer-sphere (solvent) nuclear rearrangements that accompany the electron transfer. In **Figure 1.1**, it is the energy of the reactants at the equilibrium nuclear configuration of the products. It can be observed from the exponential term in **Equation 1.1** that at low driving forces ($-\Delta G° < \lambda$), the rates increase with $-\Delta G°$. The rate will reach a maximum where the two values are equal, and then will decrease as $-\Delta G°$ continues to increase, which is also known as the inverted effect. A direct lesson from Marcus theory is that the nuclear rearrangements that accompany an electron transfer must be compensated by the reaction driving force.

In proteins, electron transfers are usually over fairly long distances. Electronic interaction between the two sites is weak, and the transition state must be formed many times before the electron transfer actually occurs, rendering the process non-adiabatic. This consideration is noted in the pre-exponential factor of **Equation 1.1**, in the electronic coupling matrix term H_{AB}.

$$k_{ET} = \sqrt{\frac{4\pi^3}{h^2 \lambda RT}} H_{AB}{}^2 \exp\left(-\frac{(\Delta G° + \lambda)^2}{4\lambda RT} \right) \qquad \text{(Eq 1.1)}$$

The electronic coupling matrix element is a description of how much overlap there is between the localized donor and acceptor wave functions; the more overlap, the better the electronic interaction. In proteins, H_{AB} is quite small. The distance dependence can be mathematically expressed, utilizing a decay factor, β, that was estimated by Hopfield to be approximately 1.4 $Å^{-1}$ (**Equation 1.2**).[3] The larger β is, the more dependent on distance the coupling is.

$$H_{AB}(r) = H_{AB}(r_0) \exp\left(-\frac{\beta(r - r_0)}{2} \right) \quad \text{(Eq 1.2)}$$

It is clear from **Equation 1.2** that the electron coupling between the electron donor and acceptor exhibits an exponential dependence on the distance between the two redox centers. This exponential dependence translates into an exponential dependence on distance for the rate of the electron transfer as well.

Is there a β that is universal to all proteins, or is β specific to each protein, each possible electron tunneling pathway? Though there was considerable argument for the former,[7] it has been observed the latter suggestion is a more accurate approximation: the bridging medium that connects donor and acceptor mediates the electronic coupling via superexchange.[8] Mathematically speaking, the medium is broken into *n* identical repeat units, and the electronic coupling matrix element is thereby described as a function of the coupling between the redox sites and their bridge ($h_{Db,}$ h_{bA}), the coupling between the bridging units themselves (h_{bb}**)**, and the energy required to actually place an electron or hole on the bridge (Δε) (**Equation 1.3**).

$$H_{AB} = \frac{h_{Db}}{\Delta\varepsilon}\left(\frac{h_{bb}}{\Delta\varepsilon}\right)^{n-1} h_{bA} \qquad \text{(Eq. 1.3)}$$

Equation 1.3 as applied to biological systems is more useful for philosophical exercises than accurate calculation, because the bridging protein medium is in actuality a complex array of bonded and non-bonded contacts. In this large array, which route does the electron take? A general approach, taken by the persistent proponents of the universal β, has conceded the heterogeneity of the medium by including a modification to their theory, packing density parameter ρ (on a scale of 0 (vacuum) to 1.0 (completely packed medium)). This ρ was found to be on average 0.76 with a (rather large) standard deviation of about 0.10.[9] While this approach can offer a general idea of electron transfer

kinetics, it does not offer the complete picture of the tunneling medium. The tunneling pathway model, which takes the more atomistic view, breaks the extensive arrays down into components linked by covalent bonds, hydrogen bonds, and through-space jumps.[10–16] Each component is assigned is own decay constant (ε_C, ε_H, ε_S, respectively). A structure-dependent searching algorithm is used to identify the tunneling pathway that best couples the two redox sites. The total electron coupling is expressed as a repeated product of the couplings for the individual components (**Equation 1.4**).

$$H_{AB} \propto \Pi\varepsilon_C \Pi\varepsilon_H \Pi\varepsilon_S \quad \text{(Eq 1.4)}$$

In summary, to render electron transfer efficient in biological systems, the protein fold creates a balance of driving force and reorganization energy. It provides adequate electronic coupling between the donor and acceptor, a well-engineered system of covalent bonds, hydrogen bonds, and through-space jumps through which the electron can tunnel.

Electron Transfer Experiments: Metal-Modified Metalloproteins

The Gray group has a long-term goal of empirically demonstrating the considerable amount of theory that has been proposed to describe electron transfer in biological systems.[17–20] Such experiments must involve the systematic manipulation of the parameters, driving force, reorganization energy, and electronic coupling.

The Gray group's plan of attack is to surface-label metalloproteins with redox-active metal complexes and to study the intramolecular electron transfer between the two metal centers. The electron transfer would be induced by laser excitation, and because the each metal had its own optical signature in each of its various oxidation states, the

state of the metals could be monitored over time. By changing the label or the metal resident to the protein, the driving force (-ΔG°) can be changed. By changing the sites of labeling (by installing histidine at various positions using site-directed mutagenesis), the distance and therefore the electronic coupling (H_{AB}) can be varied.

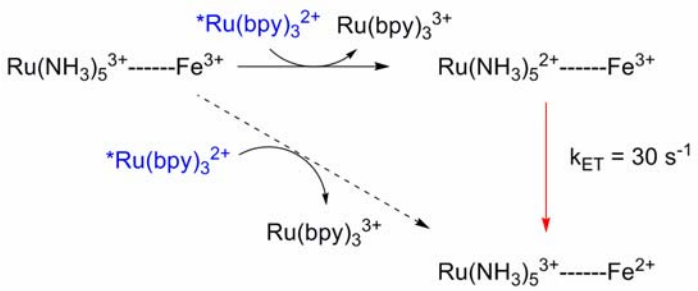

Figure 1.2. Electron transfer between $Ru(NH_3)_5^{2+}$ and Fe^{3+}. Scheme of first reported intramolecular electron transfer obtained through the use of metal-modified metalloproteins. In the study, $Ru(bpy)_3^{2+}$ was excited, generating its high-potential excited stated (highlighted in blue). It was found that both the $Ru(NH_3)_5^{3+}$ and Fe^{3+} could oxidixe $*Ru(bpy)_3^{2+}$, but that the quenching by ruthenium was faster, generating the kinetic product $Ru(NH_3)^{2+}$ in fivefold excess over the thermodynamic product Fe^{2+}, demonstrated in the figure by the hashed arrow for the slower, less-dominant phase. EDTA was utilized to scavenge $Ru(bpy)_3^{3+}$ to prevent back reaction, so that the kinetics of the intramolecular electron transfer could be observed.

The first of these systems was reported on in 1982: cytochrome *c* was labeled with $Ru(NH_3)_5^{3+}$ at the His33 site.[21] Reports on the phototriggered electron transfer quickly followed.[22,23] The electron transfer was initiated by the excitation of the photosensitizer $Ru(bpy)_3^{2+}$ with a 532 nm laser pulse; in its long-lived excited state, $*Ru(bpy)_3^{2+}$ is an excellent reducing agent. It donates an electron to the modified metalloprotein (PFe^{3+}-Ru^{3+}) system (**Figure 1.2**). While it does donate electrons to both the iron and the rutheniuim label, it was found that $*Ru(bpy)_3^{2+}$ quenching generates the reduced ruthenium complex in fivefold excess to the reduced iron product (denoted with a solid arrow in the figure). By utilizing a $Ru(bpy)_3^{3+}$ scavenger (ethylene diammine tetraacetic acid), the kinetics of the intramolecular electron transfer from the Ru^{2+} to Fe^{3+}

could be revealed and monitored. The rate of this electron transfer was determined to be 30 s^{-1}.

The utility of diimine ligands proved to be an important and useful modification to the program. The reorganization energy that accompanied Ru-diimine$^{3+/2+}$ electron transfer was observed to be smaller than that measured for $Ru(NH_3)_5^{3+/2+}$, which allowed for investigations into the inverted region (where $-\Delta G° > \lambda$).[24] Furthermore, the ruthenium-diimine photosensitizers could be directly attached to the protein (still labeling at histidine sites) and so the complications of intermolecular electron transfer could be avoided. Finally, the diimine ligands allowed for facile manipulation of the reduction potential of the label, which allowed for a systematic approach to studying the effects of driving force on the kinetics of electron transfer.[25] It was from these variations that the empirical demonstration of the inverted effect was observed (**Figure 1.3**).

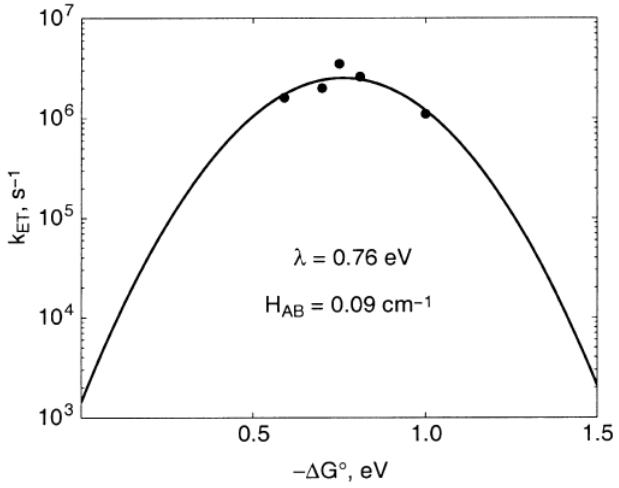

Figure 1.3. Driving force dependence of electron transfer rates in Ru-His33 cytochrome *c*. Solid line is the best fit to **Equation 1.1**; values calculated for λ and H_{AB} shown.

The metal-modified metalloprotein program has gone on to demonstrate the importance of tunneling pathways in determining electron transfer kinetics[18,26] (**Figure**

1.4). **Figure 1.4** summarizes the study of activationless ($-\Delta G° = \lambda = \sim 0.8$ eV) electron transfer in the metal-modified metalloprotein program. In these cases, because the driving force and reorganization energy are approximately equal, the exponential term in **Equation 1.1** has the value of 1, and so any change on the rate of electron transfer/tunneling should be solely dependent on the electronic interactions between the centers (i.e., H_{AB}, and, in turn, distance).

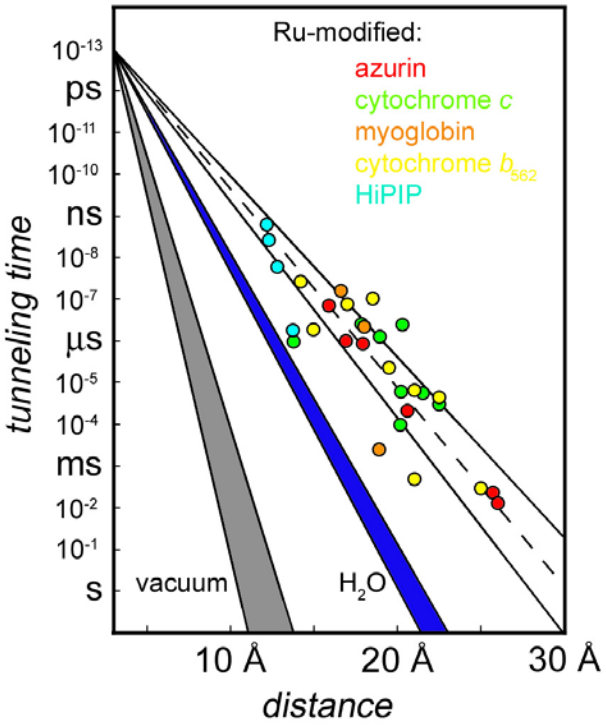

Figure 1.4. Tunneling timetable for activationless electron transfer in five different proteins (indicated above). The tunneling time is plotted in logarithmic scale against the distance traversed by the electron.[20]

In **Figure 1.4**, the tunneling times of the electron transfers in the proteins studied are plotted logarithmically against the distance between the redox centers; one should note that β is the slope of the various lines. The data display a few marked characteristics: 1) tunneling through proteins is more efficient than tunneling through

vacuum or water (β is smaller for proteins than for the other two). This is because the protein fold lowers the reorganization energy of the electron transfer event by excluding water and utilizing an expanded network of hydrogen bonds to minimize the reorganization of ligands about the metal during electron transfer;[27] 2) the protein data points are all scattered around an average β of 1.1 $Å^{-1}$, which is close to the β = 1.0 $Å^{-1}$ value found for the superexchange-mediated electron tunneling across saturated alkane bridges.[28,29] This similarity indicates that the electronic coupling in proteins is similar to the electron coupling in alkane chains, which is not completely surprising; 3) though some electron transfers happen over the same distance (i.e., ~21 Å), the kinetics of the electron transfer can vary up to three orders of magnitude; the range and the scatter that is observed across all proteins demonstrate the effect tunneling pathways have on electron transfer/tunneling kinetics.

An examination of this tunneling timetable reveals a limitation of experiments executed thus far; efficient electron transfer in proteins has been demonstrated for distances up to 15 Å in these studies. But according to the timetable, electron tunneling at longer distances take on the order of milliseconds to seconds to complete. It remains mysterious how nature can convey electrons over distances of over 30 Å on a much faster timescale in the processes that sustain life in cells.

1.3 LONG-RANGE ELECTRON TRANSFER IN PROTEINS

Photosynthesis and respiration are complementary energy transduction processes that utilize long-range electron transfer.[19,30–32] In respiration, hydrogen atoms are abstracted from organic molecules, stored, then passed into the respiratory chain, a

system of membrane-bound proteins located in cell organelles, mitochondria, or the cell membrane. The hydrogen atoms are split into protons and electrons; protons are sequestered to one side of the membrane, while electrons are passed through the chain to eventually reduce oxygen into water. The proton gradient that is generated is utilized to generate adenosine triphosphate (ATP), which serves as the currency for energy in living cells. In the light reactions of photosynthesis, photons from the sun trigger the separation of charge in a system of membrane-bound proteins. Water is oxidized to oxygen, and electrons are passed through the system to eventually generate the reduced form of nicotinamide adenine dinucleotide phosphate (NADPH) which is utilized later in the dark reactions of photosynthesis to fix carbon dioxide.

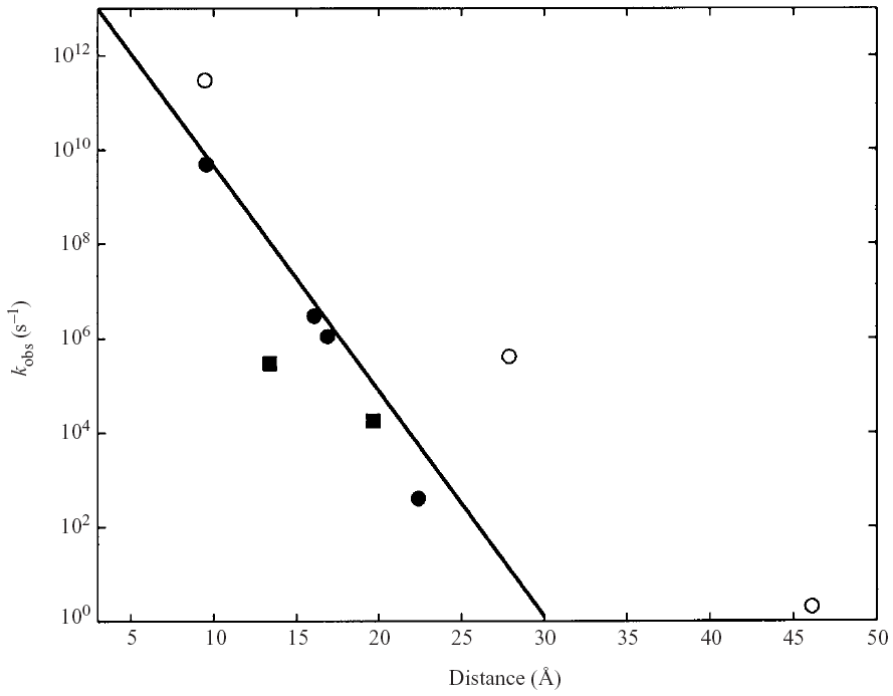

Figure 1.5. Distance dependence of observed electron transfer rates in cytochrome *c* oxidase (squares) and bacterial photosynthetic reaction centers (circles). Open circles represent transfers where multistep tunneling may be in operation.[19]

The observed electron transfer kinetics in bacterial photosynthetic reaction centers and cytochrome *c* oxidase (where oxygen is reduced to water in the respiratory chain) are plotted against the average $\beta = 1.1$ Å^{-1} value below in **Figure 1.5**.[19,33–36] One can clearly see that many of the electron transfer reactions lie very closely to the line, revealing just how well tuned this biological machinery is to serve its function! Intriguingly, three of the data points (open circles) lie well above the $\beta = 1.1$ Å^{-1} line, orders of magnitude faster than would be expected for activationless electron transfer. It is speculated that these faster kinetics can be accessed through a multistep tunneling mechanism.[34,37,38]

By this mechanism, the bridging protein medium not only electronically couples the electron donor and acceptor; it (in particular, an amino acid in the bridge) is also oxidized and reduced. Participation of this amino acid renders the long-range electron transfer a multistep tunneling process, also known as "hopping". A long-distance transfer is now broken into multiple electron tunneling steps, or "hops", which are separated by redox-active intermediates. Because electron transfer rates are exponentially dependent on distance, the kinetics of multiple short electron transfers will be orders of magnitude faster than the kinetics of one long single-step electron transfer between the donor and acceptor. It is now the latest goal of the metal-modified metalloprotein program to engineer systems to exhibit this behavior, lending experimental support towards the hypothesis.

1.4 PROTEIN-BASED RADICALS

Which amino acids can be utilized as intermediates in multistep tunneling? Amino acid radicals are actually quite common, and their roles in biology (beyond the

role in photosynthesis and respiration proposed above in the previous section) include DNA biosynthesis and repair, metabolism of assorted biomolecules, hormone synthesis, and disproportionation of hydrogen peroxide.[39] Observed amino acid radicals in these proteins include glycines, cysteines, tyrosines, tryptophans, and post-translationally modified tyrosines and tryptophans. Reduction potentials for some of the amino acids in aqueous media have been measured (and remeasured, occasionally, as there has been debate, especially over tyrosine and tryptophan) (**Table 1.1**).

Radical	E°'	Reference
$Gly^{\bullet}$	1.22 V (pH 10.5)	a
$Cys^{\bullet}$	1.33 V	b
$Tyr^{\bullet}$	0.93 V	c,d
$Trp^{\bullet}$	1.01 V, 1.05 V	c,d

Table 1.1. Measured reduction potentials of natural amino acids in solvated environments (*v.* NHE, unless otherwise specified, at pH 7). [a]Zhao, R.; Lind, J.; Merenyi, G.; Eriksen, T.E. *J. Am. Chem. Soc.* **1994**, *116*, 12010–12015. [b]Sudhar, P.S.; Armstrong, D.A. *J. Phys. Chem.* **1987**, *91*, 6532–6537. [c]Determined by cyclic voltammetry in: Harriman, A. *J. Phys. Chem.* **1987**, *91*, 6102–6104. [d]Determined by pulse radiolysis in: DeFelippis, M.R.; Murthy, C.P.; Faraggi, M.; Klapper, M.H. *Biochemistry* **1989**, *28*, 4847–4853.

An examination of **Table 1.1** reveals that the amino acids that are easiest to oxidize are tyrosine and tryptophan. These amino acids have been found at strategic locations in proteins that exhibit efficient long-range electron transfer: photosystem II,[40,41] class I ribonucleotide reductase,[42] and DNA photolyase,[43,44]. In these cases, there have already been extensive spectroscopic characterizations of tyrosine-based and tryptophan-based radicals in these sites. It is clear that these two amino acids present likely candidates through which multistep tunneling occurs, so they have been the focus of the multistep tunneling program for some time now.

1.5 MULTISTEP TUNNELING IN THE GRAY GROUP

The plan to demonstrate multistep tunneling in proteins in the Gray group is fairly straightforward; take one of the previously synthesized systems, install a tyrosine or tryptophan between the metal label and the metal resident to the protein, and demonstrate that the kinetics of electron transfer in this system are significantly enhanced (**Figure 1.6**).

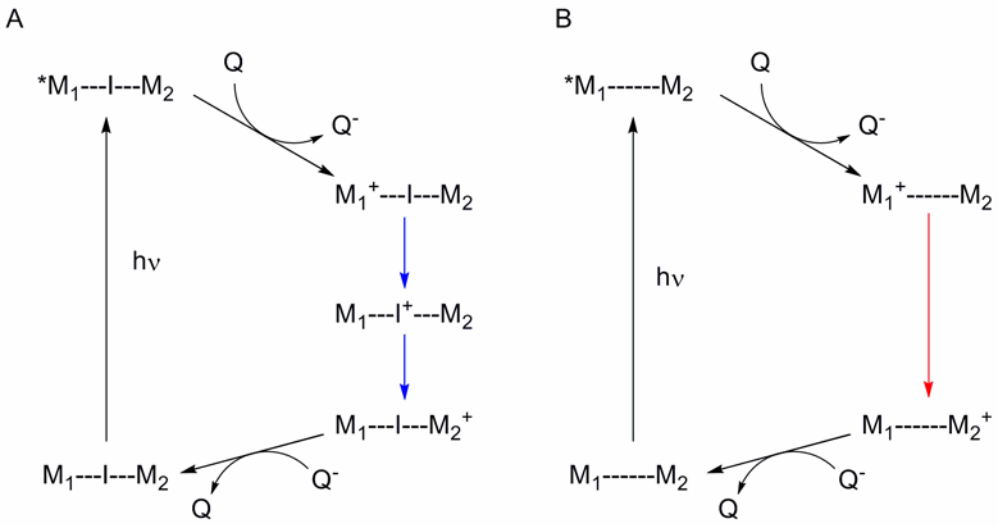

Figure 1.6. Possible plan for studying multistep tunneling in proteins. M_1 is the photosensitizer, I is the intermediate amino acid, and M_2 is the metal that is resident to the protein. **A.** Multistep tunneling: the photosensitizer is excited and, in its excited state, oxidized by an external quencher. Two electron transfers follow (blue arrows): intermediate to M_1, M_2 to I^+. Eventually, the M_2^+ is reduced by reduced quencher. **B.** Single-step tunneling: the photosensitizer is excited and, in its excited state, oxidized by an external quencher. One electron transfer (red arrow) occurs between the two redox centers. Eventually, M_2^+ is reduced by reduced quencher. It is hoped that M_2^+ will form quicker in system **A**.

Because the systems on *Pseudomonas aeruginosa* azurin exhibit very well-behaved kinetics (red data points in **Figure 1.4**),[45–47] it was selected as the protein on which the multistep tunneling experiments would be executed. Initial attempts were conducted by former graduate students Drs. William A. Wehbi[48] and Jeremiah E.

Miller,[49] as well as post-doctoral scholar Dr. Malin Abrahamsson. They labeled their proteins with the high-potential photosensitizer $Re(dmp)(CO)_3^+$, which is an excellent oxidant in either its excited state or oxidized 2+ state. Wehbi focused his studies on tyrosine (though he also did some work with cysteine), while Miller and Abrahamsson focused on tryptophan.

It was soon found, however, that, these studies were not as straightforward as previously supposed; upon oxidation, both aromatic amino acids become extremely susceptible to deprotonation, generating neutral radicals. The deprotonated amino acid radicals have lower reduction potentials, and so the driving force is not high enough to drive the subsequent electron transfer.

Circumventing the problem of deprotonation could be done in one of two ways: 1) find a system where the deprotonation of the radical cation would occur on a slower timescale than the subsequent electron transfer; or 2) find a system that was already deprotonated. Both systems have been examined in this thesis, and hopping has been probed through tyrosine, tryptophan, and 3-Nitrotyrosine (**Figure 1.7**).

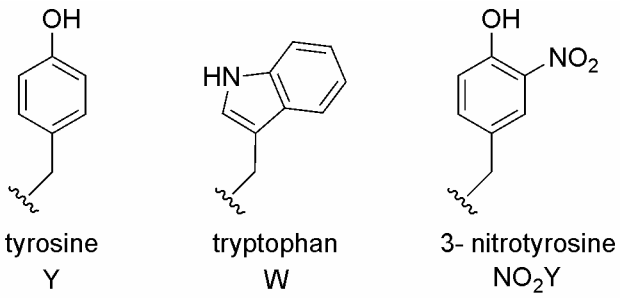

Figure 1.7. Hopping residues studied

1.6 RESEARCH OUTLINE

At the time I began my research, the research plan had been modified in two ways: first, high-potential ruthenium sensitizers would be pursued; second, the tyrosine analog 3-nitrotyrosine was to be employed as the newest hopping candidate. My research later incorporated studies utilizing both rhenium and tryptophan.

High-Potential Ruthenium Sensitizers

While the previously utilized rhenium sensitizers had the appropriate potentials for hopping studies, their optical inactivity limited the information that could be gained on their redox states. Re^0 could be traced at 500 nm, but both Re^+ and Re^{2+} were optically silent. Ruthenium dyes were an attractive alternative, because their absorbance was quite substantial in the 500 nm region,[25] and minimal in the 620 nm region, where the Cu^{2+} center of azurin absorbs.[50,51] The only limitation was that the ruthenium labels previously utilized in the metal-modified metalloprotein program were not of a high enough potential to drive electron transfer to intermediate amino acid residues. Therefore, the first goal was to install electron withdrawing groups onto the ligand to raise the potential of the metal. Chapter two summarizes the synthesis and characterization of three high-potential ruthenium photosensitizers, one of which is utilized in chapters four and five.

3-Nitrotyrosine as the Intermediate

Because deprotonation of the radical cations of both tryptophan and tyrosine appeared to complicate hopping studies, it was proposed to perturb the pK_a of the protons

by substituting onto the aromatic ring of the amino acid. If the pK_a were lowered enough, the studies could be conducted with the amino acid in only one protonation state.

Synthetic protocols for the nitration of tyrosines using tetranitromethane have been used since their development in the late 1960s.[52–58] Moreover, the Gray group has also had experience and success with the protocol: Dr. Jennifer C. Lee utilized 3-nitrotyrosine in her studies of α-synuclein structure.[58] 3-nitrotyrosine's proton has a pK_a of around 7,[54] so it is very feasible to work with the amino acid in its deprotonated state for hopping studies. The deprotonated 3-nitrotyrosininate has a reduction potential of about 1.07 V *v.* NHE,[59] which is close to that of tyrosine and tryptophan, so it should participate as an intermediate in hopping systems. Deprotonated 3-nitrotyrosinate absorbs at 428 nm, which offers a spectroscopic handle for the oxidation state of the intermediate amino acid residue. These advantages and details all made 3-nitrotyrosine an extremely attractive target for use in the engineered hopping systems. I was successful in installing the nitro group onto tyrosines in multiple sites of the protein, and was able to demonstrate that the residue could participate in redox chemistry on the protein; discussion of the protocol, and the results from the nitrotyrosine mutants are in Chapters Two and Four.

Hopping Systems

At the time I joined the multistep tunneling program, a successful hopping system had just been discovered by Dr. Malin Abrahamsson. H124/W122/All-Phe azurin was modified with $Re(dmp)(CO)_3$. When the rhenium label was excited, it induced a nearly 20 Å multistep electron transfer that occurred within 50 nanoseconds! Because the

system was the first of its kind, as much information on it had to be obtained as possible; samples were sent to Brian Crane at Cornell University, so that structural data could be obtained. The kinetics data was confirmed by ultrafast time-resolved infrared spectroscopy, done by Tony Vlček at Queen Mary, University London. I got involved on the project when temperature studies and ultrafast UV-Vis spectroscopy studies also had to be carried out on the system. Chapter Three summarizes the conclusions obtained from my data.

Inspired by this data, I expanded my studies into other systems based on this one to figure out what made hopping in this system work so well. I manipulated potentials of both metal label and intermediate, and varied distance as well. It was through these investigations that I discovered another promising hopping system. These pursuits are discussed in Chapter Four.

1.7 REFERENCES

(1) Szent-Gyorgyi, A. *Science* **1941**, *93*, 609–611.

(2) Chance, B.; Williams, G. R. *Adv. Enzymol.* **1956**, *17*, 65–134.

(3) Hopfield, J. J. *P. Natl. Acad. Sci. USA* **1974**, *71*, 3640–3644.

(4) Marcus, R. A. *Angew. Chem., Int. Ed. Eng.* **1993**, *32*, 1111–1121.

(5) Marcus, R. A. *Adv. Chem. Phys.* **1999**, *106*, 1.

(6) Marcus, R. A.; Sutin, N. *Biochim. Biophys. Acta* **1985**, *811*, 265–322.

(7) Moser, C. C.; Keske, J. M.; Warncke, K.; Farid, R. S.; Dutton, P. L. *Nature* **1992**, *355*, 796–802.

(8) McConnell, H. M. *J. Chem. Phys.* **1961**, *35*, 508–515.

(9) Moser, C. C.; Page, C. C.; Dutton, P. L. *Philos. T. Roy. Soc. B* **2006**, *361*, 1295–1305.

(10) Beratan, D. N.; Onuchic, J. N.; Hopfield, J. J. *J. Chem. Phys.* **1987**, *86*, 4488–4498.

(11) Onuchic, J. N.; Beratan, D. N. *J. Chem. Phys.* **1990**, *92*, 722–733.

(12) Onuchic, J. N.; Beratan, D. N.; Winkler, J. R.; Gray, H. B. *Annu. Rev. Bioph. Biom.* **1992**, *21*, 349–377.

(13) Beratan, D. N.; Betts, J. N.; Onuchic, J. N. *J. Phys. Chem.* **1992**, *96*, 2852–2855.

(14) Beratan, D. N.; Betts, J. N.; Onuchic, J. N. *Science* **1991**, *252*, 1285–1288.

(15) Prytkova, T. R.; Kurnikov, I. V.; Beratan, D. N. *Science* **2007**, *315*, 622–625.

(16) Beratan, D. N.; Balabin, I. A. *P. Natl. Acad. Sci. USA* **2008**, *105*, 403–404.

(17) Winkler, J. R.; Di Bilio, A. J.; Farrow, N. A.; Richards, J. H.; Gray, H. B. *Pure Appl. Chem.* **1999**, *71*, 1753–1764.

(18) Winkler, J. R. *Curr. Opin. Chem. Biol.* **2000**, *4*, 192–198.

(19) Gray, H. B.; Winkler, J. R. *Q. Rev. Biophys.* **2004**, *36*, 341–372.

(20) Gray, H. B.; Winkler, J. R. *P. Natl. Acad. Sci. USA* **2005**, *102*, 3534–3539.

(21) Yocom, K. M.; Shelton, J. B.; Shelton, J. R.; Schroeder, W. A.; Worosila, G.; Isied, S. S.; Bordignon, E.; Gray, H. B. *P. Natl. Acad. Sci. USA* **1982**, *79*, 7052–7055.

(22) Winkler, J. R.; Nocera, D. G.; Yocom, K. M.; Bordignon, E.; Gray, H. B. *J. Am. Chem. Soc.* **1982**, *104*, 5798–5800.

(23) Nocera, D. G.; Winkler, J. R.; Yocom, K. M.; Bordignon, E.; Gray, H. B. *J. Am. Chem. Soc.* **1984**, *106*, 5145–5150.

(24) Brown, G. M.; Sutin, N. *J. Am. Chem. Soc.* **1979**, *101*, 883–892.

(25) Mines, G. A.; Bjerrum, M. J.; Hill, M. G.; Casimiro, D. R.; Chang, I. J.; Winkler, J. R.; Gray, H. B. *J. Am. Chem. Soc.* **1996**, *118*, 1961–1965.

(26) Winkler, J. R.; Gray, H. B. *Chem. Rev.* **1992**, *92*, 369–379.

(27) Crane, B. R.; Di Bilio, A. J.; Winkler, J. R.; Gray, H. B. *J. Am. Chem. Soc.* **2001**, *123*, 11623–11631.

(28) Smalley, J. F.; Finklea, H. O.; Chidsey, C. E. D.; Linford, M. R.; Creager, S. E.; Ferraris, J. P.; Chalfant, K.; Zawodzinsk, T.; Feldberg, S. W.; Newton, M. D. *J. Am. Chem. Soc.* **2003**, *125*, 2004–2013.

(29) Smalley, J. F.; Feldberg, S. W.; Chidsey, C. E. D.; Linford, M. R.; Newton, M. D.; Liu, Y.-P. *J. Phys. Chem.* **1995**, *99*, 13141–13149.

(30) Ramirez, B. E.; Malmstrom, B. G.; Winkler, J. R.; Gray, H. B. *P. Natl. Acad. Sci. USA* **1995**, *92*, 11949–11951.

(31) Gray, H. B.; Halpern, J. *P. Natl. Acad. Sci. USA* **2005**, *102*, 3533.

(32) Purves, W. K.; Orians, G. H.; Heller, H. C.; Sadava, D. *Life: The Science of Biology*; Fifth ed.; Sinauer Associates, Inc.: Salt Lake City, UT, 1998.

(33) Winkler, J. R.; Malmstrom, B. G.; Gray, H. B. *Biophys. Chem.* **1995**, *54*, 199–209.

(34) Kirmaier, C.; Holten, D. *Photosynth. Res.* **1987**, *13*, 225–260.

(35) Shopes, R. J.; Levine, L. M. A.; Holten, D.; Wraight, C. A. *Photosynth. Res.* **1987**, *12*, 165–180.

(36) Ortega, J. M.; Mathis, P. *Biochemistry* **1993**, *32*, 1141–1151.

(37) Page, C. C.; Moser, C. C.; Chen, X. X.; Dutton, P. L. *Nature* **1999**, *402*, 47–52.

(38) Axelrod, H. L.; Abresch, E. C.; Okamura, M. Y.; Yeh, A. P.; Rees, D. C.; Feher, G. *J. Mol. Biol.* **2002**, *319*, 501–515.

(39) Stubbe, J.; van der Donk, W. A. *Chem. Rev.* **1998**, *98*, 705–762 and references therein.

(40) Hoganson, C. W.; Babcock, G. T. *Science* **1997**, *277*, 1953–1956.

(41) Tommos, C.; Hoganson, C. W.; Di Valentin, M.; Lydakis-Simantiris, N.; Dorlet, P.; Westphal, K.; Chu, H.-A.; McCracken, J.; Babcock, G. T. *Curr. Opin. Chem. Biol.* **1998**, *2*, 244–252.

(42) Stubbe, J.; Nocera, D. G.; Yee, C. S.; Chang, M. C. Y. *Chem. Rev.* **2003**, *103*, 2167–2202.

(43) Aubert, C.; Vos, M. H.; Mathis, P.; Eker, A. P. M.; Brettel, K. *Nature* **2000**, *405*, 586–590.

(44) Kim, S.; Sancar, A.; Essenmacher, C.; Babcock, G. T. *Proceedings of the National Academy of Sciences* **1993**, *90*, 8023–8027.

(45) Di Bilio, A. J.; Hill, M. G.; Bonander, N.; Karlsson, B. G.; Villahermosa, R. M.; Malmstrom, B. G.; Winkler, J. R.; Gray, H. B. *J. Am. Chem. Soc.* **1997**, *119*, 9921–9922.

(46) Langen, R.; Chang, I. J.; Germanas, J. P.; Richards, J. H.; Winkler, J. R.; Gray, H. B. *Science* **1995**, *268*, 1733–1735.

(47) Langen, R.; Colon, J. L.; Casimiro, D. R.; Karpishin, T. B.; Winkler, J. R.; Gray, H. B. *J. Biol. Inorg. Chem* **1996**, *1*, 221–225.

(48) Wehbi, W. A., California Institute of Technology, 2003.

(49) Miller, J. E., California Institute of Technology, 2003.

(50) Adman, E. T. *Adv. Protein Chem.* **1991**, *42*, 145–197.

(51) Solomon, E. I.; Hare, J. W.; Dooley, D. M.; Dawson, J. H.; Stephens, P. J.; Gray, H. B. *J. Am. Chem. Soc.* **1980**, *102*, 168–178.

(52) Riordan, J. F.; Sokolovsky, M.; Vallee, B. L. *J. Am. Chem. Soc.* **1966**, *88*, 4104–4105.

(53) Sokolovsky, M.; Riordan, J. F.; Vallee, B. L. *Biochemistry* **1966**, *5*, 3582–3589.

(54) Riordan, J. F.; Sokolovsky, M.; Vallee, B. L. *Biochemistry* **1967**, *6*, 358–361.

(55) Bruice, T. C.; Gregory, M. J.; Walters, S. L. *J. Am. Chem. Soc.* **1968**, *90*, 1612–1619.

(56) Riordan, J. F.; Vallee, B. L.; Hirs, C. H. W.; Serge, N. T. In *Methods in Enzymology*; Academic Press: 1972; Vol. 25, 515–521.

(57) Rischel, C.; Thyberg, P.; Rigler, R.; Poulsen, F. M. *J. Mol. Biol.* **1996**, *257*, 877–885.

(58) Lee, J. C.; Langen, R.; Hummel, P. A.; Gray, H. B.; Winkler, J. R. *P. Natl. Acad. Sci. USA* **2004**, *101*, 16466–16471.

(59) Leigh, B.S. (*personal communication).*

CHAPTER TWO

Preparation & Characterization of

Ru^{2+}- and Re^{+}-modified Pseudomonas aeruginosa *Azurins*

2.1 ABSTRACT

Three new high-potential ruthenium complexes for protein modification have been synthesized and characterized. $[Ru(trpy)(tfmbpy)]^{2+}$ has optimal redox and photophysical properties for protein electron transfer experiments. Proteins with a 3-nitrotyrosine moiety were successfully made and characterized for the investigations of hopping through nitrotyrosine. Protocols for the expression, labeling, and purification of modified proteins were developed and shown to be quite general. All together, eleven modified proteins were prepared and characterized.

2.2 INTRODUCTION

Design of Hopping Systems

The simplest hopping center has three redox centers: the photosensitizer, one intermediate aromatic amino acid, and the metal that is resident to the protein. Two "hops" accomplish the transfer of an electron between the two metal centers. **Figure 2.1** depicts two different hopping systems, with the hops in each system depicted with a blue arrow.

There are a few considerations to keep in mind when engineering a hopping system. For instance, in the systems described in **Figure 2.1**, 1) the system will be installed on a protein, so the protein must be easy to manipulate and fairly stable; 2) the

protein to be utilized ought to have a reduction potential that is fairly low, so that hopping is favorable; 3) the reduction potential of the intermediate must be low enough to be oxidized by the metal label, but high enough to drive the subsequent oxidation of the metal resident to the protein; and 4) the reduction potential of the metal label's excited state, or its oxidized state must be high enough to drive the entire process.

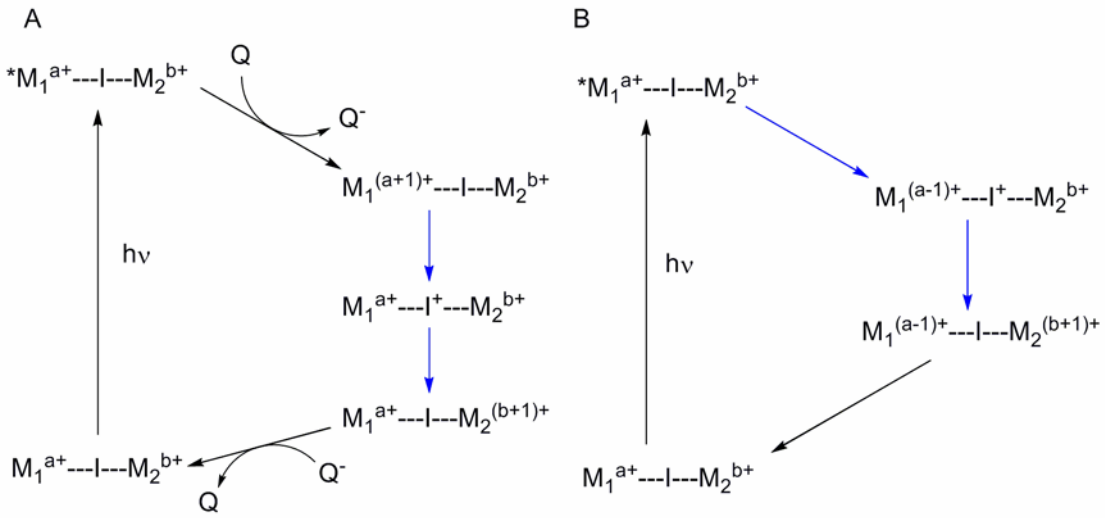

Figure 2.1. Two different hopping systems. In both cases, the two hops are highlighted in blue. **A.** The photosensitizer M_1 is excited then oxidized by an external quencher Q. Intermediate I reduces the oxidized M_1, and is then reduced by M_2. The oxidized M_2 is eventually reduced by the reduced Q and the system returns to ground state. **B.** The photosensitizer M_1 is excited and then reduced by the intermediate I. Oxidized I is reduced by M_2, then single-step charge recombination occurs to regenerate the ground state system.

Pseudomonas aeruginosa *azurin*

The cupredoxin azurin from *Pseudomonas aeruginosa* is an ideal protein on which to execute hopping studies. Azurin is a small, 128 residue protein that shuttles electrons between cytochrome 551 and nitrite reductase in the denitrifying chains in bacteria.[1,2] The cupredoxins are known for their intense blue color, which originates in the unique binding motif of the copper center.[3-6] The copper is held in a trigonal bipyramidal geometry; His46, His117, and Cys112 bind the metal in the equatorial plane,

and the sulfur of Met121 and the carbonyl oxygen of Gly45 ligate axially (**Figure 2.2**). The ligand-to-metal charge transfer from the Cys112 into the copper gives azurins (and for that matter, all type I copper proteins) their color. The reduction of the copper is measured to be approximately 0.31 V *v*. NHE.[7]

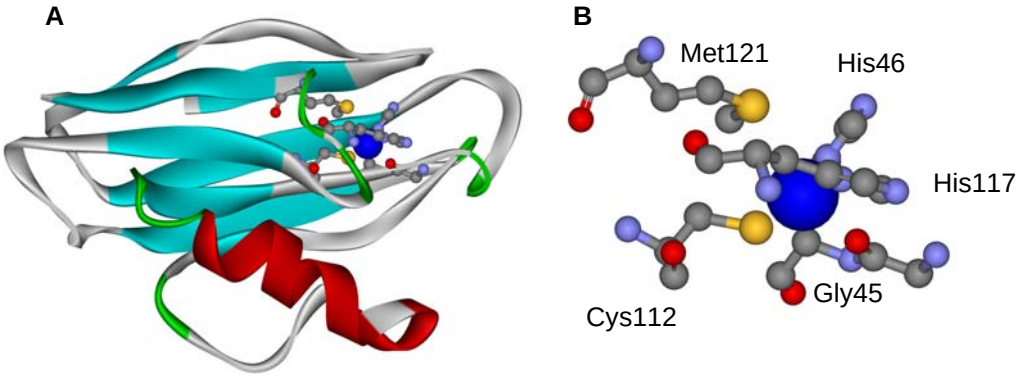

Figure 2.2. Crystal structure of *Pseudomonas aeruginosa* azurin (PDB code 1AZU). **A.** Total structure, 128 amino acids, β-barrel structure comprising eight anti-parallel beta strands. **B.** The ligands of the copper in *P. aeruginosa* azurin; trigonal bipyramidal coordination: His46, H117, Cys112 ligate the metal on the equatorial plane. The sulfur of Met121 and the carbonyl oxygen of Gly45 coordinate axially.

Protocols were developed to express *Pseudomonas aeruginosa* azurin and the structure appeared to be quite robust to mutations.[8] Because the protein has an appropriate potential, and is easy to work with, it has been utilized before in the metal-modified metalloprotein program. Electronic coupling of β-sheet structures was studied utilizing azurin's β-barrel structure.[9,10] The kinetics of electron transfer were fairly well-behaved, plotting out almost linearly on a distance *v*. log rate plot, the distance-decay β value being calculated to be approximately 1.00 $Å^{-1}$.

Furthermore, electron transfer studies done on single crystals of azurin revealed the electron transfer kinetics were the same in azurin, regardless of whether or not the protein was in a crystal or in solution.[11] This substiated the studies done before, as it was

now clear that the structures in the solution studies were similar to the natural structure of the system. The report also included crystal structures of the reduced forms of azurin, which illustrated that upon the metal's reduction, the ligands did not reorient themselves, making inner-sphere reorganization energy quite small; the coordination environment is constrained by a "cage" of hydrogen bonds, in a cluster of hydrophobic residues.

Given the plethora of established protocols for expressing and labeling azurin mutants, its well-behaved kinetics, as well as appropriate reduction potential, it is clearly one of the most attractive proteins on which to build hopping systems. Only a few adjustments have to be made to make the system appropriate: the wild-type surface H83 will be mutated to prevent mislabeling when targeting the other sites, and the resident tyrosines (Tyr72 and Tyr108) and tryptophan (Trp48) will be mutated so that any rate enhancement exhibited (or radicals observed) will be derived from the system of interest. All hopping systems are constructed on the All-Phe azurin mutant: W48F/Y72F/H83Q/Y108F, and will be hereafter abbreviated simply as Az.

Previously labeled sites of the appropriate distance (~20–25 Å) for hopping studies include the wild-type surface His83 and sites 107, 124, and 126, so they are the first choices for metal modification. The hopping residue will be installed along the established tunneling pathways from these sites to the copper.

Reduction Potentials & Photosensitizers

When investigating hopping, the reduction potentials of all redox centers involved must be considered (**Table 2.1**). The reduction potential of one metal center is fixed: the $Cu^{2+/+}$ couple of azurin is measured to have a reduction potential of 0.31 V *v*. NHE.[7]

redox couple	E° (V *v.* NHE)	reference
$Cu^{2+/+}$	0.31	a
$Ru(bpy)_2(im)(HisX)^{3+/2+}$	1.08	b
$Re(phen)(CO)_3(HisX)^{2+/+}$	2.0	c
$TrpH^{\bullet+}/TrpH$	1.15	d
$Trp^{\bullet}/TrpH$	1.01	d
$Trp^{\bullet}/Trp^{-}$	0.41	e
$TyrH^{\bullet+}/TyrH$	1.45	f
$Tyr^{\bullet}/TyrH$	0.91	d,g,h
$Tyr^{\bullet}/Tyr^{-}$	0.72	d,g,h
$NO_2Tyr^{\bullet}/NO_2Tyr^{-}$	1.07	i

Table 2.1. Estimated reduction potentials for redox couples relevant to multistep electron tunneling studies. [a]Pascher, T,; Karlsson, B.G.; Nordling, M.; Malmstrom, B.G.; Vanngard, T. *Eur. J. Biochem.* **1993**, *212*, 289–296. [b]Di Bilio, A.J.; Hill, M.G.; Bonander, N.; Karlsson, B.G.; Villahermosa, R.M.; Malmstrom, B.G.; Winkler, J.R.; Gray, H.B. *J. Am. Chem. Soc.* **1997**, *119*, 9921–9922. [c]Connick, W.B.; Di Bilio, A.J.; Hill, M.G.; Winkler, J.R.; Gray, H.B. *Inorg. Chim. Acta* **1995**, *240*, 169–173. [d]Harriman, A. *J. Phys. Chem.*, **1987**, *91*, 6102–6104. [e]calculated, given potential in ref.d and pK data from Remers, W.A. in *Indoles: Part One*; Houlihan, W.J., Ed.; Wiley-Interscience: New York, 1972, Vol. 25, 1-226. [f]calculated, given the potential in refs. d,g,h, and pKs mentioned therein. [g]Sjödin, M., Styring, S., Åkermark, B., Sun, L., Hammarström, L. *J. Am. Chem. Soc.*, **2000**, *122*, 3932–3936. [h]Magnuson, A.; Frapart, Y.; Abrahamsson, M.; Horner, O.; Akermark, B.; Sun, L.; Girerd, J.J.; Hammarström, L. *J. Am. Chem. Soc.* **1999**, *121*, 89–96. [i]Leigh, B.S. (*unpublished results*).

Previous attempts by former Gray group graduate students Drs. William A. Wehbi[12] and Jeremiah E. Miller[13] to engineer systems to exhibit hopping kinetics through tyrosine and tryptophan were thwarted by one very frustrating complication; once oxidized, the radical cation is easily deprotonated and the reduction potential of the resulting neutral radical is not high enough to drive the subsequent tunneling reaction (**Figure 2.3**).

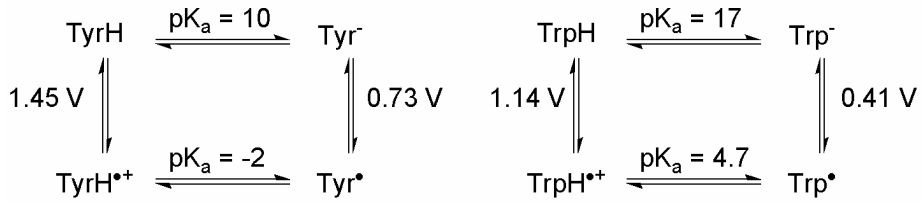

Figure 2.3. Reduction potentials and pK_as of relevant oxidation/protonation states of tryptophan and tyrosine[14-17]

In order to avoid problems of deprotonation, it is proposed to study hopping through the tyrosine analog 3-nitrotyrosine. The pK_a of the proton is measured to be around 7; if the hopping experiments on the system are executed at a pH above 7 the residue will already be deprotonated, so there will only be one reduction potential to worry about. The relevant reduction potential is measured to be 1.07 V *v*. NHE,[18] which is well within range of those of tyrosine and tryptophan, so the residue will likely participate in hopping. Finally, installation of the nitro group onto tyrosine is easily achieved utilizing protocols established in the late 1960s.[19-23] A tyrosine will be introduced to the site of interest using site-directed mutagenesis, and the protein will be exposed to tetranitromethane to achieve the substitution.

In the choice of metal label, a high-potential photosensitizer will have to be utilized; if either of the strategies in **Figure 2.1** are to work, the reduction potential of either the excited ($*M_1^{a+}$) or oxidized ($M_1^{(a+1)+}$) states must be high enough to drive the overall electron transfer. Wehbi and Miller's first attempts were carried out with the rhenium compounds, $Re(phen)(CO)_3^+$ and $Re(dmp)(CO)_3^+$ (dmp = 4,7-Dimethyl-1,10-phenanthroline). Both the $*Re^+$ and Re^{2+} states have high reduction potentials (**Figure 2.4**).

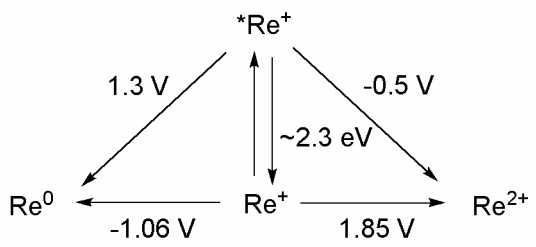

Figure 2.4. Modified Latimer diagram of $Re(phen)(CO)_3^{+}$.[24] Constructed from values obtained in acetonitrile, using a Ag/AgCl reference electrode.

Rhenium, while being of the appropriate reduction potential, is optically inactive in both Re^{+} and Re^{2+} states, which limits the information that can be obtained on the metal's oxidation state. The Gray group has had considerable experience working with ruthenium photosensitizers in the metal-modified metalloprotein program,[9,10,25-28] so it is natural to once more consider this oft-used option. The reduction potential of $Ru(bpy)_2(im)(HisX)^{3+/2+}$ is 1.08 V *v.* NHE, so it is still a bit too low for the proposed studies. However, the potential of the metal can be tuned through substitution onto the bipyridine ligand framework. This approach has been utilized before in the investigation of the effect of driving force on electron transfer kinetics.[26] The highest potential accessed in these studies was 1.26 V *v.* NHE, which was achieved by installing amides in the 4,4' positions. It is hoped that by substituting with an even more electron-deficient group, such as trifluoromethyl, the potential can be raised even more. For this reason, labels utilizing bis-trifluoromethyl-substituted bipyridine (tfmbpy) ligands will be pursued for this newest generation of hopping systems.

Chapter Outline

This chapter provides the protocols used in the synthesis of all the metal-modified metalloprotein systems studied in this dissertation. First, the synthesis and

characterization of metal labels are addressed; more than one ruthenium label was synthesized, but one was clearly easier to work with, and had appropriate photophysical and electrochemical properties. Secondly, the preparation of protein, including the preparation of the 3-nitrotyrosine-substituted mutants is outlined. Through the course of studying the nitration reaction, unfolding studies were made, the results of which are also included. Thirdly, protocols to install the label onto the protein surface are listed. The experimental section includes extensive details on the synthesis of these systems, as well as on how samples were prepared for laser spectroscopy measurements.

2.3 RESULTS AND DISCUSSION

Metal Labels

$[Ru(tfmbpy)_2(im)_2]^{2+}$

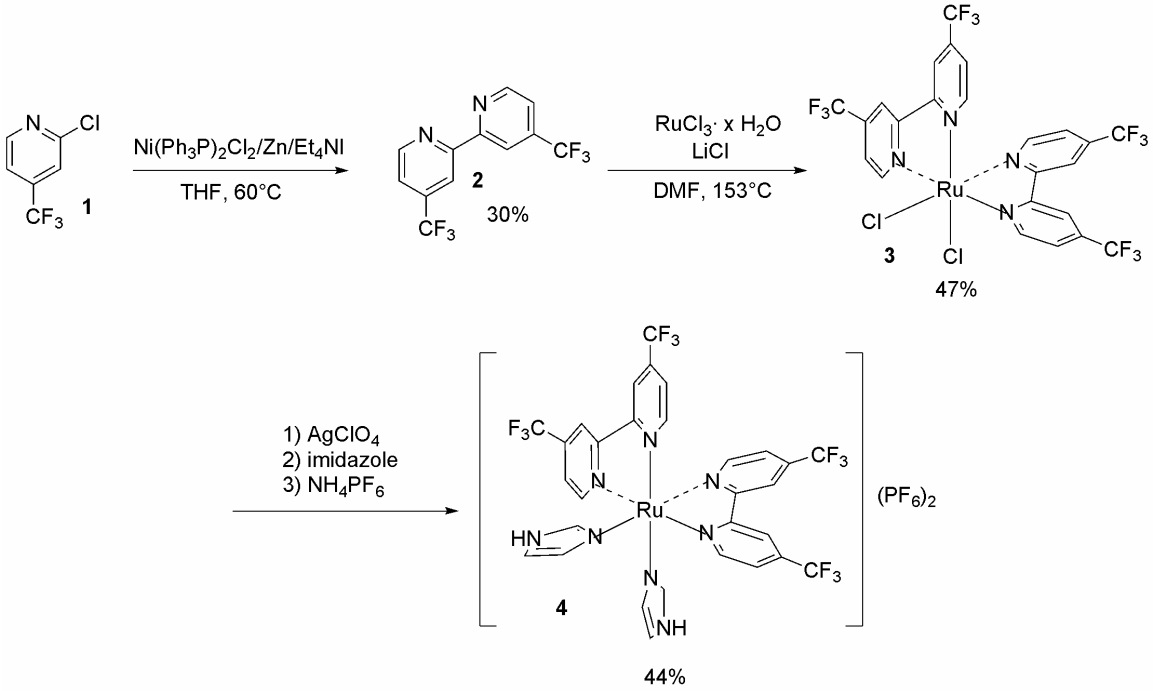

Scheme 2.1. Synthesis of $[Ru(tfmbpy)_2(im)_2](PF_6)_2$

$[Ru(tfmbpy)_2(im)_2]^{2+}$ was synthesized as described in **Scheme 2.1**; only a few modifications had to be made to the established protocol to achieve synthesis of the compound. The nickel-catalyzed coupling reaction of the monomer (**1**) afforded tfmbpy (**2**) in low yields. The ligand was installed onto the ruthenium to generate $Ru(tfmbpy)_2Cl_2$ (**3**) in moderate yield. Due to the unreactive nature of the $Ru(tfmbpy)_2Cl_2$ compound, many different methods were attempted to generate the imidazole-ligated product (**4**). It was found that removal of the chlorines with silver to generate an acetone-ligated intermediate was essential. Subsequent addition of the imidazole generated the product.

The absorbance and fluorescence spectra of $[Ru(tfmbpy)_2(im)_2](PF_6)_2$ in acetone are shown in **Figure 2.5**. The metal-to-ligand charge transfer from the t_{2g} to π^* of the tfmbpy ligand is observed at 514 nm and excitation at this wavelength results in emission that maximizes at 707 nm in water. The lifetime of the excited state was found to be 33 ns in water (**Figure 2.6**). This lifetime is much shorter than is desired; traditionally, ruthenium labels for electron transfer studies have had lifetimes of at least 100 ns. [9,10,25-28] However, it has been observed that lifetimes of excited states are generally longer in organic solvents and on protein than they are in aqueous environments. This supposition was confirmed: the lifetime was extended to 42 ns in acetone, and 51 ns in acetonitrile. While the lifetime of the excited state is still quite short, it is suspected that it may extend further still when the label is attached onto the protein.

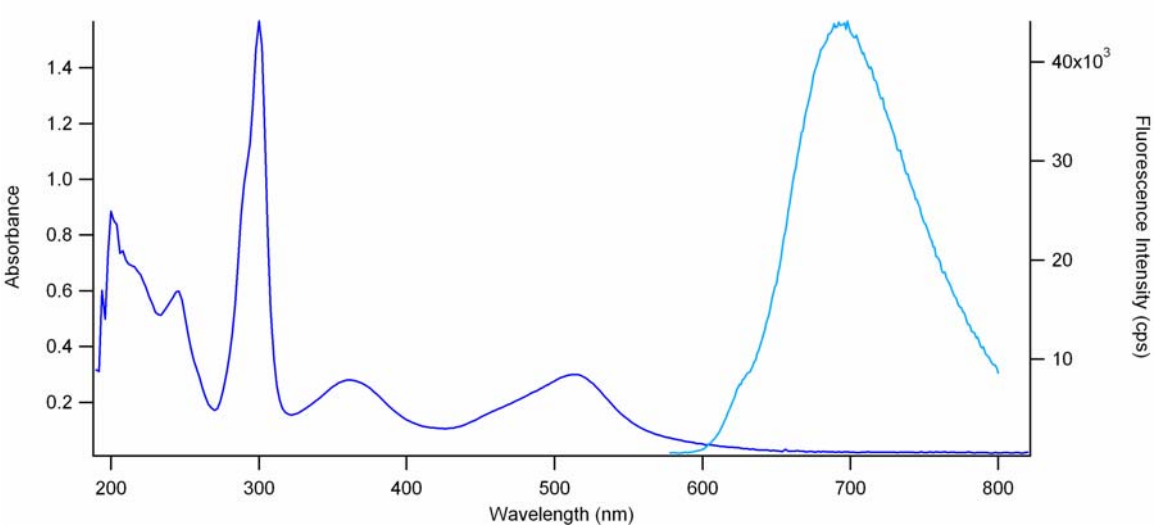

Figure 2.5. Absorption (dark blue) and emission (light blue) spectra of $[Ru(tfmbpy)_2(im)_2](PF_6)_2$ in acetone

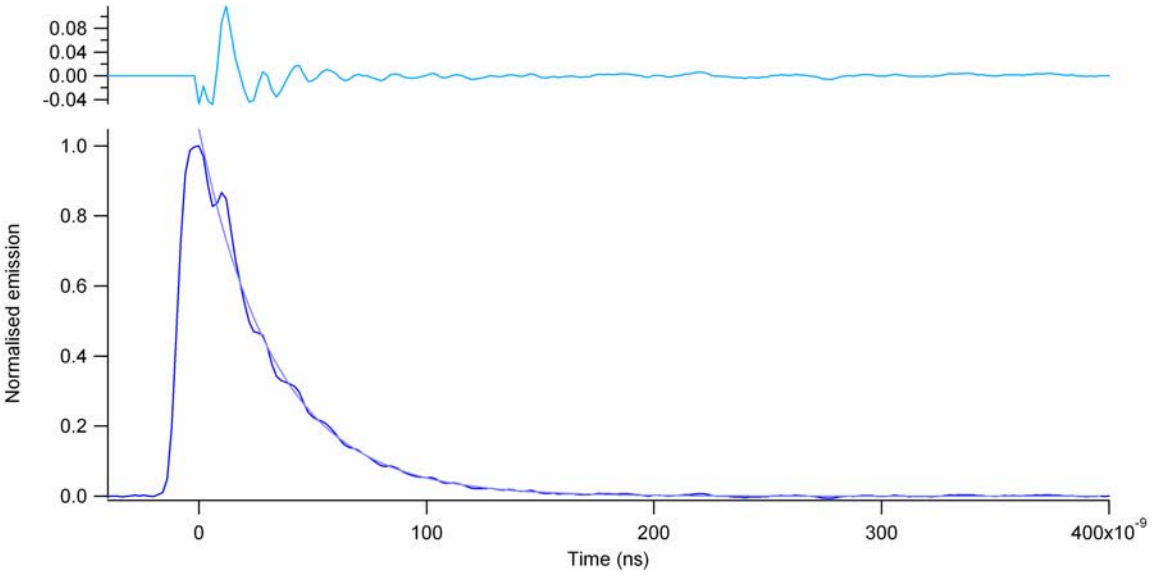

Figure 2.6. Time-resolved emission of $*[Ru(tfmbpy)_2(im)_2](PF_6)_2$ in water. λ_{ex} = 514 nm, λ_{em} = 707 nm. Fit to single exponential function, τ = 33 ns

The 3-2-1 Architecture

The Gray group has previously worked with the tridentate-bidentate-monodentate architecture (referred hereafter as 3-2-1) on ruthenium: $[Ru(trpy)(bpy)]^{2+}$ was installed on plastocyanin (trpy = 2,2';6'2"-terpyridine, bpy = 2,2'-bipyridine).[28] The measured

reduction potential of $[Ru(trpy)(bpy)(im)]^{3+/2+}$ was found to be 1.09 V *v*. NHE. So a similar approach to raising the metal's reduction potential by utilizing electron-deficient ligands was to be utilized here. The $[Ru(Cl\text{-}trpy)(bpy)(im)]^{2+}$ and $[Ru(trpy)(tfmbpy)(im)]^{2+}$ compounds were targeted because Cl-trpy was found to be commercially available and the tfmbpy had already been made for the previous study. In addition, the $[Ru(trpy)(bpy)(im)]^{2+}$ compound was synthesized for easy comparison of spectroscopic and electrochemical properties.

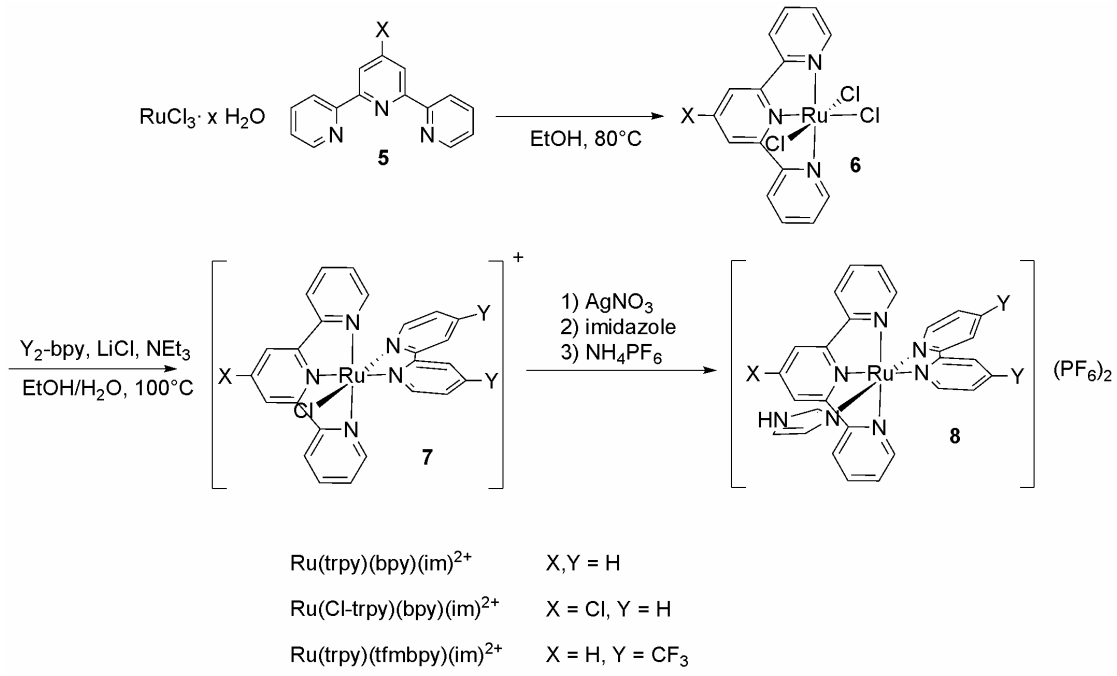

Scheme 2.2. Synthesis of 3-2-1 ruthenium compounds

Synthesis of these complexes proved to be quite facile (**Scheme 2.2**). Protocols had been established in the literature and were followed with minor modifications. The trpy ligand (**5**) was easily attached to the ruthenium to generate the $Ru(trpy)Cl_3$ species (**6**). The ruthenium was reduced and attached to a bidentate ligand in the following slower step to generate the Ru(trpy)(bpy)Cl cation (**7**). Because of the previous success

using silver in the $Ru(tfmbpy)_2(im)_2$ reaction, the same method was tried, and the model compound (**8**) was obtained. The method proved to be robust to changes in reactant structure. Using more electron-withdrawing ligands slowed reactions down and yielded less compound (**Table 2.2**).

molecule	time	overall yield
$Ru(trpy)(bpy)(im)^{2+}$	5 days	43%
$Ru(Cl\text{-}trpy)(bpy)(im)^{2+}$	8 days	25%
$Ru(trpy)(tfmbpy)(im)^{2+}$	15 days	14%

Table 2.2. Overall yields and overall time taken to synthesize three 3-2-1 architecture ruthenium compounds

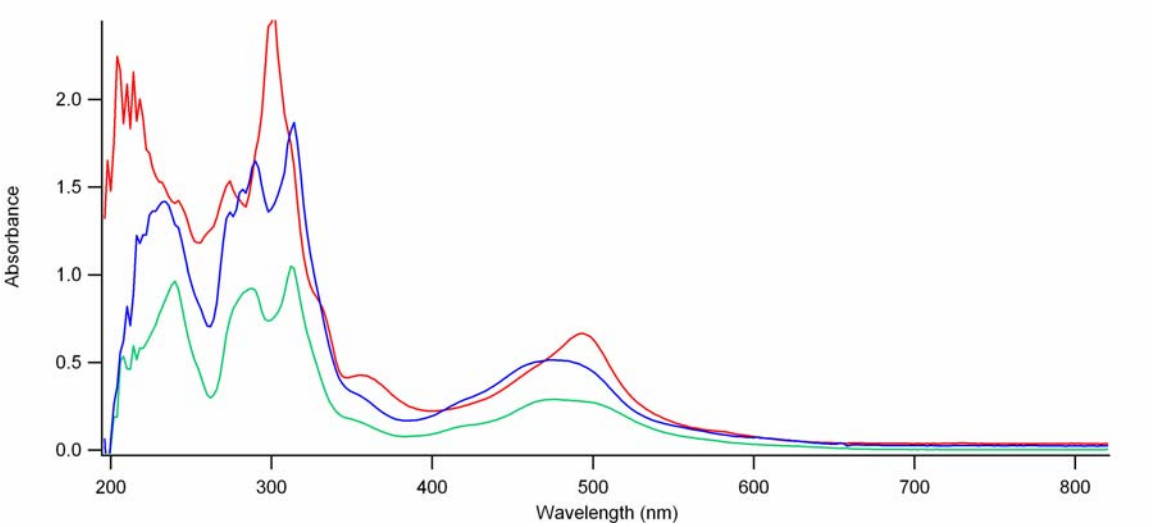

Figure 2.7. UV-VIS spectra of three ruthenium sensitizers in acetonitrile. Red trace is $Ru(trpy)(tfmbpy)(im)^{2+}$, λ_{max} = 494 nm. Green trace is $Ru(Cl\text{-}trpy)(bpy)(im)^{2+}$, λ_{max} = 480 nm. Blue trace is $Ru(trpy)(bpy)(im)^{2+}$, λ_{max} = 475 nm.

Absorption measurements were made on the three compounds in acetonitrile (**Figure 2.7**). The peaks around the 470–500 nm region were assigned metal-to-ligand charge transfers (MLCTs) from the t_{2g} orbitals to the π^* of the bpy and trpy analog

ligands. The sharper peaks at 300–350 nm were assigned as the π to π* of the bpy and trpy ligands.

There is an expected red shift resulting from the installation of the π* energy-lowering electron-withdrawing groups onto the ligands. Installation of the trifluoromethyl groups on bpy shifts the MLCT more than the chloro on the trpy ligand.

This trend manifests itself in the fluorescence spectra as well. The [Ru(trpy)(tfmbpy)(im)]$(PF_6)_2$ emission was observed at 725 nm (**Figure 2.8**), extremely red-shifted from the [Ru(Cl-trpy)(bpy)(im)]$(PF_6)_2$ emission, which was observed at 700 nm. Still bluer than that is the emission of the unmodified [Ru(trpy)(bpy)(im)]$(PF_6)_2$, which can be found at 695 nm.

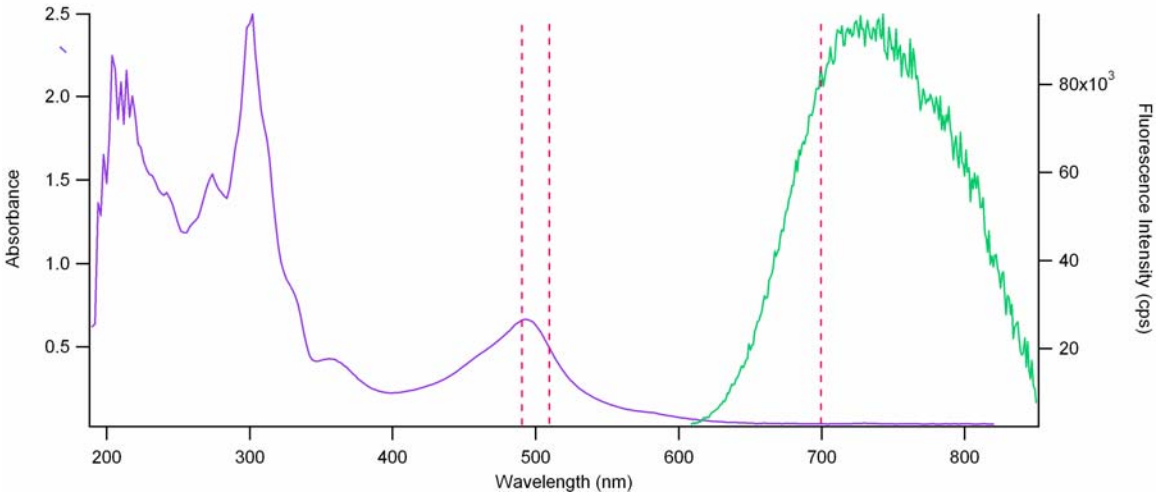

Figure 2.8. Absorption (purple) and emission (green) spectra of [Ru(trpy)(tfmbpy)(im)]$(PF_6)_2$ in acetonitrile. Wavelengths of interest are highlighted with the hashed pink line. The photosensitizer will be excited at either 490 nm or 510 nm, and Ru^{2+} will be monitored at the other, with the use of a long-pass filter. $*Ru^{2+}$ will be monitored at 700 nm.

The cyclic voltammetry (CV) measurements exhibited similar (and the hoped for) trend (**Figure 2.9**). Due to solubility issues, CV measurements had to be executed in

acetonitrile. The tfmbpy clearly accomplishes the goal of raising the potential of the ruthenium dye (**Table 2.3**).

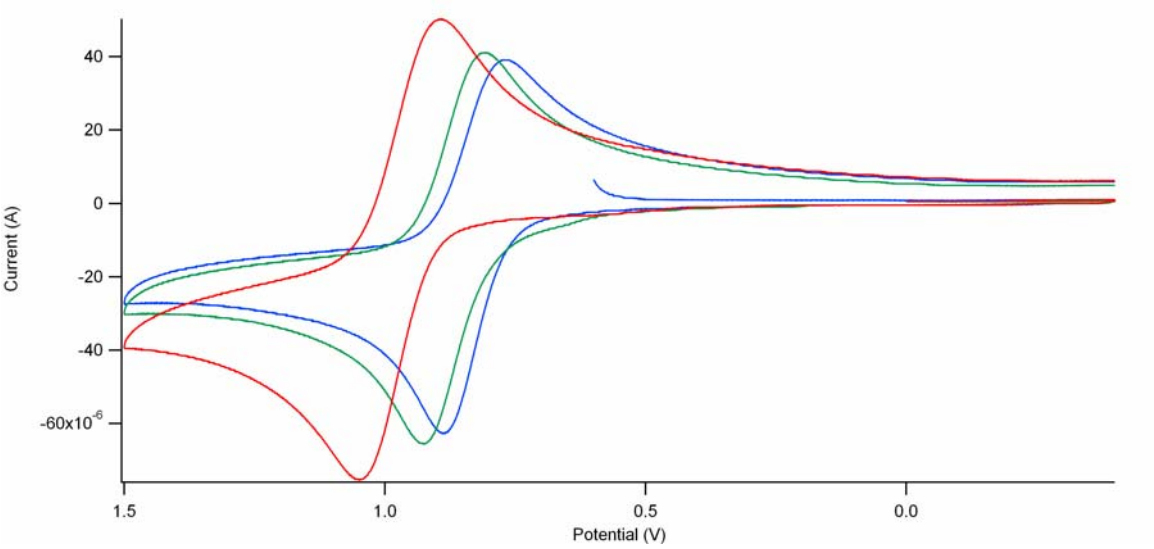

Figure 2.9. Cyclic voltammograms of three ruthenium sensitizers. Red trace is Ru(trpy)(tfmbpy)(im)$^{2+}$. Green trace is Ru(Cl-trpy)(bpy)(im)$^{2+}$. Blue trace is Ru(trpy)(bpy)(im)$^{2+}$.

molecule	E (V *v.* Ag/$AgNO_3$, in ACN)
Ru(trpy)(bpy)(im)	0.83
Ru(Cl-trpy)(bpy)(im)	0.87
Ru(trpy)(tfmbpy)(im)	0.97

Table 2.3. Reduction potentials of three ruthenium sensitizers. Measured at room temperature in acetonitrile. Silver/silver nitrate reference electrode

The lifetime of the excited state of *[Ru(trpy)(tfmbpy)(im)]$^{2+}$ was found to be approximately 33 ns in water. The reduction potential of the $Ru^{2+/+}$ couple was also measured. A modified Latimer diagram was constructed from the data obtained (**Figure 2.10**). Because **Figure 2.4** was constructed on potentials *v.* Ag/AgCl, it is not fair to compare the two values. However, it can be observed, based on the results described in the later chapters, that *[Ru(trpy)(tfmbpy)(im)]$^{2+}$ does not have as high a potential as

*Re^{+} with either phen or dmp as ligand, and the $Ru^{3+/2+}$ couple does not have as high a potential as $Re^{2+/+}$.

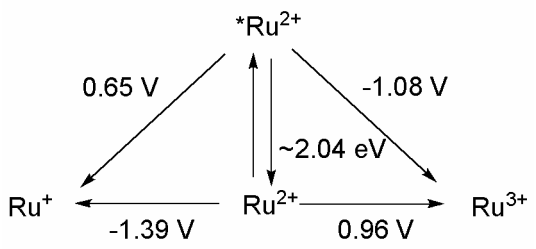

Figure 2.10. Modified Latimer diagram of Ru(trpy)(tfmbpy)(im). Constructed from values obtained in acetonitrile, using a $Ag/AgNO_3$ reference electrode

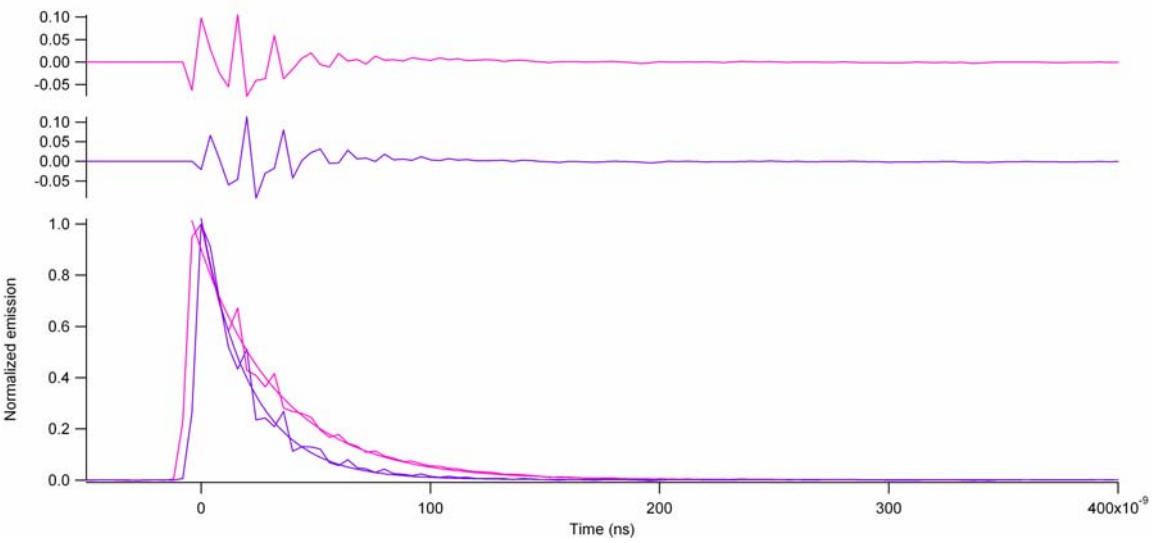

Figure 2.11. Emission data: Ru(trpy)(tfmbpy)$(im)^{2+}$ without (pink) and with (purple) quencher. 25 μM [Ru(trpy)(tfmbpy)(im)]$(PF_6)_2$ in 50 mM NaP_i, pH 7.7, 80 mM methyl viologen. λ_{ex} = 510 nm, λ_{em} = 700 nm. τ = 33 ns without quencher, 21 ns with quencher

Because it seemed likely that Ru^{3+} would be need to be accessed during photochemical measurements, quenchers were tested. *[Ru(trpy)(tfmbpy)(im)]$^{2+}$ has a disappointingly short lifetime, so there was a worry that the excited state would not live long enough for the intermolecular quench to occur. Indeed, $Ru(NH_3)_6^{2+}$ and lower (< 50

mM) concentrations of methyl viologen did not succeed in oxidizing *Ru^{2+}. However, 80 mM methyl viologen was found to accomplish the desired goal (**Figure 2.11**).

There was a small disadvantage to using methyl viologen, however; in its reduced state, methyl viologen absorbs in the 600 nm region, which complicates transient absorption studies done to probe Cu^{2+} generation. It was soon found, however, that the labeled proteins did not need to for the ruthenium to be oxidized to the Ru^{3+} state in order for interesting kinetics to occur. Further experiments with methyl viologen as a quencher were discontinued.

Rhenium

Despite its optical inactivity, rhenium's high potential was too much of a benefit to ignore. Systems were still pursued utilizing $[Re(dmp)(CO)_3]^+$. This proved to be a wise decision: the two successful hopping systems utilize Re^+. Brian S. Leigh was generous enough to provide the $[Re(dmp)(CO)_3(H_2O)]OTf$ needed for protein labeling, and Dr. Angel J. Di Bilio provided the model compound $[Re(dmp)(CO)_3(im)]OTf$ for control measurements. Procedures to make both species can be found in Dr. Jeremiah E. Miller's thesis.[13]

Azurin

Site-Directed Mutagenesis & Expression of Mutants

As discussed above, a few mutations have to be made to *Pseudomonas aeruginosa* azurin to facilitate successful hopping experiments. The surface His83 is changed into a Gln, and resident Tyr72, Tyr108, Trp48 are changed into Phe. This

mutant is misleadingly but still appropriately named the All-Phe mutant (**Figure 2.12**). All further site-directed mutagenesis was executed on the plasmid carrying the All-Phe azurin mutant. Established protocols were assiduously followed;[13] expression of desired mutants was achieved with little difficulty. Yuling Sheng executed site-directed mutagenesis and expressed most of the mutants needed for the studies described.

```
          10         20         30         40         50
AECSVDIQGNDQMQFNTNAITVDKSCKQFTVNLSHPGNLPKNVMGHNFVLSTAADMQ

  60         70         80         90         100        110
GVVTDGMASGLDKDFLKPDDSRVIAQTKLIGSGEKDSVTFDVSKLKEGEQFMFFCTF

      120
PGHSALMKGTLTLK
```

Figure 2.12. Sequence of All-Phe azurin. The mutations to the wild type are highlighted; H83Q in red, and W48F, Y72F, and Y108F are highlighted in blue.

Nitration of Tyrosine

Tyrosine was inserted into the sites of interest using site-directed mutagenesis. Previously established nitration protocols were followed, in which the protein was exposed to tetranitromethane. Protocols were obtained from Bert Tsunyin Lai, Dr. Jennifer C. Lee, and Prof. Michele McGuirl (University of Montana). UV-VIS spectra were obtained to confirm nitration of the tyrosine (**Figure 2.13**). The first mutant on which nitration was attempted was H107/Y110/Az(Cu^{2+}). This was an unfortunate selection, as the tyrosine was unreactive to tetranitromethane at this site, and proved to remain so in all future attempts, even after a successful protocol had been developed. A strategy was undertaken to unfold the protein, nitrate the residue, and allow the protein refold. The strategy with complete unfolding of the protein was unsuccessful; while it appeared that the tyrosine had been nitrated, the protein would not refold. It has been

previously observed that tetranitromethane oxidizes cysteines, resulting in disulfide bridges and sulfinic acids.[29] It is likely that unfolding the protein exposes the copper-ligating Cys112 and possibly the disulfide bridging Cys3 and Cys26 to oxidations that disrupt the protein's structure. To circumvent this problem, unfolding studies were carried out to probe the possibility of loosening the protein structure just enough to expose the tyrosine for nitration, but not lose copper ligation. These experiments are listed and discussed below in the next section; the conditions that seemed optimal for nitration trials were either 40% methanol or 3 M urea. Both conditions were attempted; the reaction in methanol was not at all successful, and the reaction run in 3 M urea resulted in a miniscule yield of the desired product, the greater percentage of product being the oxidized unfolded azurin.

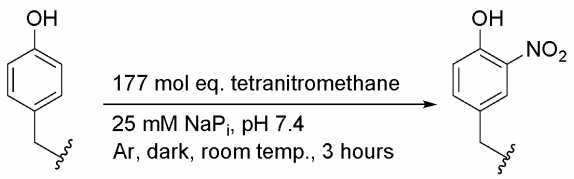

Scheme 2.3. Nitration of tyrosine

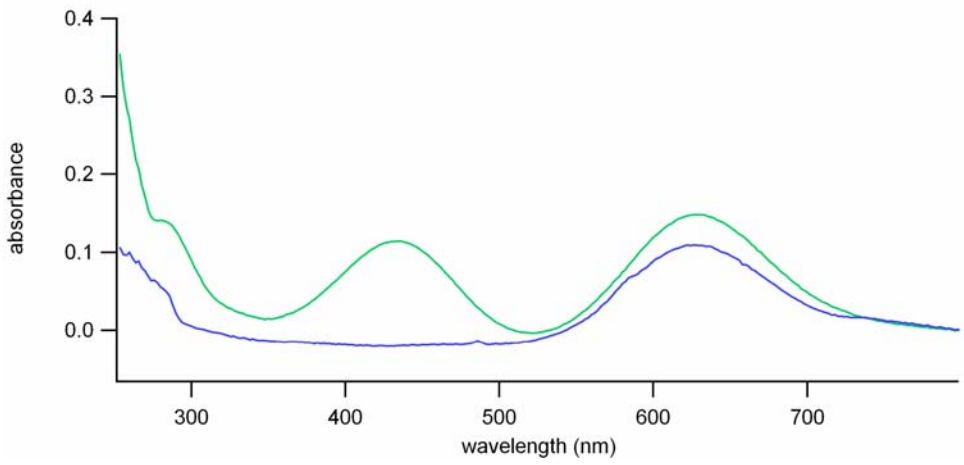

Figure 2.13. UV-VIS of successful nitration. Blue trace is H107/Y109/Az(Cu^{2+}) in 25 mM NaP$_i$. Green trace is H107/YNO$_2$109/Az (Cu^{2+}) in 25 mM DEA, pH 8.8.

When nitration was attempted on H107/Y109/Az(Cu^{2+}) without any denaturants, the tyrosine was nitrated without any difficulty. It is likely that the tyrosine at the 110 site was simply not exposed enough to react. The protocol utilized to nitrate at the 109 site was also utilized to successfully nitrate at the 122 site (**Scheme 2.3**).

Routinely, the protein was nitrated prior to labeling, for labeling was the lower-yielding reaction of the two. Once nitrated, the protein would be purified using anion exchange chromatography.

It was important to purify either the nitrated unlabeled protein or the nitrated labeled protein using cation-exchange chromatography. Purification using cation-exchange chromatography at either stage yielded two major products; one green in color, and one blue, both of the same mass. The blue product is the expected and desired mutant; at pH 4.52, the nitrotyrosine should be protonated, and thus not absorb at 434 nm. The green product was pursued and studied, but no productive or interesting results came of the studies; it remains unclear what, exactly, it is, though it is conjectured that it is a side-product of the nitration reaction with an altered protein structure.

Once the purity of the sample was ascertained by mass spectrometry, the protein was then ready for labeling reactions.

Unfolding Studies

Unfolding studies were carried out in varying concentrations of methanol and urea in the hopes of finding a concentration of denaturant that would perturb secondary structure, but leave copper binding undisturbed. The copper coordination was monitored by UV-VIS spectroscopy and the extent of secondary structure was measured using

circular dichroism (CD). The resulting unfolding conditions would be employed in a nitration reaction, so the buffer used in these studies was the 50 mM sodium phosphate, pH 8.0 that was to be used in the reaction. The mutant used for these studies was H107/Y110/Az(Cu^{2+}).

The results of the experiments done with methanol are shown in **Figures 2.14–2.16**. Measurements were made on eleven samples of azurin, with increasing concentrations of methanol, every 10% from 0 to 100%. The UV-VIS spectra indicate that the protein is aggregating with increased concentrations; the baseline is migrating upwards with every sample. At around 80% methanol, solubility became a problem. The measurement at 40% methanol, indicated in **Figure 2.14** with a solid line, shows the copper center intact, as well as minor aggregation. The CD spectra show strange incongruity, but the measurement at 40% methanol clearly displays the predicted behavior; less secondary structure compared to wild type. 40% methanol was determined to be the optimal concentration of methanol to achieve the desired effect on the protein.

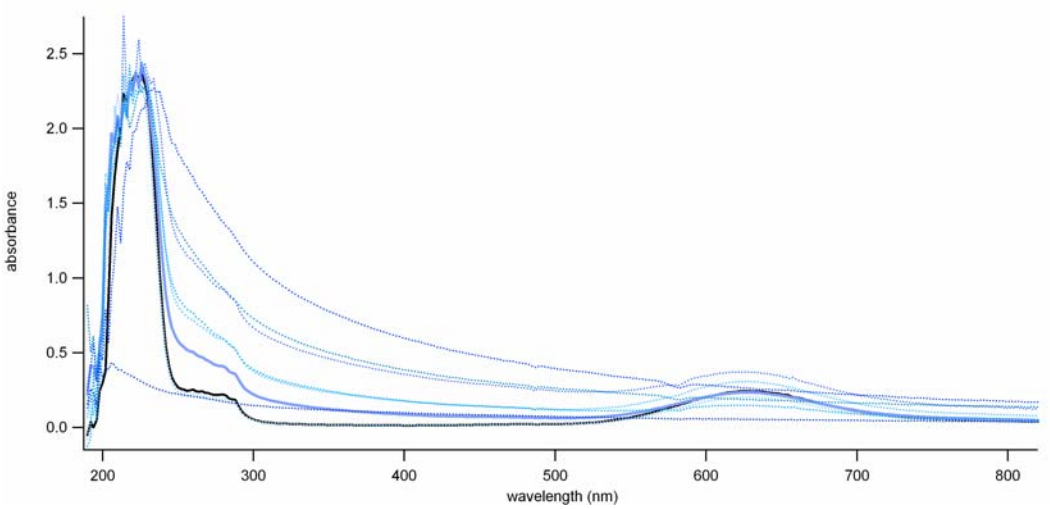

Figure 2.14. UV-VIS spectra of azurin in increasing concentrations of methanol. 4 μM H107/Y110/Az(Cu^{2+}) in 50 mM NaP_i, pH 8 in 1 mm path length cuvette. Data for increasing concentrations of methanol (0–100% v/v, a sample at each 10% increment) are displayed in gradient of shades; the lightest shades are of the lesser methanol concentrations, the darker are for the more concentrated. The control measurement without methanol is indicated in black. The spectrum at 40% methanol is solid blue.

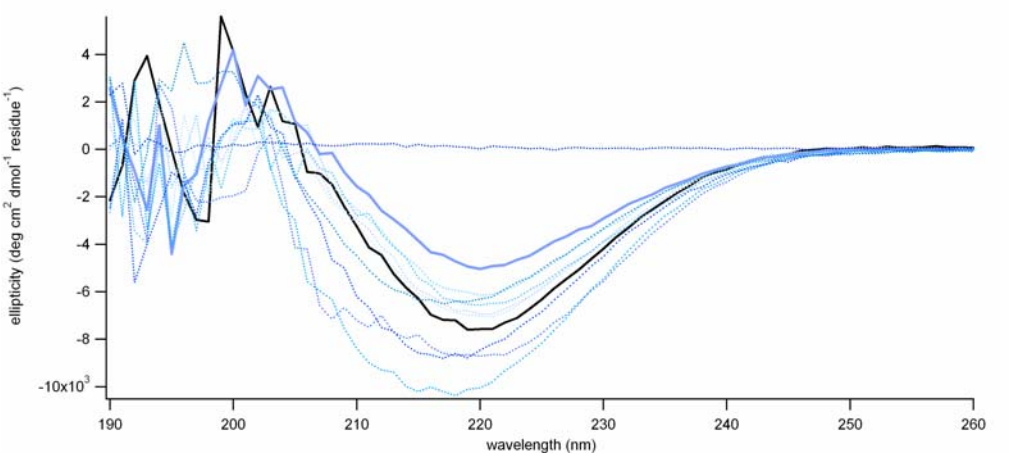

Figure 2.15. CD spectra of azurin in increasing concentrations of methanol. 4 μM H107/Y110/Az(Cu^{2+}) in 50 mM NaP_i, pH 8 in 1 mm path length cuvette. Data for increasing concentrations of methanol (0–100% v/v, a sample at each 10% increment) are displayed in gradient of shades; the lightest shades are of the lesser methanol concentrations, the darker are for the more concentrated. The control measurement without methanol is indicated in black. The spectrum at 40% methanol is solid blue.

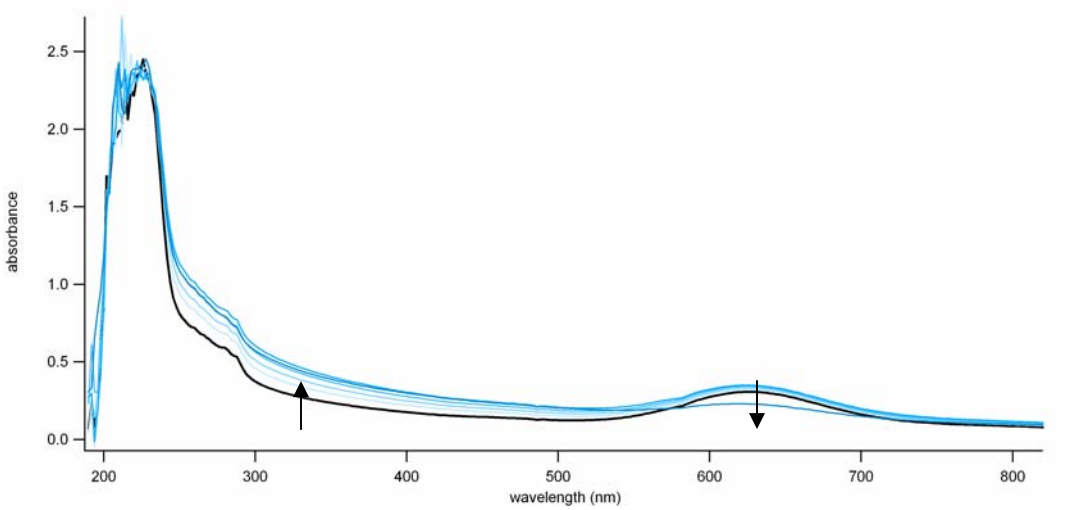

Figure 2.16. UV-VIS of azurin in 50% methanol over time. 4 μM H107/Y110/Az(Cu^{2+}) in 50% methanol/50 mM NaP_i, pH 8 in 1 mm path length cuvette. Spectra were taken immediately, 2, 5, 10, 30, and 270 minutes after the sample was made; darker shades for more time elapsed.

The 50% methanol/50% buffer sample was monitored to check for denaturation over time; while aggregation occurred over the span of the first 30 minutes, diminished binding of the copper center was not evident. Four and a half hours later, aggregation and unfolding of the Cu^{2+} center has rendered the sample useless. While these experiments were not executed on the 40% methanol sample, it is clear that there is a limit to the reaction time; it would defeat the purpose of finding optimal conditions if these optimal conditions also destroyed the reactants.

The results of the experiments done with urea are shown in **Figures 2.17–2.22**. Measurements were made on nine samples of azurin, with increasing concentrations of urea, every 1 M increment from 0 to 8 M. These experiments yielded more aesthetically pleasing and predictable results; the UV-VIS reveals no aggregation; simply deterioration structure and copper binding site. The CD measurements also demonstrate the same aesthetically pleasing predictability. It was found, however, that the samples had not

been given enough time to equilibrate before measurements; the measurements were therefore repeated in 24 hours.

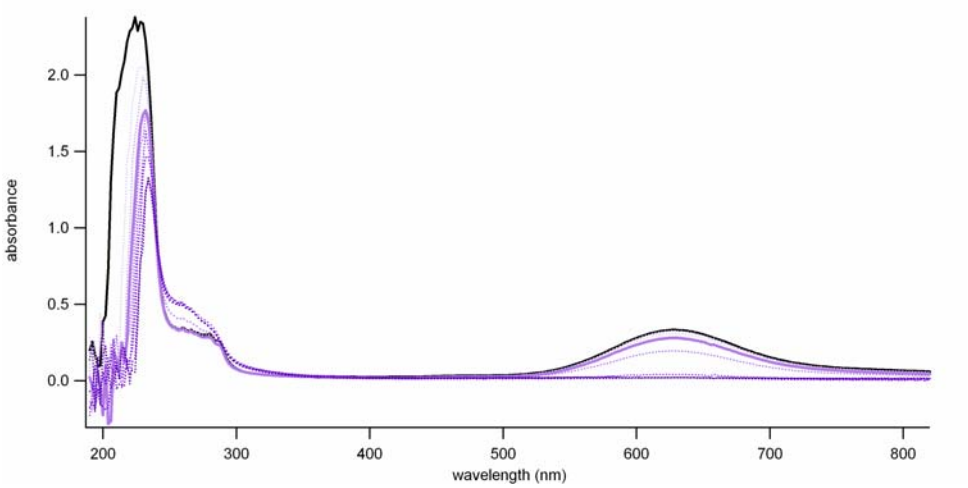

Figure 2.17. UV-VIS spectra of azurin in increasing concentrations of urea. 5 μM in H107/Y110/Az(Cu^{2+}) in 50 mM NaP_i, pH 8 in 1 mm path length cuvette. Data for increasing concentrations of urea (0–8 M, a sample at each 1 M increment) are displayed in gradient of shades; the lightest shades are of the lesser urea concentrations, the darker are for the more concentrated. The control measurement without urea is indicated in black. The spectrum at 3 M urea is solid purple.

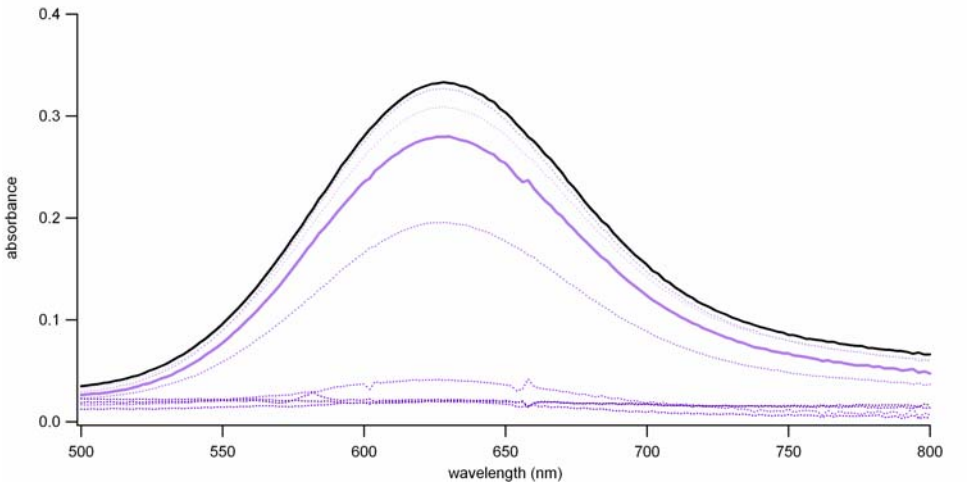

Figure 2.18. Zoom in of 500–800 nm region of **Figure 2.17**. 5 μM H107/Y110/Az(Cu^{2+}) in 50 mM NaP_i, pH 8 in 1 mm path length cuvette. Data for increasing concentrations of urea (0–8 M, a sample at each 1 M increment) are displayed in gradient of shades; the lightest shades are of the lesser urea concentrations, the darker are for the more concentrated. The control

measurement without urea is indicated in black. The spectrum at 3 M urea is solid purple.

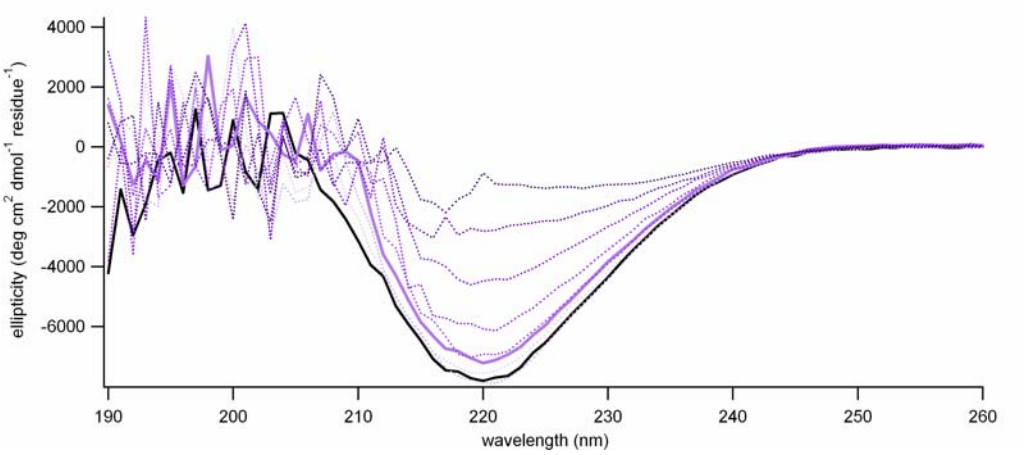

Figure 2.19. CD spectra of azurin in increasing concentrations of urea. 5 μM H107/Y110/Az(Cu^{2+}) in 50 mM NaP_i, pH 8 in 1 mm path length cuvette. Data for increasing concentrations of urea (0–8 M, a sample at each 1 M increment) are displayed in gradient of shades; the lightest shades are of the lesser urea concentrations, the darker are for the more concentrated. The control measurement without urea is indicated in black. The spectrum at 3 M urea is solid purple.

Measurements made after equilibration demonstrate a clear choice for optimal conditions; the UV-VIS spectra reveal that the copper center has deteriorated in samples with 4 M or higher concentrations of urea (**Figures 2.20–2.21**). The CD spectra indicate that at concentrations lesser than 3 M, azurin retains much of its secondary structure (**Figure 2.22**). Given these observations, 3 M urea (after the protein has been allowed to equilibrate in the solution) seems to be at the perfect point, where the copper center maintains its integrity and the secondary structure is being compromised to only a minor degree.

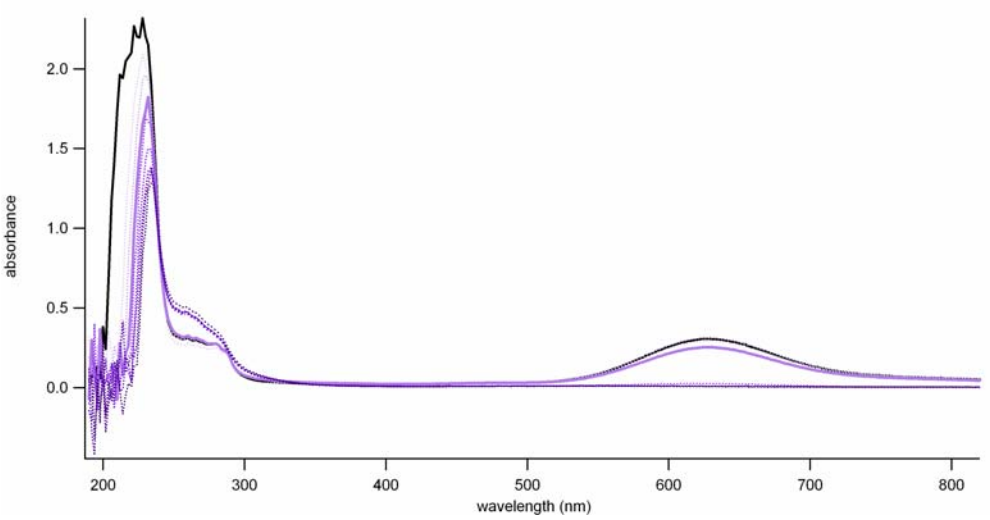

Figure 2.20. UV-VIS spectra of azurin in increasing concentrations of urea, 24 hours. 5 μM H107/Y110/Az(Cu^{2+}) in 50 mM NaP_i, pH 8 in 1 mm path length cuvette. Data for increasing concentrations of urea (0–8 M, a sample at each 1 M increment) are displayed in gradient of shades; the lightest shades are of the lesser urea concentrations, the darker are for the more concentrated. The control measurement without urea is indicated in black. The spectrum at 3 M urea is solid purple.

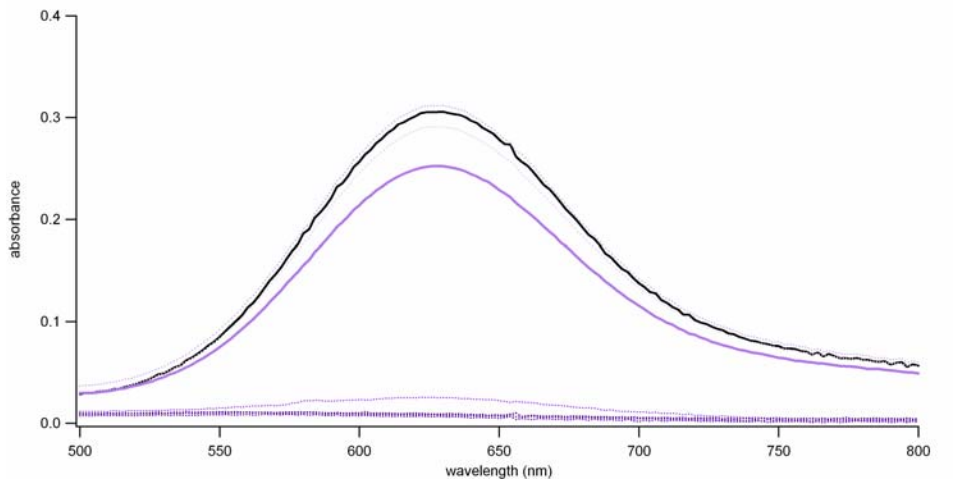

Figure 2.21. Zoom in of 500–800 nm region of **Figure 2.20**. 5 μM H107/Y110/Az(Cu^{2+}) in 50 mM NaP_i, pH 8 in 1 mm path length cuvette. Data for increasing concentrations of urea (0–8 M, a sample at each 1 M increment) are displayed in gradient of shades; the lightest shades are of the lesser urea concentrations, the darker are for the more concentrated. The control measurement without urea is indicated in black. The spectrum at 3 M urea is solid purple.

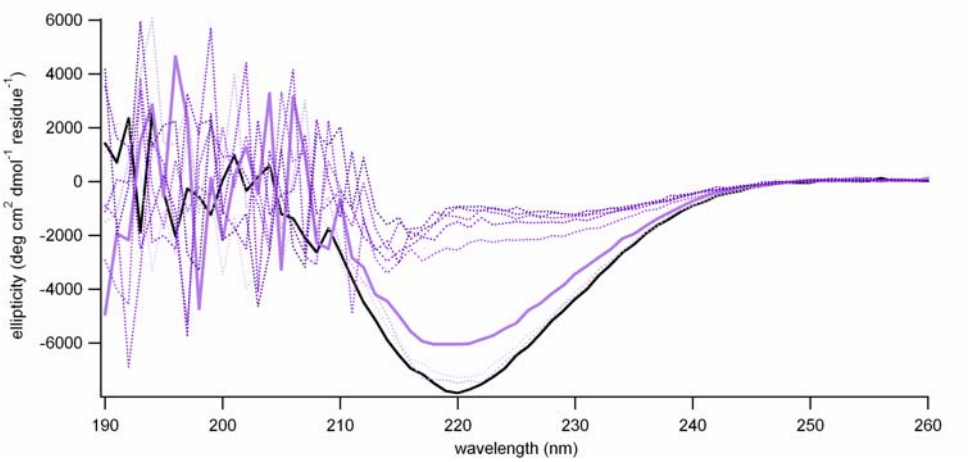

Figure 2.22. CD spectra of azurin in increasing concentrations of urea, 24 hours. 5 μM H107/Y110/Az(Cu^{2+}) in 50 mM NaP_i, pH 8 in 1 mm path length cuvette. Data for increasing concentrations of urea (0–8 M, a sample at each 1 M increment) are displayed in gradient of shades; the lightest shades are of the lesser urea concentrations, the darker are for the more concentrated. The control measurement without urea is indicated in black. The spectrum at 3 M urea is solid purple.

Metal-Labeled Azurin

$[Ru(tfmbpy)_2(im)(HisX)]^{2+}$

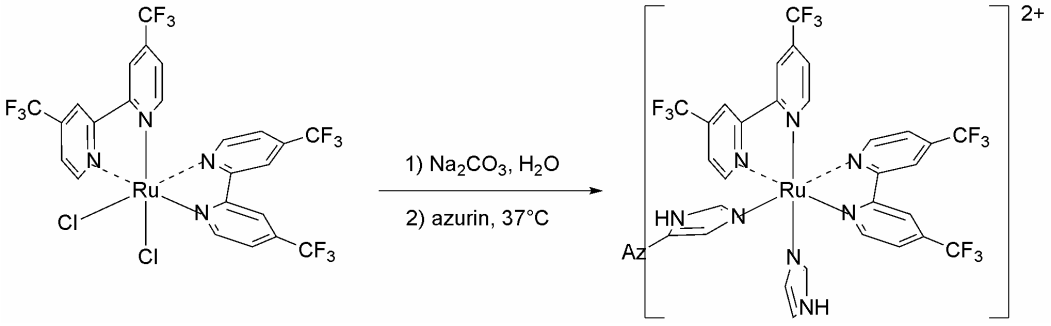

Scheme 2.4. Generation of $Ru(tfmbpy)_2CO_3$ and installation onto azurin

Installing $[Ru(tfmbpy)_2(im)]^{2+}$ label onto the protein proved to be too difficult. Traditionally, the $Ru(bpy)_2CO_3$ species is made from $Ru(bpy)_2Cl_2$ in preparation for the labeling reaction (**Scheme 2.4**).[30-32] The carbonate is a labile leaving group and allows for facile generation of the $Ru(bpy)_2(H_2O)_2^{2+}$ intermediate, which attaches onto the

protein. The $Ru(tfmbpy)_2CO_3$ was a difficult species to generate, no doubt owing the unreactivity of the $Ru(tfmbpy)_2Cl_2$ complex.

Beyond this complication, another disadvantage of this labeling system was recognized: previous flash-quench experiments with $[Ru(bpy)_2(im)(HisX)]^{2+}$-labeled protein indicated that upon excitation, the imidazole ligand was found to exchange with water.[33] This might not have necessarily been the outcome of the studies with the electron-deficient tfmbpy-subtituted analog, but this possibility, coupled with the unreactivity of complex certainly rendered $[Ru(tfmbpy)_2(im)(HisX)]^{2+}$ less exciting a label prospect.

$[Ru(trpy)(tfmbpy)(HisX)]^{2+}$

The established labeling protocol involves stripping the chloride away from $[Ru(trpy)(tfmbpy)Cl]^{+}$ and precipitating silver chloride, leaving the aquo intermediate ready for substitution onto protein. While previously reported labelings with $[Ru(trpy)(bpy)]^{2+}$ took a mere 24 hours at room temperature,[28] the unreactive nature of the $[Ru(trpy)(tfmbpy)]^{2+}$ required a two-week, 37°C incubation time (**Scheme 2.5**). Nonetheless, a moderate amount of labeled protein could be isolated, and so the label and protocol were used to modify proteins in various sites.

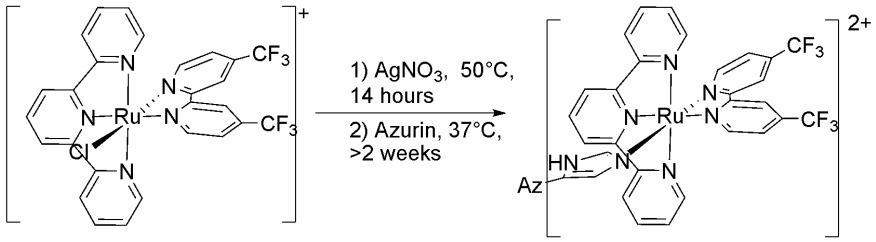

Scheme 2.5. Generation of $[Ru(trpy)(tfmbpy)(H_2O)]NO_3$ followed by installation onto azurin

Labeled azurin was separated from unlabeled by running the product mixture of labeled and unlabeled protein sample through a chelating column. The labeled protein product was confirmed by UV-VIS spectroscopy (**Figure 2.23**). It was further purified by ion exchange chromatography, checked for purity using mass spectrometry, and stored in the dark at 4°C in 25 mM NaOAc, pH 4.52. Prior to laser spectroscopy measurements, stored labeled protein was once more purified using the chelating column and ion exchange chromatography. Mass spectrometry and UV-VIS spectroscopy was carried out on the sample to confirm sample purity.

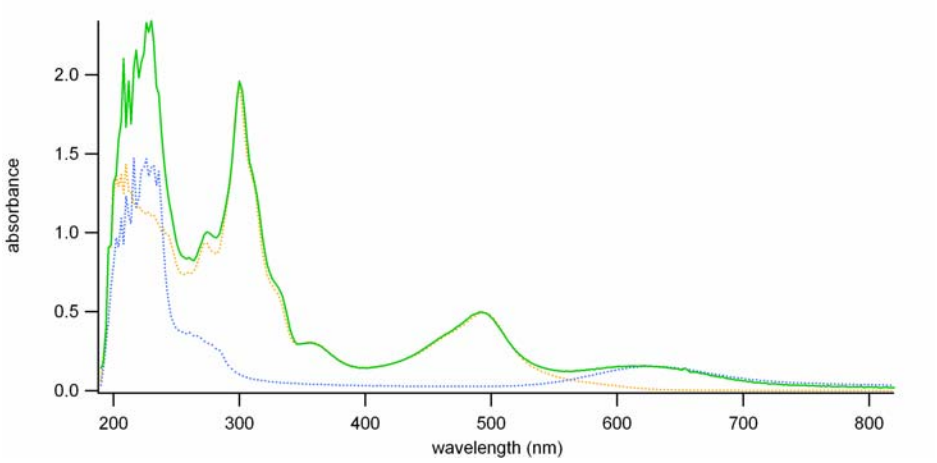

Figure 2.23. UV-VIS spectrum of $[Ru(trpy)(tfmbpy)]^{2+}$-labeled azurin. Green trace is $Ru(trpy)(tfmbpy)(H107)/Y108/Az(Cu^{2+})$. Blue trace is $H107/Y108/Az(Cu^{2+})$. Orange trace is $[Ru(trpy)(tfmbpy)(im)](PF_6)_2$. All samples were made in 25 mM NaP_i, pH 7.2.

$[Re(dmp)(CO)_3(HisX)]^+$

Protocols to install rhenium labels onto proteins are very well established,[24] and were followed accordingly. A different approach to purification was taken; a different chelating column was used to separate unlabeled from labeled protein, and while the column remained the same, a different gradient was used in cation-exchange

chromatography. For the nitrotyrosine mutants, an anion-exchange chromatography was executed after. Purity of the sample was ascertained by mass spectrometry. If the sample was stored before laser spectroscopy experiments, chelating, cation-exchange, and anion-exchange chromatography would once more be executed to ensure purity of the sample.

Labeled Proteins

Protein	Chapter
Re124/W122/Cu^{2+}	3
Ru124/W122/Cu^{2+}	4
Ru124/W122/Zn^{2+}	4
Ru124/F122/Zn^{2+}	4
Ru124/$YNO_2$122/Cu^{2+}	4
Re124/$YNO_2$122/Cu^{2+}	4
Ru126/W122/Cu^{2+}	4
Re126/W122/Cu^{2+}	4
Re126/F122/Cu^{2+}	4
Ru83/F48/Cu^{2+}	5
Ru83/Y48/Cu^{2+}	5

Table 2.4. Labeled proteins studied in this dissertation, and the chapters that discuss them. $[Ru(trpy)(tfmbpy)]^{2+}$ labeling is abbreviated as Ru and $[Re(dmp)(CO)_3]^{+}$ labeling is abbreviated Re.

2.4 CONCLUSIONS

Three high-potential ruthenium sensitizers were synthesized in the pursuit of a photosensitizer that was both high-potential and optically active. This was accomplished through the use of installing electron-withdrawing groups onto the ligand framework. Difficulties were encountered with the initially pursued $[Ru(tfmbpy)_2(im)(HisX)]^{2+}$ when it was found that substitution onto the protein was not straightforward. Utilizing the 3-2-1 architecture of $[Ru(trpy)(bpy)(HisX)]^{2+}$ proved to be more successful.

$[Ru(trpy)(tfmbpy)(HisX)]^{2+}$ was proven to be of high potential and could be installed onto the protein.

Site-directed mutagenesis and protein expression garnered desired mutants. To gain the nitrotyrosine moiety, the tyrosine mutant was first expressed, and established protocol was followed to nitrate the residue using tetranitromethane. The position of the tyrosine was shown to be extremely important in determining the success of the reaction. Unfolding studies were executed on a mutant of azurin to probe if unfolding the protein would assist in exposing the residue for nitration reactions; it was found that unfolding, even to a small degree, still allows destructive side reactions.

Protocols to label and purify hopping systems are outlined; only minor revisions had to be made to established protocol to achieve the desired results. In total, eleven azurin mutants were labeled, characterized, and studied throughout the course of this dissertation, the results of which are described in the following chapters.

2.5 EXPERIMENTALS

Materials

2-Chloro-4-(triflouromethyl)pyridine was purchased from Matrix Scientific. All other reagents were purchased from Aldrich. Dry THF was obtained from the solvent columns. Absolute EtOH was obtained from Aaper. Other reagent-grade solvents were purchased from VWR and were used without further purification.

Resources and Instrumentation

Prior to June 2007, DNA sequencing was obtained from the Caltech Sequence and Structure Analysis Facility. After June 2007, the sequences were obtained from Laragen. Mass spectrometry on small molecules was carried out by Dr. Lionel Cheruzel or Dr. Mona Shahgholi at the mass spectrometry facility at Caltech. Mass spectrometry on protein samples were carried out at the Beckman Institute Protein/Peptide Micro Analytical Laboratory by Dr. Jie Zhou.

UV-VIS spectra were taken on an Agilent 8453 UV-VIS spectrometer. Steady-state fluorescence measurements were made using a Fluorolog Model FL3-11 fluorometer equipped with a Hamamatsu R928 PMT. ^{1}H-NMR spectra were obtained on a Varian Mercury spectrometer operating at 300 MHz in Caltech's NMR Facility. CD spectra were taken on an Aviv 62ADS spectropolarimeter (Aviv Associates, Lakewood, NJ). CV measurements were made using a Model 660 Electrochemical Workstation (CH-Instrument, Austin, TX). Laser spectroscopy, unless otherwise specified, was executed using the Nanosecond-I setup in the Beckman Institute Laser Resource Center.

Synthesis & Characterization of Ruthenium Model Compounds

$Ru(trpy)Cl_3$[34], $[Ru(trpy)(bpy)(im)](PF_6)_2$[35] were synthesized following previously reported protocols.

4,4'-bis(trifluoromethyl)-2,2'-bipyridine (tfmbpy)

A literature preparation was modified to obtain this ligand.[36]

Under argon, $Ni(Ph_3P)_2Cl_2$ (3.92 g, 6 mmol), zinc dust (1.96 g, 30 mmol), and Et_4NI (5.14 g, 20 mmol) were added to a 100 mL Schlenck flask equipped with a stir bar. Dry THF (40 mL) was added and the mixture was stirred at room temperature for 30 minutes. The mixture turned dark red. In a second 25 mL round-bottom flask and under argon, 2-chloro-4-trifluoromethylpyridine was added to 10 mL dry THF. The chloro-pyridine solution was added to the reaction pot via cannula transfer. The reaction was heated for three days at 60°C with stirring to yield a dark brown-black solution. The flask was then cooled to room temperature and added into 200 mL aqueous ammonia and extracted into 200 mL of a 1:1 mixture of benzene and diethyl ether. The aqueous phase was washed with 1:1 benzene/ether mixture (100 mL, 2 times). The combined organic layers were then washed with water and brine, dried over $MgSO_4$, and filtered. The mixture was then concentrated down to yield a brown oil. Subsequent column chromatography performed on silica gel with 20% dichloromethane/hexanes (R_f = 0.2) yielded a white powder. The ^{1}H-NMR matches that given in the literature. Yield: 1.14 g (39%).

$Ru(tfmbpy)_2Cl_2 \cdot 2H_2O$

The synthesis of this compound was modified from a preparation taken from literature.[37]

$RuCl_3 \cdot 2.5\ H_2O$ (169 mg, 0.67 mmol), tfmbpy (394 mg, 1.35 mmol), LiCl (189 mg, 4.47 mmol), and 1.1 mL DMF were added to a two dram vial equipped with a stir bar. The vial was sealed with a Teflon screw-cap and the reaction was stirred at reflux for 24 hours. The reaction mixture was then cooled to room temperature, added to 50 mL

reagent-grade acetone, and stored at -10°C overnight. Filtering yielded a red-purple solution and dark purple powder. The powder was washed three times with water (5 mL) and three times with diethyl ether (5 mL), and dried on a vacuum line. Yield: 252 mg (47%). The ^{1}H-NMR was checked against literature.

$[Ru(tfmbpy)_2(im)_2](PF_6)_2$

The synthesis of this compound was modified from a preparation taken from literature.[37]

$Ru(tfmbpy)_2Cl_2 \cdot 2.5\ H_2O$ (200 mg, 0.25 mmol), $AgClO_4$ (156 mg, 0.75 mmol), and 25 mL reagent-grade argon-sparged acetone were added to a 100 mL round-bottom flask equipped with a stir bar. The mixture was stirred at room temperature overnight, and the AgCl precipitate was removed by filtration. The mixture was added to a 50 mL round-bottom flask with stir bar. Imidazole (68 mg, 1 mmol) was added to the mixture under argon. A condenser was then attached and sealed off with a septum. The reaction was heated at reflux with stirring for 3 days. After cooling the reaction to room temperature, the mixture was concentrated to approximately one-third of its original volume and added to 17 mL water. NH_4PF_6 was added to precipitate out the dark purple powder product. The powder was isolated by filtration and washed with a generous amount of water and diethyl ether. The product was then dried on the vacuum line. Yield: 123 mg (44%). ^{1}H-NMR (d_6-DMSO), δ: 9.37 (s, 2H), 9.28 (s, 2H), 9.19 (d, 2H, J = 6 Hz), 8.27 (d, 2H, J = 6 Hz), 8.20 (dd, 2H, J = 6.6 Hz, < 1 Hz), 7.81 (s, 2H), 7.73 (dd, 2H, 6.6 Hz, < 1 Hz), 7.30 (s, 1H), 6.71 (s, 1H).

[Ru(trpy)(tfmbpy)Cl]Cl

A literature preparation was modified for the synthesis of this compound.[35]

$Ru(trpy)Cl_3$ (200 mg, 0.45 mmol), tfmbpy (133 mg, 0.45 mmol), and LiCl (114 mg, 2.69 mmol) were added to a 100 mL round-bottom flask equipped with a stir bar. 45 mL 75% absolute EtOH/water was added to the flask. Finally, 0.1 mL NEt_3 was added as reductant. The mixture was heated to reflux and stirred for 6 hours. The reaction mixture was filtered while still hot and the filtrate was concentrated down to approximately one-third its original volume. It was then stored at 4°C overnight. The resulting purple-black precipitate was collected by filtration and washed two times with 5 mL portions of 3 N HCl, one time with minimal reagent grade acetone, and three times with 10 mL portions of diethyl ether. Yield: 225 mg (71%). ^{1}H-NMR (d_6-DMSO), δ: 10.34 (d, 1H, 6 Hz), 9.60 (s, 1H), 9.35 (s, 1H), 8.86 (d, 2H, J = 8 Hz), 8.71 (d, 2H, J = 8 Hz), 8.46 (dd, 1H, J = 8 Hz, < 1 Hz), 8.31 (t, 1H, J = 8 Hz), 8.02 (td, 2H, J = 8 Hz, 1 Hz), 7.74 (d, 1H, J = 6 Hz), 7.66 (d, 2H, J = 4.5 Hz), 7.43 (dd, 1H, J = 4.5 Hz), 7.36 (td, 2H, J = 6 Hz, < 1 Hz).

[Ru(trpy)(tfmbpy)(im)]$(PF_6)_2$

[Ru(trpy)(tfmbpy)Cl]Cl (100 mg, 0.143 mmol), $AgNO_3$ (73 mg, 0.429 mmol), and 14.3 mL water were added to a 25 mL round-bottom flask equipped with a stir bar. The reaction stirred at 50°C for 24 hours. The AgCl precipitate was filtered from the red solution. The solution was added to a 50 mL round-bottom flask equipped with a stir bar. To this solution was added imidazole (48 mg, 0.715 mmol). The reaction was then stirred at reflux for 6 days. The reaction mixture was then cooled, and the AgCl that continued to precipitate at this stage was then removed by filtration. NH_4PF_6 was added

to precipitate the product, a dark red-orange powder. The product was isolated by filtration and washed with ether. Yield: 72 mg (51%). ^{1}H-NMR (d^6-DMSO), δ: 9.66 (s, 1H), 9.45 (s, 1H), 8.86 (d, 2H, J = 8.4 Hz), 8.75 (m, 3H), 8.342 (m, 2 H), 8.15 (td, 2H, J = 6 Hz, < 1 Hz), 7.89 (d, 2H, J = 5.4 Hz), 7.74 (d, 1H, J = 5.7 Hz), 7.50 (m, 3H), 7.23 (s, 1H), 7.03 (s, 1H), 6.04 (s, 1H).

[Ru(trpy)(bpy)Cl]Cl

The method used above on the preparation of [Ru(trpy)(tfmbpy)Cl]Cl was followed for the synthesis of this complex.

The amounts used for this synthesis: $Ru(trpy)Cl_3$ (100 mg, 0.23 mmol), bpy (36 mg, 0.23 mmol), LiCl (49 mg, 1.15 mmol), 0.15 mL NEt_3, and 23 mL 75% EtOH/water. The mixture was stirred at reflux for 24 hours. The product was a metallic black powder. Yield: 72 mg (56%). ^{1}H-NMR (d_6-DMSO), δ: 10.1 (d, 1H), 8.89 (d, 1H, J = 7.5 Hz), 8.80 (d, 2H, J = 7.8 Hz), 8.68 (d, 2H, J = 8.1 Hz), 8.62 (dd, 2H, J = 7.2 Hz, < 1 Hz), 8.34 (m, 1H), 8.20 (t, 1H, J = 8.1 Hz), 8.05 (td, 1H, J = 6 Hz), 7.97 (m, 2H), 7.76 (td, 1H, J = 8 Hz), 7.60 (d, 2H, J = 4.8 Hz), 7.33 (m, 3H), 7.06 (m, 1H).

[Ru(trpy)(bpy)(im)](PF$_6$)$_2$

The method used in the preparation of [Ru(trpy)(tfmbpy)(im)]$(PF_6)_2$ was followed for the synthesis of this complex.

The amounts used for this synthesis: [Ru(trpy)(bpy)Cl]Cl (50 mg, 0.082 mmol), $AgNO_3$ (42 mg, 0.246 mmol), and 8.2 mL of water were stirred at 50°C overnight. After addition of imidazole (28 mg, 0.41 mmol), the reaction was heated to reflux and stirred

for 24 hours. The product is a dark red-orange solid. Yield: 57 mg (Quantitative Yield). ^{1}H-NMR (d_6-DMSO), δ: 8.95 (d, 1H), 8.78 (m, 5H), 8.52 (d, 1H, J = 4.8 Hz), 8.38 (m, 1H), 8.26 (t, 1H), 8.12 (t, 2H, J = 7 Hz), 7.93 (m, 2H), 7.81 (d, 2H, J = 5.1 Hz), 7.51 (t, 2H, J = 6.3 Hz), 7.37 (d, 1H, J = 5.7 Hz), 7.18 (m, 2H), 7.0 (s, 1H), 6.02 (s, 1H).

Ru(Cl-trpy)Cl$_3$

The method used above on the preparation of Ru(trpy)Cl$_3$ was followed in the synthesis of this complex.

The amounts used in this synthesis: RuCl$_3$·2.5 H$_2$O (253 mg, 1 mmol), Cl-trpy (268 mg, 1 mmol), and 125 mL absolute EtOH. The reaction was stirred at reflux for 6.5 hours. The product is a light brown powder. Yield: 375 mg (72%).

[Ru(Cl-trpy)(bpy)Cl]Cl

The method used above on the preparation of [Ru(trpy)(tfmbpy)Cl]Cl was followed in the synthesis of this complex.

The amounts used in this synthesis: Ru(Cl-trpy)Cl$_3$ (200 mg, 0.42 mmol), bpy (131 mg, 0.84 mmol), LiCl (118 mg, 2.8 mmol), 0.1 mL NEt$_3$, and 44 mL 75% EtOH/water. This mixture was stirred at reflux for 6 hours. The product was a metallic black powder. Yield: 94 mg (35%). ^{1}H-NMR (d_6-DMSO), δ: 10.06 (d, 1H, J = 5.4 Hz), 9.09 (s, 2H), 8.93 (d, 1H, J = 8 Hz), 8.78 (d, 2H, J = 7.8 Hz), 8.65 (d, 1H, J = 7.8 Hz), 8.37 (m, 1H), 8.02 (m, 3H), 7.78 (m, 1H), 7.64 (d, 2H, J = 5.4 Hz), 7.42 (m, 3H), 7.06 (t, 1H).

[Ru(Cl-trpy)(bpy)(im)]$(PF_6)_2$

The method used above on the preparation of [Ru(trpy)(tfmbpy)(im)]$(PF_6)_2$ was followed in the synthesis of this compound.

The amounts used: [Ru(Cl-trpy)(bpy)Cl]Cl (70 mg, 0.11 mmol) and $AgNO_3$ (56 mg, 0.33 mmol) were stirred in 11 mL water at 50°C for 24 hours. After filtering off the AgCl and adding imidazole (37 mg, 0.55 mmol) the reaction was heated to reflux and stirred for 2 days. The product was an orange powder. Yield: 87 mg (quantitative yield). ^{1}H-NMR (d_6-DMSO), δ: 9.07 (s, 2H), 8.94 (d, 1H, J = 7.8 Hz), 8.80 (d, 2H, J = 8.4 Hz), 8.69 (d, 1H, J = 8.4 Hz), 8.46 (m, 1H), 8.36 (m, 1H), 8.12 (t, 2H, J = 8 Hz), 7.91 (m, 2H), 7.81 (d, 2H, J = 5.7 Hz), 7.49 (m, 3H), 7.14 (m, 2H), 6.9 (s, 1H), 5.99 (s, 1H).

Protein Protocols

Site-Directed Mutagenesis

All mutagenesis experiments were performed using the QuikChange mutagenesis kit (Stratagene). The appropriate primers were ordered from Invitrogen. The template DNA, W48F/Y72F/H83Q/Y108F-azurin, was obtained from Brian Leigh. Sequences were checked by DNA sequencing. Yuling Sheng executed site-directed mutagenesis for most of the mutants obtained.

Expression of Mutant Proteins

Following previously established protocol,[24,38] the plasmids of the generated mutants were transformed into BL21 (DE3) Single Competent Cells (Novagen) and the bacteria were plated on LB-plates containing the antibiotic ampicillin. Colonies were

selected and inoculated in a 3 mL starter TB culture, supplemented with ampicillin (60 mg/mL). They were shaken for 7–8 hours at 37°C and the result was a cloudy beige solution. This solution was used to inoculate 6 x 1L TB media (70 mg/mL ampicillin) and the flasks were shaken for 20 hours at 37°C.

Cells were isolated by centrifuging the resulting mixture for 10 minutes at 5000 rpm. The cells were resuspended in sucrose solution and centrifuged for 10 min at 5000 rpm. The cells were then resuspended in cold $MgSO_4$ buffer solution and the mixture was allowed to stand for 10 minutes at 4°C, allowing for the bloated cells to lyse. The mixture was then centrifuged for 30 minutes at 10,000 rpm to isolate the lysed cell remains. The yellow supernatant was collected and 1 mL of the protease inhibitor PMF solution/100 mL supernatant was added. The solution was added to enough 1M NaOAc pH = 4.5 solution so that the final concentration of the NaOAc was 0.025 M. $CuSO_4 \cdot 5H_2O$ was added to the solution (0.25 g/50 mL). This mixture was allowed to stand for another week and stored at 4°C, allowing for precipitation of any undesirable protein and any other debris. (Azurin does not precipitate at this pH.) The mixture was then centrifuged at 5,000 rpm at 4°C for 10 minutes and the protein mixture was decanted and concentrated. The blue protein was purified by cation-exchange chromatography (see below) and stored in 25 mM NaOAc at 4°C until use. To check concentration of the protein, $\varepsilon(628\text{ nm}) = 5900\ M^{-1}cm^{-1}$.

Nitration of Tyrosine

Into a 25 mL round-bottom flask, 8.5 mL of a 70 μM solution of azurin in 25 mM NaP_i, pH 8 (though KP_i, pH 7.4 and 7.8 also work), was added. A concentrated stock

solution of azurin of known concentration was usually kept on hand, and was diluted to make this solution each time. The solution was stirred under argon for fifteen minutes, after which 1.5 mL of 1% v/v tetranitromethane/absolute ethanol was added dropwise via syringe in the dark. The reaction was stirred in the dark for 3 hours, after which it was opened up to air and run down a PD-10 desalting column to separate the protein from the tetranitromethane. Conversion can be checked for by exchanging the protein into pH 7.8 buffer and taking a UV-VIS spectrum. The protein was then purified using anion-exchange chromatography prior to being labeled.

Labeling Protein

To label the protein with $[Ru(trpy)(tfmbpy)]^{2+}$, the protocol developed by Dr. Angel Di Bilio was followed with minor modification.

[Ru(trpy)(tfmbpy)Cl]Cl (10 mg, 0.014 mmol) and $AgNO_3$ (5 mg, 0.028 mmol) were added to a 2 dram vial equipped with a stir bar. The mixture was stirred in 1.4 mL water at 70°C for 24 hours. The resulting precipitate was filtered off, yielding a red-orange solution. To this solution, sodium phosphate was added until the pH of the solution was 7.2–7.8. If label precipitated, more water was added. This solution was utilized for the labeling.

Azurin was concentrated as much as it could be, resulting in a solution of 1–5 mM azurin. This solution was distributed among 1.7 mL Eppendorf tubes, 200 μL added to each. 1.3 mL label solution was added to each tube. The tubes were placed in a 37°C heating block and kept in the dark for 10 days.

The protein was isolated from excess label using Amicon Ultra-15 10,000 MWCO tubes (Millipore). Due to the high excess of ruthenium, the sample had to be washed extensively. Removal of the label is important; while the remaining label will be separated from protein on the chelating column (and it is straightforward to remove from the column), it is still preferable to load as little ruthenium onto the column as possible. After washing, the sample was purified by chelating column and cation-exchange chromatography, and, if the sample was a nitrotyrosine mutant, anion-exchange chromatography. The resulting protein is dark olive green in color. Purity was confirmed by mass spectrometry.

To label the protein with rhenium, a protocol outlined by Dr. Jeremiah Miller was used.[13] The only changes made to the protocol were in the workup; PD-10 columns were found to be not necessary. Upon removal from the heating block, the protein was concentrated using Amicon Ultra-15 10,000 MWCO tubes and exchanged into 25 mM NaOAc, pH 4.52. The sample was allowed to stand at 4°C in the dark for 4 days to precipitate remaining rhenium. The sample was removed from the precipitate and washed further. Removal of excess rhenium is crucial in this case; rhenium is extremely difficult to remove from the chelating column. The sample was then purified using the chelating column, cation-exchange chromatography, and, in the cases utilizing nitrotyrosine, anion-exchange chromatography. The resulting protein is blue in color. The purity of the sample was checked with mass spectrometry.

Purification of Azurin

It cannot be emphasized enough that, to obtain pure samples of protein, clean FPLC columns must be used. Columns were always cleaned after the purification of each mutant, and cleaning procedures are detailed below. Column manuals should also be consulted for pepsin protocol when rigorous cleaning is desired (i.e., in times of frequent use, once every three months, in times of low use, once every six months/every time purification is started up again).

Chelating Column

The chelating column used was 5 mL HiTrap chelating column (GE Healthcare). Solutions used for HiTrap are listed below in **Table 2.5**.

Buffer	Composition
Buffer A	20 mM NaP_i, 750 mM NaCl, pH 7.2
Buffer B	20 mM NaP_i, 750 mM NH_4Cl, pH 7.2
Cu solution	100 mM $CuSO_4$
EDTA solution	25 mM NaEDTA, pH 8.8

Table 2.5. Solutions for HiTrap Chelating Column.

A flow rate of 2 to 4 mL/min was utilized in this protocol.

In preparation for protein purification, the column was equilibrated to Buffer A by running 15 mL of the buffer through the column. After equilibration, 2 mL Cu solution was loaded onto the column and the column was allowed to equilibrate. If not enough copper was added, another 1 mL of the Cu solution was loaded. After copper was loaded on the column, 15 mL Buffer B was run through to remove excess copper. 30 mL of Buffer A was run through afterwards to equilibrate the column for protein purification.

The sample loaded onto the column for purification was 200–500 μM, and can always be less; it is not recommended to be much more concentrated, as overloading the column will result in no separation at all. Usually, 1.5 mL of the protein solution was loaded onto the column each run. The sample was loaded onto the column using buffer A.

Separation by chelating column is straightforward; the exposed histidine of the unlabeled protein will bind to the copper of the column and become immobilized. The labeled protein, where the label blocks access to the histidine, will not be deterred and simply pass through the column. The method utilized is summarized below in **Table 2.6**.

mLs into run	% Buffer B
0	0
25	0
27	100
60	100
62	0
75	0

Table 2.6. Method utilized to purify labeled proteins on the chelating column

The copper was stripped off the column after use, or between mutants. To remove the copper, 2 mL EDTA solution was loaded onto the column and the column was allowed to equilibrate. If any copper remained on the column (evident from lingering color on the column), EDTA loading and equilibration was repeated until the copper was removed.

If copper precipitated on the column, removal was achieved by preparing a 10 mL superloop with 10 mL EDTA solution. The solution was slowly loaded onto the column, at a rate of 0.01 or 0.1 mL/min, and was left thus for approximately 8–10 hours.

If rhenium precipitated on the column, a methanol gradient was run, often more than once, to remove the metal. In this method, the flow rate was ~1 mL/min. The column should not remain under 100% methanol for too long.

mLs into run	% Buffer B
0	0
50	100
100	0
130	0

Table 2.7. Methanol gradient method run to remove metal labels from chelating columns and ion-exchange columns. Buffer A is milli Q water, buffer B is HPLC grade methanol.

After use, the column was stored in 20% absolute ethanol/milli Q water.

Cation-Exchange Chromatography

Cation-exchange chromatography was accomplished using a Mono S HR 10/10 column (GE Healthcare). It was executed on proteins after metallation and prior to labeling, proteins after labeling (subsequent to the chelating column), and prior to laser experiments. Solutions used for Mono S are listed below in **Table 2.8**.

Buffer	Composition
Buffer A	25 mM NaOAc, pH 4.52
Buffer B	300 mM NaOAc, pH 4.52
EDTA solution	25 mM NaEDTA, pH 8.8
Acetate solution	2 M NaOAc
Base solution	2 M NaOH
Salt solution	2 M NaCl

Table 2.8. Solutions for Mono S column

The MonoS column used in these studies was a bit old, so the flow rate had to be kept to 1 to 2 mL/min.

In preparation for purification, 30 mL Buffer B was run through the column, then 50 mL Buffer A. The sample loaded onto the column for purification was 200–500 μM, and can always be less; it is not recommended to be much more concentrated, as overloading the column will result in no separation at all. Usually, 1.5 mL of the protein solution was loaded onto the column each run. The sample was loaded onto the column using buffer A.

The active component of the resin of the Mono S column is $–CH_2\text{-}SO_3^-$. Proteins are separated by their cationic charge. Apo azurin usually goes straight through the column. Zinc and copper-substituted azurins usually elute at around 20% Buffer B. The gradient must be proceeded through slowly to achieve separation (**Table 2.9**). For optimal purification, the gradient was held when the blue band of protein started moving on the column, and was continued only when the last of the protein had come off the column.

mLs into run	% Buffer B
0	0
25	0
125	100
145	100
147	0
180	0

Table 2.9. Method utilized to purify azurin on the Mono S column

Every few runs, even if the runs were being done on the same mutant, the column was subjected to a quick cleaning: the column was turned upside down, and equilibrated to milli Q water. The following sequence was then executed: 2 mL load salt solution,

equilibration, 2 mL load acetate solution, equilibration, 2 mL load salt solution, equilibration, 2 mL load base solution, equilibration, 2 mL load salt solution, equilibration. If a different mutant was going to be purified on the column, this cleaning sequence was repeated a few more times.

If orange or yellow residue remained on the column, metal label was contaminating the column. The column was turned upside down and the methanol gradient (delineated above in **Table 2.7**) was executed.

If zinc azurin was being purified, the Mono S column was subjected to at least five 2-mL loads of the EDTA solution to remove any copper on the column, so that copper contamination can be avoided.

When not in use, the column was stored in 20% absolute ethanol/milli Q water.

Anion-Exchange Chromatography

Anion-exchange chromatography was accomplished using a Mono Q HR 10/10 column (GE Healthcare). It was executed on proteins with nitrotyrosine after the nitration reaction and after labeling (subsequent to the chelating column), and prior to laser experiments. Solutions used for Mono Q are listed below in **Table 2.10**.

Buffer	Composition
Buffer A	50 mM DEA, pH 8.8
Buffer B	50 mM DEA, 1 M NaCl, pH 8.8
Acetate solution	2 M NaOAc
Base solution	2 M NaOH
Salt solution	2 M NaCl

Table 2.10. Solutions used for Mono Q

In preparation for purification, 30 mL Buffer B was run through the column, then 50 mL Buffer A. The sample loaded onto the column for purification was 200–500 μM, and can always be less; it is not recommended to be much more concentrated, as overloading the column will result in no separation at all. Usually, 1.5 mL of the protein solution was loaded onto the column each run. The sample was loaded onto the column using buffer A.

The active component of the resin of the Mono Q column is $–CH_2\text{-}N(CH_3)_3^+$. Proteins are separated by their anionic charge. Because the column is being carried out at high pH, if the tyrosine has been nitrated, it should be in the deprotonated form and should be separated on the column from non-nitrated azurin. The non-nitrated azurin usually elutes early, often not even needing Buffer B for elution. Nitrated azurin elutes at around 50% Buffer B. The gradient must be proceeded through slowly to achieve separation (**Table 2.11**). For optimal purification, the gradient was held when the blue-green band of protein started moving on the column, and was continued only when the last of the protein had come off the column.

mLs into run	% Buffer B
0	0
25	0
125	100
145	100
147	0
180	0

Table 2.11. Method utilized to purify azurin on the Mono Q column

Every few runs, even if the runs were being done on the same mutant, the column was subjected to a quick cleaning: the column was turned upside down, and equilibrated to milli Q water. The following sequence was then executed: 2 mL load salt solution,

equilibration, 2 mL load acetate solution, equilibration, 2 mL load salt solution, equilibration, 2 mL load base solution, equilibration, 2 mL load salt solution, equilibration. If a different mutant was going to be purified on the column, this cleaning sequence was repeated a few more times.

If orange or yellow residue remained on the column, metal label was contaminating the column. The column was turned upside down and the methanol gradient (delineated above in **Table 2.7**) was executed.

When the column was not in use, it was stored in 20% absolute ethanol/milli Q water.

Electrochemical Measurements

Measurements were made with the help of Brian S. Leigh. Measurements were made on a Model 660 Electrochemical Workstation (CH-Instrument, Austin, TX) in a two-compartment cell with a glassy carbon working electrode, a platinum wire counter electrode, and a silver/silver nitrate reference electrode. 100 mM tetrabutylammonium tetrafluoroborate was prepared in dry degassed acetonitrile as electrolyte. Measurements were carried out at room temperature.

Circular Dichroism Measurements

CD spectra were taken on an Aviv 62ADS spectropolarimeter (Aviv Associates, Lakewood, NJ). Measurements were carried out in a 1 mm cuvette at room temperature. Accompanying UV-VIS measurements were also measured with the 1 mm cuvette. Data was recorded between 190 nm and 260 nm with a band-pass of 1.5 nm.

Laser Spectroscopy & Analysis

Time-resolved emission and absorbance measurements were made on custom-made laser setup Nanosecond-I in the Beckman Institute Laser Resource Center. The laser setup has already been thoroughly outlined and explained elsewhere,[24] so only basic details are summarized here. A frequency-tripled Nd:YAG laser from Spectra-Physics emits 355 nm pulses, 10 ns in duration. Measurements carried out on rhenium systems were excited by this laser. Measurements carried out on the ruthenium systems were excited by laser light from a Spectra-Physics MOPO, which was pumped by the Nd:YAG. The laser power was adjusted using a quarter-wave plate so that the laser light exciting the sample had a power of 1 mJ/pulse. For the most part, transient absorption was probed for with white light from a xenon arc lamp, which was run in a continuous mode, or set to generate 500 μs pulses of brighter light. Transient absorption measurements at 632.8 nm were made using a HeNe laser probe to limit the collection of emission from the label at that wavelength.

Sample Preparation

25 to 50 μM samples of protein in freshly made 25 mM KP_i buffer, in the pH range 7.0 to 7.8, were added to 1 cm path length cuvettes and degassed by fifteen quick pump purges, stirring under argon for fifteen minutes, and another quick fifteen pump purges. Generation of bubbles in the sample during the degassing was unavoidable, but was kept to a minimum by careful watching of the sample.

To reduce the copper center for certain measurements, sodium dithionite was added until the blue color of the sample disappeared. This sample was washed with

buffer to remove excess dithionite; if the blue reappeared, more dithionite would be added and washing would be repeated. The sample was then added to the cuvette and degassed as described above.

To reduce the copper center in samples with nitrotyrosine residues, dithionite could not be used; the dithionite reduced the nitrotyrosine to aminotyrosine. Instead, the green sample was placed in the cuvette with a stir bar and a small scrap of Pt mesh (1 mm by 3 mm) and the solution was deaerated and put under hydrogen gas for 15 minutes, deaerated and put under hydrogen gas for another 4 to 8 hours (the reaction time depended on which mutant was being reduced). It is important that the stir bar agitates the scrap of Pt. Because the H_2/Pt reduction, as well as reducing the copper, also reduces any oxygen present into water, no further degassing was necessary, though the sample was usually put under argon for laser experiments.

Data Analysis

The data obtained from the Nanosecond-I laser setup was analyzed using Igor Pro 5.01 (WaveMetrics, Inc., Lake Oswego, OR). Data was fit with a non-linear least-square algorithm to function with single (n=1), double (n=2), or triple (n=3) exponential decays (**Equation 2.1**). The reported τ values are calculated from the k_n obtained from the fit (**Equation 2.2**).

$$I(t) = c_0 + \sum_n c_n e^{-k_n t} \quad \text{Eq. 2.1}$$

$$\tau_n = \frac{1}{k_n} \quad \text{Eq. 2.2}$$

2.6 REFERENCES

(1) Sutherland, I. W.; Wilkinson, J. F. *J. Gen. Microbiol.* **1963**, *30*, 105–112.

(2) Antonini, E.; Finazzi-Agro, A.; Avigliano, L.; Guerrieri, P.; Rotilio, G.; Mondovi, B. *J. Biol. Chem.* **1970**, *245*, 4847–4849.

(3) Solomon, E. I.; Hare, J. W.; Dooley, D. M.; Dawson, J. H.; Stephens, P. J.; Gray, H. B. *J. Am. Chem. Soc.* **1980**, *102*, 168–178.

(4) Adman, E. T. *Adv. Protein Chem.* **1991**, *42*, 145–197.

(5) Gray, H. B.; Malmstrom, B. G.; Williams, R. J. P. *J. Biol. Inorg. Chem* **2000**, *5*, 551–559.

(6) Solomon, E. I.; Randall, D. W.; Glaser, T. *Coordin. Chem. Rev.* **2000**, *200-202*, 595–632.

(7) Pascher, T.; Karlsson, B. G.; Nordling, M.; Malmstrom, B. G.; Vanngard, T. *Eur. J. Biochem.* **1993**, *212*, 289–296.

(8) Chang, T. K.; Iverson, S. A.; Rodrigues, C. G.; Kiser, C. N.; Lew, A. Y. C.; Germanas, J. P.; Richards, J. H. *P. Natl. Acad. Sci. USA* **1991**, *88*, 1325–1329.

(9) Langen, R.; Chang, I. J.; Germanas, J. P.; Richards, J. H.; Winkler, J. R.; Gray, H. B. *Science* **1995**, *268*, 1733–1735.

(10) Langen, R.; Colon, J. L.; Casimiro, D. R.; Karpishin, T. B.; Winkler, J. R.; Gray, H. B. *J. Biol. Inorg. Chem* **1996**, *1*, 221–225.

(11) Crane, B. R.; Di Bilio, A. J.; Winkler, J. R.; Gray, H. B. *J. Am. Chem. Soc.* **2001**, *123*, 11623–11631.

(12) Wehbi, W. A., California Institute of Technology, 2003.

(13) Miller, J. E., California Institute of Technology, 2003.

(14) Harriman, A. *J. Phys. Chem.* **1987**, *91*, 6102–6104.

(15) Magnuson, A.; Frapart, Y.; Abrahamsson, M.; Horner, O.; Akermark, B.; Sun, L.; Girerd, J. J.; Hammarstrom, L.; Styring, S. *J. Am. Chem. Soc.* **1999**, *121*, 89–96.

(16) Sjodin, M.; Styring, S.; Akermark, B.; Sun, L.; Hammarstrom, L. *J. Am. Chem. Soc.* **2000**, *122*, 3932–3936.

(17) Remers, W. A. In *Indoles, Part One*; Houlihan, W. J., Ed.; Wiley-Interscience: New York City, 1972; Vol. 25, 1–226.

(18) Leigh, B.S. (*unpublished work*).

(19) Riordan, J. F.; Sokolovsky, M.; Vallee, B. L. *J. Am. Chem. Soc.* **1966**, *88*, 4104–4105.

(20) Sokolovsky, M.; Riordan, J. F.; Vallee, B. L. *Biochemistry* **1966**, *5*, 3582–3589.

(21) Riordan, J. F.; Sokolovsky, M.; Vallee, B. L. *Biochemistry* **1967**, *6*, 358–361.

(22) Bruice, T. C.; Gregory, M. J.; Walters, S. L. *J. Am. Chem. Soc.* **1968**, *90*, 1612–1619.

(23) Riordan, J. F.; Vallee, B. L.; Hirs, C. H. W.; Serge, N. T. In *Methods in Enzymology*; Academic Press: 1972; Vol. 25, 515–521.

(24) Miller, J.; Di Bilio, A,; Wehbi, W.A.; Green, M.T.; Museth, A.K.; Richards, J.H.; Winkler, J.R.; Gray, H.B. *BBA Bioenergetics* **2004**, *1655*, 59–63.

(25) Winkler, J. R.; Gray, H. B. *Chem. Rev.* **1992**, *92*, 369–379.

(26) Mines, G. A.; Bjerrum, M. J.; Hill, M. G.; Casimiro, D. R.; Chang, I. J.; Winkler, J. R.; Gray, H. B. *J. Am. Chem. Soc.* **1996**, *118*, 1961–1965.

(27) Di Bilio, A. J.; Hill, M. G.; Bonander, N.; Karlsson, B. G.; Villahermosa, R. M.; Malmstrom, B. G.; Winkler, J. R.; Gray, H. B. *J. Am. Chem. Soc.* **1997**, *119*, 9921–9922.

(28) Di Bilio, A. J.; Dennison, C.; Gray, H. B.; Ramirez, B. E.; Sykes, A. G.; Winkler, J. R. *J. Am. Chem. Soc.* **1998**, *120*, 7551–7556.

(29) Sokolovsky, M.; Harell, D.; Riordan, J. F. *Biochemistry* **1969**, *8*, 4740–4745.

(30) Johnson, E. C.; Sullivan, B. P.; Salmon, D. J.; Adeyemi, S. A.; Meyer, T. J. *Inorg. Chem.* **1978**, *17*, 2211–2215.

(31) Durham, B.; Pan, L. P.; Long, J. E.; Millett, F. *Biochemistry* **1989**, *28*, 8659–8665.

(32) Durham, B.; Pan, L. P.; Hahm, S.; Long, J.; Millett, F. *Adv. Chem. Ser.* **1990**, 181–193.

(33) Arjara, G. (*unpublished results*).

(34) Sullivan, B. P.; Calvert, J. M.; Meyer, T. J. *Inorg. Chem.* **1980**, *19*, 1404–1407.

(35) Takeuchi, K. J.; Thompson, M. S.; Pipes, D. W.; Meyer, T. J. *Inorg. Chem.* **1984**, *23*, 1845–1851.

(36) Chan, K. S.; Tse, A. K. S. *Synthetic Commun.* **1993**, *23*, 1929–1934.

(37) Sullivan, B. P.; Salmon, D. J.; Meyer, T. J. *Inorg. Chem.* **1978**, *17*, 3334–3341.

(38) Sheng, Y. (*unpublished results*).

CHAPTER THREE

Dramatic Acceleration of Electron Flow through Azurin

3.1 ABSTRACT

Re(dmp)$(CO)_3$(H124)/W122/Az(Cu^+) exhibits electron transfer kinetics that are much faster than expected for single-step electron tunneling. We have structurally characterized the system; the orientation of the tryptophan with respect to the phen ligand of the label is suggestive of a pseudo-stacking interaction that may encourage rapid electron transfer from the amino acid to electronically excited rhenium. The change in CO-stretching frequencies throughout the process also allows characterization of ultrafast events using time-resolved infrared spectroscopy. These findings and the characterization of excited rhenium at visible wavelengths with picosecond time resolution have allowed for generation of a model that accounts for the electron transfer events in this system.

3.2 INTRODUCTION

The System

Three β-strands extend from the ligands that coordinate azurin's copper center. The system discussed in this chapter and the next is on the Met121 arm of azurin (**Figure 3.1**). Coordination of the metal is at the 124 site, which is approximately 19 Å away from the copper site. A tryptophan is installed at the 122 site.

Unlike in previously studied tryptophan systems,[1] once oxidized, the tryptophan radical cation was not deprotonated; rather, the subsequent electron transfer from the copper to the radical cation was faster! The two-step electron transfer utilizing this tryptophan radical cation exhibited kinetics much faster than that expected for single-step tunneling. This system is the first metal-modified metalloprotein to empirically demonstrate hopping.

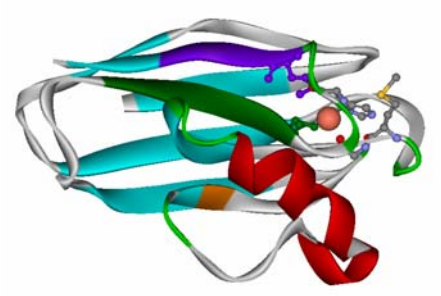

Figure 3.1. *Pseudomonas aeruginosa* azurin (PDB code: 1AZU). The Met121 arm is highlighted in purple.

Chapter Outline

Because this system is the first to exhibit such kinetics, it has been thoroughly characterized in collaboration with a number of laboratories. This chapter will discuss results obtained from these collaborations, as they all contributed in establishing the current model for the electron transfer events of the system. The system has been studied using time-resolved UV-VIS spectroscopy with both 10 ns and 10 ps lasers, time-resolved IR spectroscopy with a 150 fs laser, and structurally characterized by x-ray crystallography. Temperature studies were carried out to assess the thermodynamics of the initial electron transfer between the tryptophan and the rhenium excited state. The results are discussed in the order they were obtained.

Three mutants were prepared for these studies: Re124/W122/Az(Cu^{2+}), Re124/Y122/Az(Cu^{2+}), and Re124/F122/Az(Cu^{2+}). A. Katrine Museth was the first to express and isolate the mutant; Malin Abrahamsson labeled the protein.

A simplified schematic of the events described in the following section is presented below. (**Scheme 3.1**).

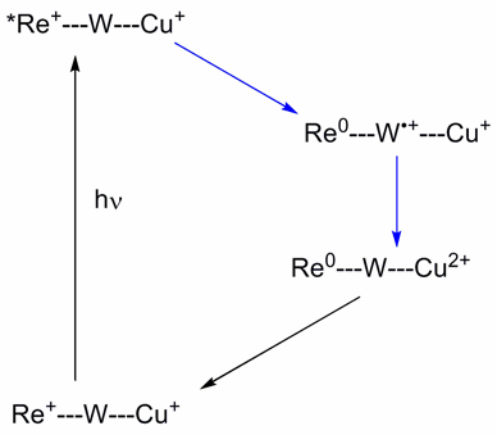

Scheme 3.1. Events after sample excitation. The blue arrows depict the multistep tunneling event.

3.3 RESULTS & DISCUSSION

Proteins for these studies were made using the protocols described in **Chapter 2**. It should be observed here that the rhenium label oxidation states in many of the schemes utilized in this chapter are simplifications: "*Re^{+}" is in actuality *$Re^{2+}(dmp^{\bullet-})(CO)_3$, and that "$Re^{0}$" is in actuality $Re^{+}(dmp^{\bullet-})(CO)_3$.[2]

Time-Resolved UV-VIS Spectroscopy with a 10 ns Laser

Re124/W122/Az(Cu^{+}) was excited with a 10 ns laser. Within 50 ns of sample excitation, formation of Cu^{2+} was observed (**Figure 3.2**, black trace). This is much faster than expected for single-step electron tunneling over a distance ~19 Å! The back ET

reaction can also be tracked; Re^{0} (500 nm, **Figure 3.2**, red trace) and Cu^{2+} kinetics both indicate that it occurs in about 3 μs.

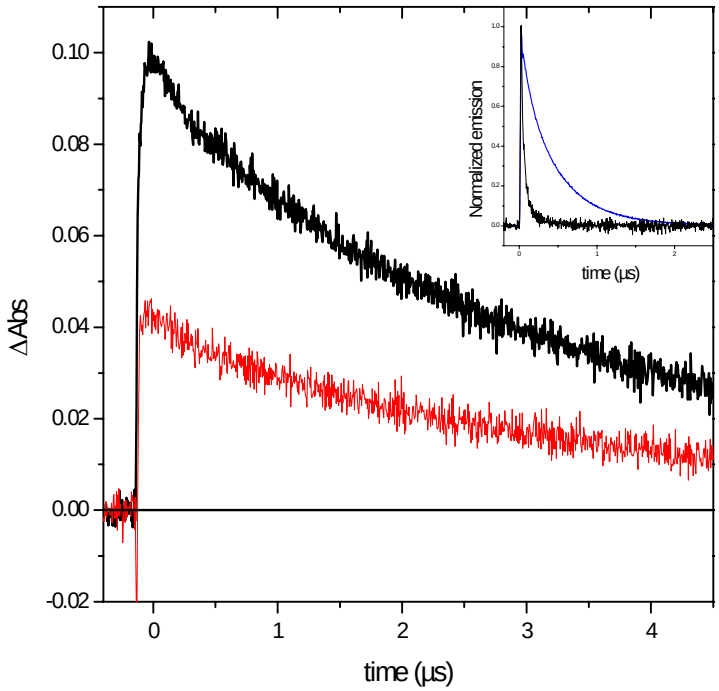

Figure 3.2. Transient absorption of Re124/W122/Az(Cu^{+}). 60 μM Re124/W122/Az(Cu^{+}) in 50 mM KPi pH 7.16. λ_{ex} = 355 nm, λ_{obs} = 628.5 nm (black) and 500 nm (red). Inset: Fluorescence decay at λ_{em} = 595 nm for Re124/W122/Az(Cu^{+}) (black) and Re124/F122/Az(Cu^{+}) (blue)[3]

The quenching of the excited state $*Re^{+}$ is not observed in either Re(H124)/F122/Az(Cu^{+}) or Re(H124)/Y122/Az(Cu^{+}), substantiating the hypothesis that the tryptophan is likely responsible for these enhanced kinetics. Additionally, Cu^{2+} was not formed when Re124/F122/Az(Cu^{+}) or Re124/Y122/Az(Cu^{+}) were excited in similar conditions.

Structural Characterization

A comparison of the x-ray crystal structures of the rhenium-labeled W122 mutant and the rhenium-labeled wild-type K122 variant (**Figure 3.3**) demonstrates a curious and

interesting feature: in the W122 variant (**Figure 3.3B**), the rhenium is oriented such that the dmp ligand is in pseudo π-stacking interaction with the tryptophan residue. The ligand and aromatic ring are within van der Waals contact (~4 Å), which could serve to enhance electron transfer through the tryptophan in an efficient manner. The crystal structure also establishes the distance between the rhenium and copper atoms as 19.4 Å.

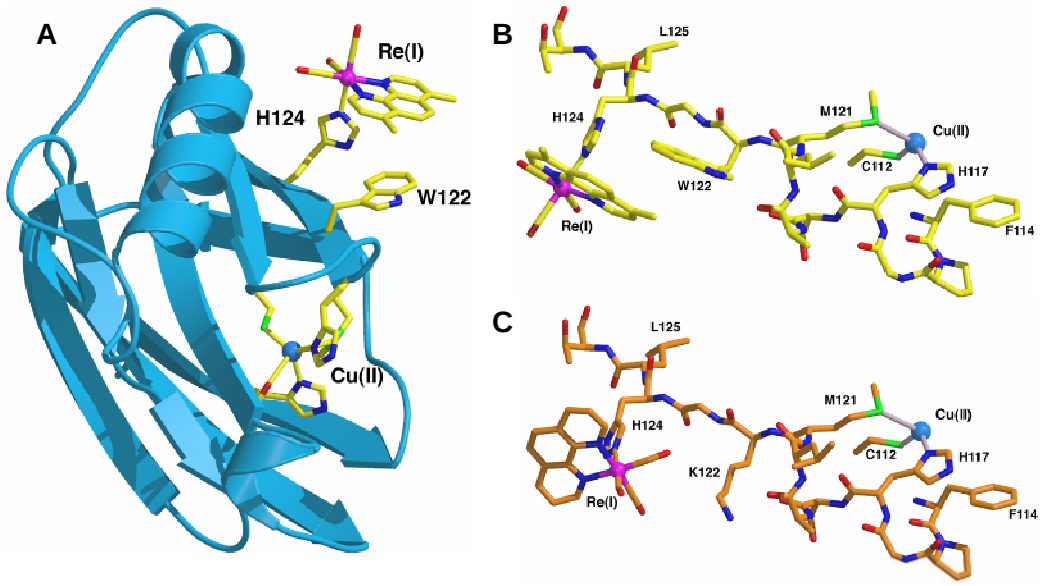

Figure 3.3. Crystal structures of Re-labeled azurins.[3] **A.** Full structure of Re124/W122/Az (Cu^{2+}). **B.** Zoom of area of interest: the electron transfer pathway. **C.** The same area of interest in Re124/Az(Cu^{+}).[3,4]

Time-Resolved IR Spectroscopy

The IR-active CO stretching frequencies of the rhenium ligand offer another mechanism by which to monitor electron transfer events. Samples were excited with a 150 fs laser and monitored using infrared detectors. These ultrafast measurements garnered information on the early events right after photoexcitation (**Figure 3.4**).

The ground state rhenium label's carbonyl stretching frequencies at 1920 and 2030 cm^{-1} are bleached immediately after the excitation. New absorbances instantly

appear and are fully developed at ~1960, 2012, and ~2040 cm^{-1}, which are attributed to the $*^3$Re excited state (denoted MLCT in **Figure 3.4**).[2] The $*^3$Re excited state absorbances decay with several time constants in the range of 10 ps to 50 ns (measured at 1950–1060 cm^{-1}) and the bleach recovers with ~20 ns and ~3 μs kinetics. A small population of Re^0 (denoted ET in **Figure 3.4**) is present within 1 picosecond after excitation. This population continues to grow over time in three phase with time constants of 10 ps, 300–400 ps, and 20–30 ns, followed by a 3 μs decay.

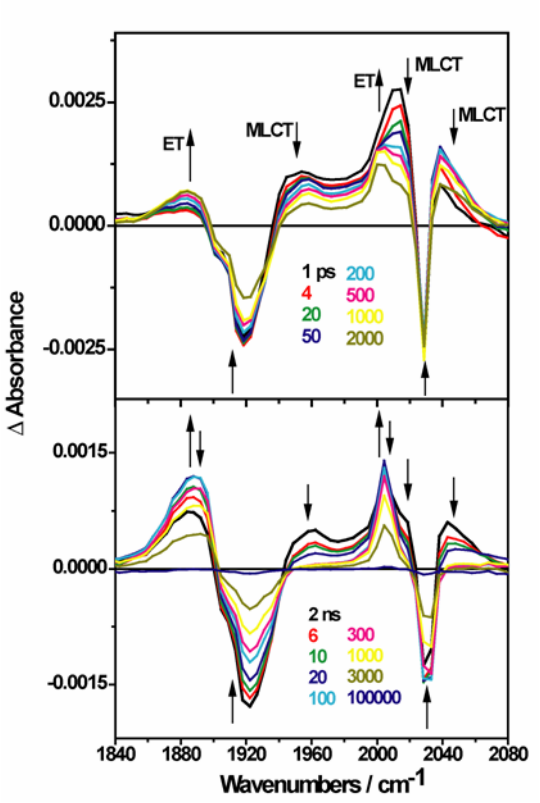

Figure 3.4. Difference time-resolved IR spectra of Re124/W122/Az(Cu^+). Measured in D_2O, pD 7.0 phostphate buffer at selected time delays after 400 nm, ~150 fs excitation. Upper panel: picoseconds. Lower panel: nanoseconds

The measurements made on the other mutants indicated that the tryptophan was absolutely essential for the rapid formation of Re^0: the reduced complex also appeared

when Cu^{2+}- and Zn^{2+}-substituted variants of the mutant were excited, but did not form in studies of Re124/Y122/Az(Zn^{2+}).

Temperature Studies

Because the driving force of the W122 to $*Re^{+}$ electron transfer seemed to be quite low, it was suspected that at lower temperatures, multistep tunneling would be shut down, as the activation barrier would no longer be achieved (**Figure 1.1**). Temperature studies were conducted to confirm this hypothesis.

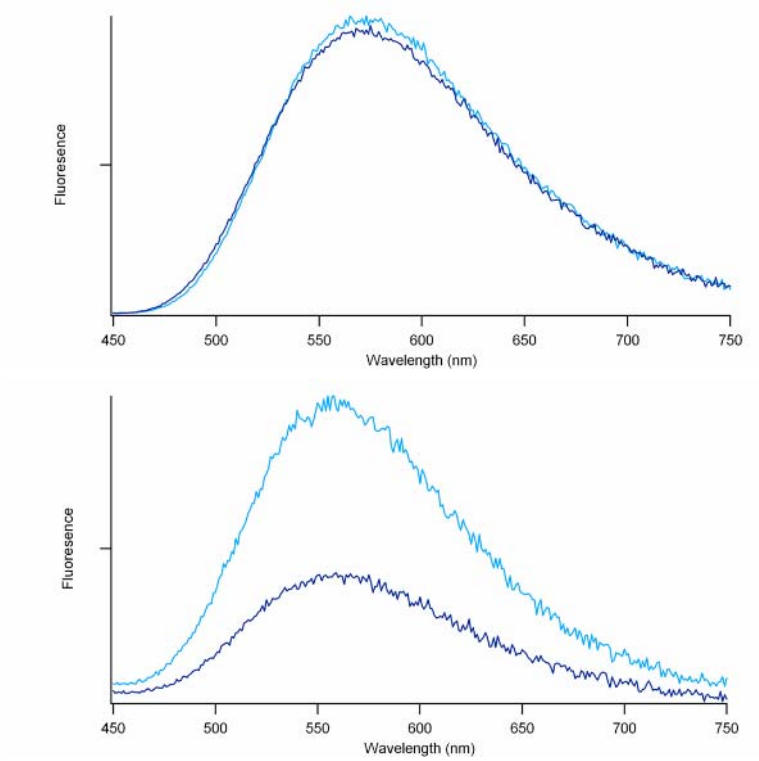

Figure 3.5. Fluorescence spectra of Re (top) and Re124/W122/Az(Cu^{+}) (bottom) at 25°C (dark blue) and -20°C (light blue). ~125 μM Re, 65% glycerol/25 mM KP_i, pH 7.4. 50 μM Re124/W122/Az(Cu^{+}), 65% glycerol/25 mM KP_i, pH 7.4. λ_{ex} = 355 nm

The temperature studies were conducted at room temperature and -20°C, which was the lowest the temperature bath would allow. Glycerol was added to samples as a

cryo-protectant. It can be seen that the temperature change has little effect on the fluorescence of the label (**Figure 3.5, top**). However, for the metal-labeled protein, the fluorescence increases with the decrease in temperature (**Figure 3.5, bottom**). This increase in fluorescence is a sign that the quenching due to the tryptophan is not occurring as much, presumably because the activation barrier is not as easily accessed as it was at room temperature.

Time-Resolved UV-VIS Spectroscopy with a 10 ps Laser

Time-resolved UV-VIS spectroscopy was carried out at faster time scales using a 10 ps laser to furnish more information on the system: fluorescence of the excited state $*Re^{+}$ was monitored with a streak camera.

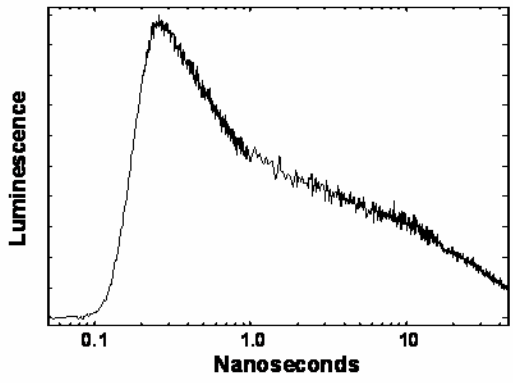

Figure 3.6. Time-resolved emission of Re124/W122/Az(Cu^{+}). 60 μM Re124/W122/Az(Cu^{+}), 50 mM KP_i, pH 7.16. (λ_{ex} = 355 nm, λ_{obs} = 500 nm)

Analysis of this data revealed a biphasic excited-state decay pattern (τ_1 = 400 ps, τ_2 = 26 ns) (**Figure 3.6**). A protocol was developed to deconvolve the instrument response function from the data to garner more accurate fits; the protocol is described below in **Section 3.5**.

The Model

The data obtained from transient absorption, emission, and infrared measurements were fit to **Scheme 3.2** to garner the elementary rate constants for each step of the mechanism. It is gratifying when the data sets for three different spectroscopic methods all fit very well to the same model.

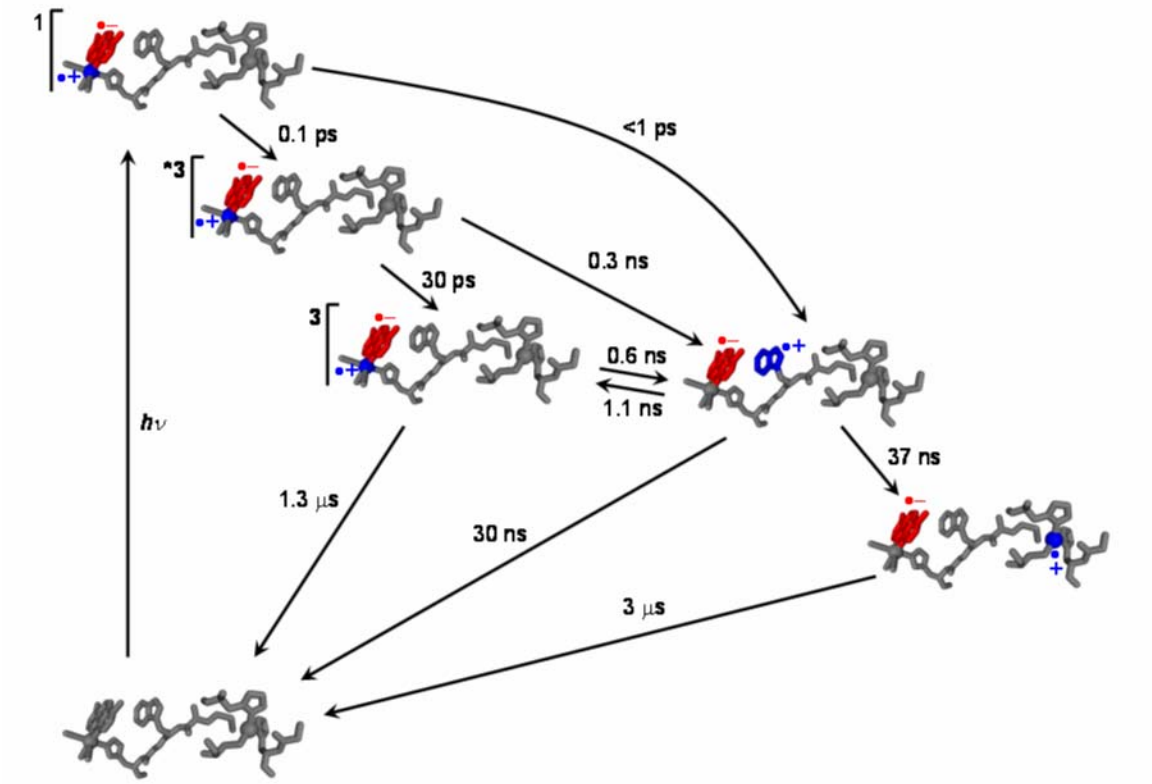

Scheme 3.2. Kinetics model of photoinduced electron transfer in Re124/W122/Az(Cu^+). Light absorption produces electron (red) and hole (blue) separation in the MLCT-excited *Re^+. Migration of the hole to copper *via* W122 is complete in less than 50 ns. Charge recombination proceeds on the microsecond timescale.[3] The *$Re^{2+}(dmp^{\bullet-})(CO)_3$ is the more accurate depiction of what has been simplified as "*Re^+", and $Re^+(dmp^{\bullet-})(CO)_3$ is the more accurate depiction of the "Re^0" state.

Upon excitation, the $*^1Re^+$ excited state is generated, which undergoes an extremely fast (~150 fs) intersystem crossing to a triplet excited state $*^3Re^+$. Subpicosecond generation of Re^0 is attributable to electron transfer from the W122 to $*^1Re^+$. The ~10 ps formation of Re^0 is attributed to a parallel relaxation and reduction of the $*^3Re^+$ excited state by tryptophan, based on previous work done on other rhenium-modified azurins.[2] No evidence for Re^0 formation was observed in proteins containing F122 or Y122 mutations; the electron source for these reductions must be the indole of W122. The ~400 ps kinetics phase is attributed to equilibration between $^3Re^+$ state and Re^0-$W^{\bullet+}$ and the ~20 ns process corresponds to reduction of $W^{\bullet+}$ by the Cu^+ to generate Cu^{2+}.

The analysis of the reaction kinetics reveals that the reduction potential of $*Re^+$ is just 14 mV greater than that of $W122^{\bullet+/0}$. This is sufficient for very rapid electron transfer between the adjacent dmp ligand and indole ring. This electron transfer does not occur in the tyrosine and tryptophan mutants because their reduction potentials are more than 200 mV above the the reduction potential of $*Re^+$ ($E°(*Re^{+/0}) = 1.4$ V *v.* NHE[5]).

Hopping Map

A true confirmation of the multistep tunneling mechanism was found through the construction of a hopping map (**Figure 3.7**)

Utilizing the distances from the crystallographic data, previously determined λ values, and **Equation 1.1**, a contour map was constructed, depicting the change in overall electron transfer rates if the driving forces of the overall process (x-axis in **Figure 3.7**) and first tunneling step (y-axis in **Figure 3.7**) were varied. The black dot on the graph

represents the potentials of Re(dmp)$(CO)_3$(H124)/W122/Az(Cu^+) system; the calculated value for the process, 87 ns, is within the same order of magnitude of the observed value 37 ns, thereby substantiating our hypothesis that multistep electron tunneling is occurring. Additionally, the two-step hopping is 250 times faster than the calculated single-step tunneling mechanism for the distance and driving force of the Re(dmp)$(CO)_3$(H124)/W122/Az(Cu^+) system.

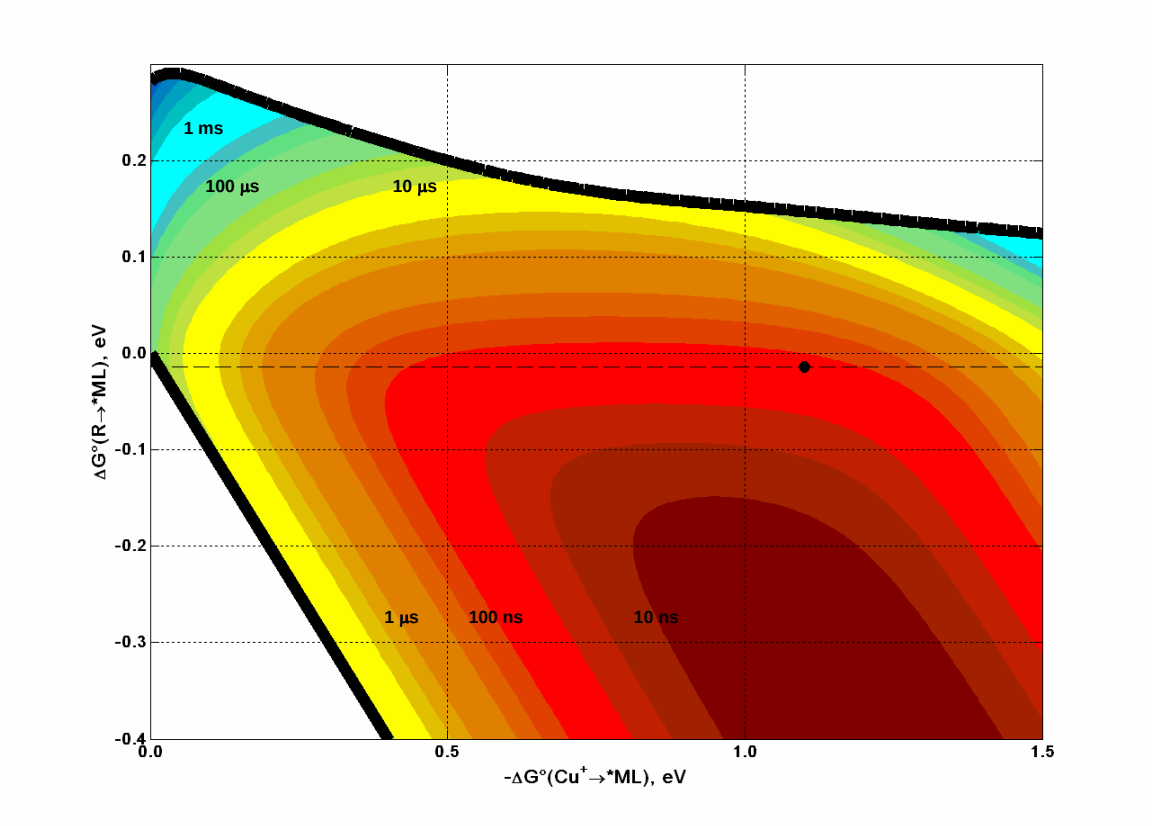

Figure 3.7. Two-step hopping map for electron tunneling through Re-modified azurin. Colored contours reflect electron transfer timescales as functions of the driving forces for the first tunneling step (R→*ML) and the overall electron transfer (Cu^+→*ML). The black dot is located at the coordinates for Re(dmp)$(CO)_3$(H124)/W122/Az(Cu^+). The arrow illustrates the transport time expected if the $Cu^{2+/+}$ potential were high enough to oxidize water.

3.4 CONCLUSIONS

The protein system Re(dmp)$(CO)_3$(H124)/W122/Az(Cu^+) exhibits electron transfer rates that are much faster than expected for a single-step tunneling mechanism. The system was structurally characterized and the kinetics were studied using time-resolved UV-VIS and IR spectroscopies. A multistep tunneling scheme was proposed and the model was fit to the data; the data were all in excellent agreement with the model. Furthermore, a hopping map was constructed to confirm that the theory behind multistep tunneling could accurately predict the electron transfer kinetics of this system. The calculated value was within an order of magnitude of the observed, and the theory is thereby supported by these studies.

3.5 EXPERIMENTALS

Rhenium-labeled proteins were prepared as described in **Chapter 2**.

Collaborators

The substantial amount of data accumulated for this project would not have been accomplished without the help of many collaborators. Crystollographic work was accomplished with Jawahar Sudhamsu and Prof. Brian R. Crane at Cornell University. Time-resolved IR spectroscopy was executed with Ana Maria Blanco-Rodriguez and Prof. Antonín Vlček, Jr. at Queen Mary, University of London, as well as Drs. Kate L. Ronayne and Michael Towrie at the STFC Rutherford Appleton Laboratory. Fits and calculations of the complex systems were done in corroboration with Dr. Jay R. Winkler of the Beckman Institute at Caltech.

Temperature Studies

Temperature studies were carried out on a Fluorolog Model FL3-11 fluorometer equipped with a Hamamatsu R928 PMT and a temperature bath. Samples were prepared and degassed in 1-cm-path-length cuvettes in 65% glycerol/25 mM KP_i, pH 7.4. The sample was excited at 355 nm.

Laser Spectroscopy with a 10 ps Laser

Time-resolved UV-VIS spectroscopy on ultrafast time scales was executed on a customized setup in the Beckman Institute Laser Resource Center. The sample was excited using the third harmonic of a 10 picosecond Nd:YAG laser (Spectra-Physics) at 355 nm (76 MHz, ≤ 5 mW power) and the emission was detected at 90° to the excitation beam using a picosecond streak camera (Hamamatsu C5680). Magic angle conditions were used in the measurements. Rhenium fluorescence was selected with a 420 nm long-pass filter (LPF). The streak camera was used in photon counting mode. Samples were prepared and degassed in 1-cm-path-length cuvettes in the same manner as samples were prepared for laser spectroscopy measurements executed on Nanosecond-I.

Data Analysis

Data obtained from the picosecond laser system was analyzed using MATLAB (The MathWorks). Streak camera images were converted to text files for analysis using the program streak_a.m. A non-negative least-square algorithm was used to fit the data to exponential decays (**Equation 2.1**) (Program max_ent.m). MATLAB programs that were used for data analysis are available in the **Appendix**.

There was concern over whether or not the kinetics observed were too fast for the instrument to detect. Therefore, instrument response was measured and used to deconvolute the data for better fits.

The instrument response was measured by scattering light into milli Q water. Unfortunately some fluorescence was still detected, so the instrument response data was fitted to garner better results for the protocol. The curve was asymmetric, and so was split in half and each half was fit to a Gaussian function (**Figure 3.8**). This function was used as the instrument response curve for the deconvolution protocol.

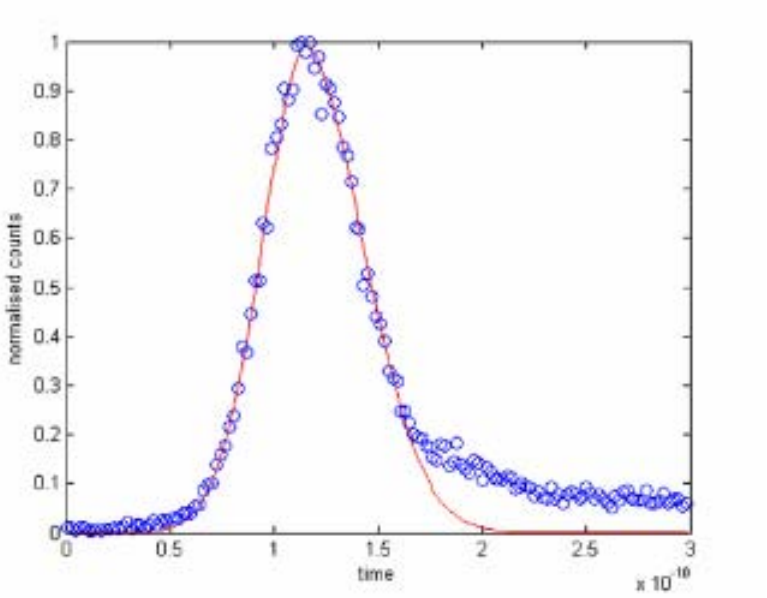

Figure 3.8. Instrument response data fitted to Gaussian functions (red). Data (blue dots) were split in half from the maximum. The early half was fit in its entirety to a Gaussian function. The second half was truncated when it appeared that the fluorescence of the sample was interfering with the response curve.

To convolve the instrument response curve to a theoretical function, MATLAB's 'fminsearch' function was utilized, for which a functions 'crystal' and 'multiexp_conv' were written.

Function 'crystal' took initial guesses of variables, a response vector, an experimental data vector, and a time vector.

Given the initial parameters, function 'crystal' computed a theoretical curve across the given time vector, and then utilized convolved the theoretical curve to a response curve 'O'. O was compared to the experimental data vector and chi square was computed.

MATLAB's 'fminsearch' function changes variables of a function until it minimizes its output value. For this case, the variables changed were summarized in a vector, pram. The 'options' had to be changed to increase the number of iterations to be done; the universal minimum was desired, not a local one.

The function was called with the command:

```
>y=fminsearch(@(x) crystal(x,R,E,t),pram,options)
```

The values for the optimized pram were recalled by running function crystal on pram after the minimization was completed. An example of the output function is shown in **Figure 3.9**.

The fitting procedure discussed here was used as a diagnostic method to check whether or not a more rigorous deconvolution program would need to be written for accurate fitting. The complete protocol undertaken to fit data from all spectroscopic measurements made requires extensive experience and understanding of MATLAB; further fitting was done in heavy collaboration with Dr. Jay R. Winkler.

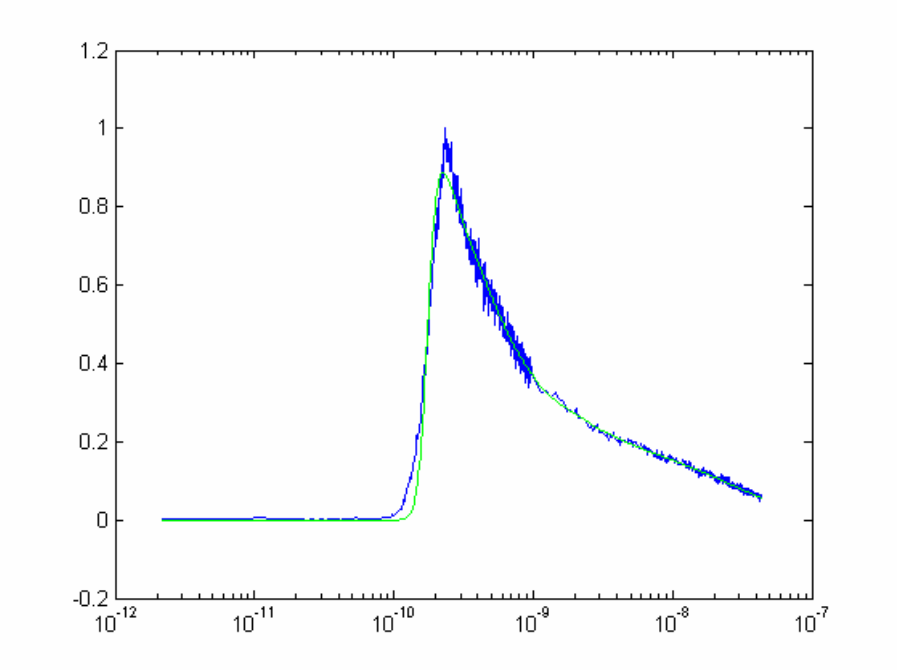

Figure 3.9. A function generated using 'fminsearch' and function 'crystal'. Fit to data collected on Re124/W122/Az(Cu^{+}). Y-axis is normalised emission. Blue is the data to be fitted. Light green curve is the O(t) that was computed to have the lowest chi-square value.

3.6 REFERENCES

(1) Miller, J. E., California Institute of Technology, 2003.

(2) Blanco-Rodriguez, A. M.; Busby, M.; Gradinaru, C.; Crane, B. R.; DiBilio, A. J.; Matousek, P.; Towrie, M.; Leigh, B. S.; Richards, J. H.; Vlcek, A.; Gray, H. B. *J. Am. Chem. Soc.* **2006**, *128*, 4365–4370.

(3) Shih, C.; Museth, A. K.; Abrahamsson, M.; Blanco-Rodriguez, A. M.; Di Bilio, A. J.; Sudhamsu, J.; Crane, B. R.; Ronayne, K. L.; Towrie, M.; Vlcek, A., Jr.; Richards, J. H.; Winkler, J. R.; Gray, H. B. *accepted for publication into Science*.

(4) Sudhamsu, J.; Crane, B. (*personal communication*).

(5) Connick, W. B.; Di Bilio, A. J.; Hill, M. G.; Winkler, J. R.; Gray, H. B. *Inorg. Chim. Acta* **1995**, *240*, 169–173.

CHAPTER FOUR

Controlling Electron Hopping

4.1 ABSTRACT

Systematic perturbations were made to the working hopping system Re(dmp)$(CO)_3$(H124)/W122/Az(Cu^+). All together, eight metal-modified azurins were made for the studies. Ruthenium and rhenium labels are attached to H124 or H126; tryptophan and 3-nitrotyrosine are installed at the 122 site. More often than not, electron transfer is observed between the amino acid and the metal label. However, subsequent electron transfer from the copper to the oxidized amino acid does not occur, except in the case of one mutant, Re126/W122/Az(Cu^+). The electron transfer kinetics observed on this system indicate that a second hopping system has been discovered.

4.2 INTRODUCTION

The System

With the working hopping system Re(dmp)$(CO)_3$(H124)/W122/Az(Cu^+) in hand, attention turned towards: 1) installing a nitrotyrosine at the 122 site and observing hopping through the tyrosine analog; 2) perturbing the pseudo-stacking interaction that had been observed between the W122 and the dmp ligand of the rhenium (**Chapter 3**, Structural Characterization); and 3) challenging the robustness of the working hopping system by changing the driving forces of the first electron transfer reaction and the overall process. To that end, the proteins studied were still on the Met121 arm; labeling

was done on either the 124 site or the 126 site, which is estimated to be another 5 Å away from the copper center. A high-potential ruthenium label was used to perturb the reduction potential of the metal label and 3-nitrotyrosine was also installed in the 122 site to perturb the potential at the amino acid site.

Chapter Outline

The chapter is divided into two components. In the first, the metal labels and intermediates are changed, keeping the two sites constant: the metal label is installed at H124 and the intermediate amino acid is installed at the 122 site. In the second part of the chapter, the label is moved two amino acid residues farther down the Met121 arm, increasing distance between the two metal and label another ~5 Å.

4.3 RESULTS AND DISCUSSION

The Importance of Reduction Potentials in Hopping

The proteins discussed in this section include Ru124/W122/Az(Cu^{2+}), Ru124/W122/Az(Zn^{2+}), Ru124/F122/Az(Zn^{2+}), Ru124/$YNO_2$122/Az(Cu^{2+}), and Re124/$YNO_2$122/Az(Cu^{2+}). These proteins were prepared using the methods described in **Chapter 2**. Zn^{2+}-substituted azurins are used for control measurements; Zn^{2+} does not react, and so any electron transfer observed in these systems should be between the aromatic amino acid residue and the metal label.

Ru124/W122/Az(Cu^{2+})

In the first system discussed, a high-potential ruthenium dye $[Ru(trpy)(tfmbpy)]^{2+}$ replaces the Re at the 124 site.

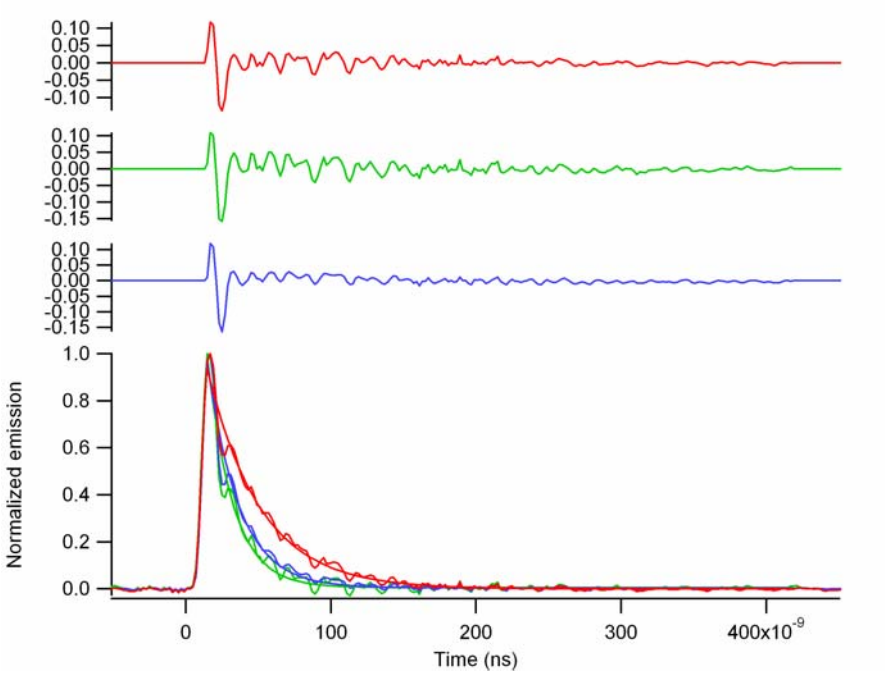

Figure 4.1. Time-resolved emission of Ru124/W122/Az(Cu^{2+}) and (Cu^{+}). 10 μM Ru124/W122/Az(Cu^{2+}), 25 mM KP_i, pH 7.14. λ_{ex} = 490 nm, λ_{em} = 700 nm. Red trace is Ru model compound, [Ru(trpy)(tfmbpy)(im)]$(PF_6)_2$ in 25 mM KP_i, pH 7.16, τ = 37 ns. Green trace is Ru124/W122/Az(Cu^{2+}), τ = 18 ns. Blue trace is Ru124/W122/Az(Cu^{+}), τ = 18 ns.

The time-resolved emission data on Ru124/W122/Az(Cu^{+}) and Ru124/W122/Az(Cu^{2+}) both show the same diminished lifetime of the excited state $*Ru^{2+}$ compared to that of the model compound (**Figure 4.1**). This indicates that the excited state is being quenched in the system. Because the lifetime was the same in both Cu^{+} and Cu^{2+} states, the quenching is likely not due to copper. In comparison, the $*Ru^{2+}$ in Ru124/F122/Az(Zn^{2+}) was measured to have a lifetime of 40 ns, indicating that the diminishment of lifetime is likely due to the W122. Time-resolved absorption data recorded at the 510 nm wavelength, which tracks the ground state Ru^{2+}, first displays a

bleach, and then quick recovery (**Figure 4.2**). It is perhaps unfair to discuss the lifetimes extracted from the fitting of this data; the signal is quite small, and lifetimes on the order of 10 ns do test the instrument's response. However, it is clear from the time-resolved absorption spectroscopy that Ru^{2+} is recovered faster in these systems than it is in the model compound. More importantly, no prolonged bleaching is evident in these systems, indicating that the subsequent oxidation of Cu^{+} in the Cu^{+} case does not occur, as Ru^{2+} would not recover so quickly if it did. Rather, what likely happens is that tryptophan oxidizes the $*Ru^{2+}$, and very quick recoupling occurs, faster than the initial quench. This back reaction is still faster than deprotonation of the tryptophan radical cation (**Scheme 4.2**).

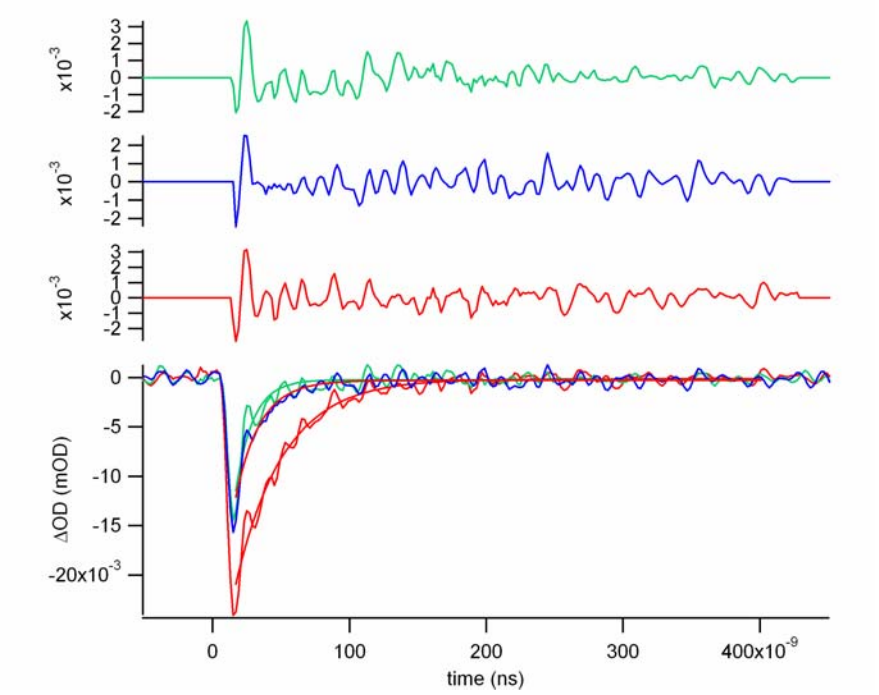

Figure 4.2. Transient absorption of Ru124/W122/Az(Cu^{2+}) and (Cu^{+}). λ_{ex} = 490 nm, λ_{obs} = 510 nm. Red trace is Ru model compound, [Ru(trpy)(tfmbpy)(im)]$(PF_6)_2$ in 25 mM KP_i, pH 7.16, τ = 37 ns. Green trace is 10 μM Ru124/W122/Az(Cu^{2+}), 25 mM KP_i, pH 7.16, τ = 12 ns. Blue trace is 10 μM Ru124/W122/Az(Cu^{+}), 25 mM KP_i, pH 7.16, τ = 17 ns.

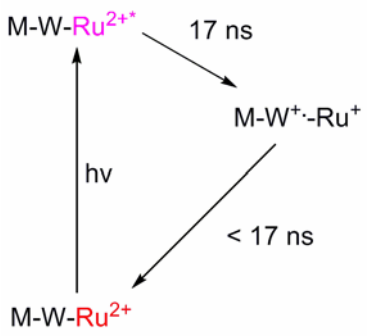

Scheme 4.1. Events after sample excitation in Ru124/W122/Az($Cu^{2+/+}$) systems. Colors indicate species observed spectroscopically.

Re124/$YNO_2$122/Az(Cu^{2+})

In this system, the perturbation was at the amino acid site; the rhenium label was installed at 124, and 3-nitrotyrosine was installed at the 122 site.

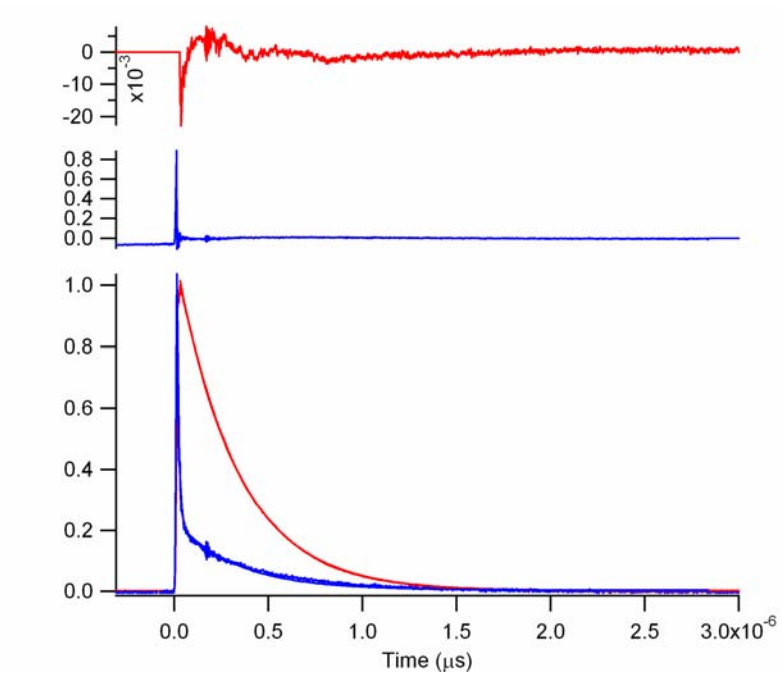

Figure 4.3. Time-resolved emission of Re124/$YNO_2$122/Az(Cu^{+}). ~40 μM Re124/$YNO_2$122/Az(Cu^{2+}), 25 mM KP_i, pH 7.8. λ_{ex} = 355 nm, λ_{em} = 560 nm. Red trace is Re model compound, [Re(dmp)$(CO)_3$(im)]OTf in 25 mM KP_i, pH 7.8, τ = 320 ns. Blue trace is Re124/$YNO_2$122/Az(Cu^{+}), which was fit to a function with two decays, one set at 320 ns. τ = 10 ns

Time-resolved emission data revealed extremely promising results (**Figure 4.3**). While the excited state $*Re^{+}$ of the model compound lives quite long, the $*Re^{+}$ in $Re124/YNO_2122/Az(Cu^{+})$ does not live long at all; indeed, if the data were fit to a function with biphasic decay, the faster phase is fitted to a value of around 10 ns, which challenges the instrument response of the Nanosecond-I laser setup. It is unsurprising that the transient absorption studies done at 434 nm to track the YNO_2^{-} state garnered inconclusive, small bleaches that were too narrow to be considered more than laser scatter; the kinetics are likely too fast for accurate data to be obtained on the 10 ns laser setup. Disappointingly, no Cu^{2+} generation was found when probed for at 632.8 nm, so no subsequent electron transfer between the copper and oxidized nitrotyrosyl radical is observed. Time-resolved emission data done on the 10 ps laser was attempted but frustrated when it was observed that the sample had undergone some aggregation (owing to excessive exposure to H_2/Pt reduction conditions).

The extremely efficient quenching of the $*Re^{+}$ state indicates that electron transfer between the nitrotyrosine residue and the $*Re^{+}$ is much more favorable than that seen in the Re124/W122 case; this is possible if the driving force of this electron transfer is no longer near that of the $*Re^{+}$, but rather, larger and downhill, making the transfer closer to activationless in barrier. $*Re^{+}$ emission data and lack of Cu^{2+} formation indicate that quick charge recombination of the reduced Re^{0} and $YNO_2^{\bullet}$ occurs, owing to a combination of the close distance between the metal label and amino acid residue, and a better driving force for the charge recombination than $Cu^{+}/YNO_2^{\bullet}$ electron transfer.

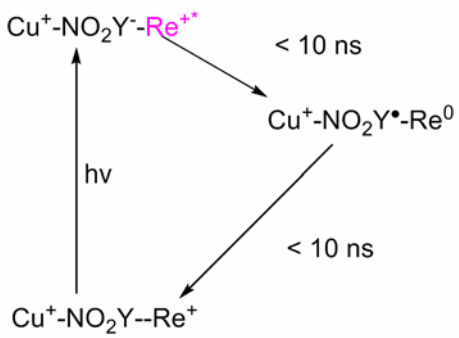

Scheme 4.2. Events after sample excitation in Re124/YNO$_2$122/Az(Cu$^+$) systems. Colors indicate species observed spectroscopically.

Ru124/YNO$_2$122/Az(Cu^{2+})

In this system, the perturbation was at the both the label and amino acid sites; a ruthenium label was installed at 124, and 3-nitrotyrosine was installed at the 122 site.

Because E°(*Ru^{2+}/Ru$^+$) did not seem to be as high as E°(*Re$^+$/Re^0), it was hoped that more spectroscopic information could be garnered on these systems; the driving force of the initial electron transfer would not be as high, slowing the electron transfer enough for detection with the 10 ns laser system. This hypothesis was true to a certain extent; quenching of the excited state was clear. However, to extract truly accurate kinetics data on this system, measurements done on a faster laser system will be necessary.

Studies done on the Ru124/YNO$_2$122/Az(Cu^{2+}) system were conducted at pHs 4.71 and 7.71 in the hopes of proving NO$_2$Y$^-$ as an electron donor in the quenching of the *Ru^{2+}; at pH 4.71, the nitrotyrosine residue would be protonated, and so would likely not participate in electron transfer.

So it was surprising when it was observed that both protonated and deprotonated samples exhibited quenching of the *Ru^{2+} excited state, regardless of the copper oxidation state (**Figures 4.4 and 4.5**). The fits to the faster decays in both emission and

transient absorption are for mere comparison; again, these lifetimes challenge the response time of the instrument; for data that appropriately details the events of $*Ru^{2+}$, measurements ought to be done with a faster laser system. Quenching in either pH is within error, so it is also unfair to suppose that one sample displays quenching to a greater extent to the other. What *is* clear from **Figures 4.4 and 4.5**, however, is that the $*Ru^{2+}$ is quenched at both pH 4.71 and 7.71. No Cu^{2+} formation was observed at either pH in the Cu^{+} measurements, indicating that the process is once again restricted to electron transfer between the metal label and the residue. To probe for NO_2Y^{-} bleaching, the transient absorption was measured at 434 nm in the pH 7.71 samples. Unfortunately, the broad MLCT of the Ru^{2+} overlaps at this wavelength, so it is unclear whether or not the bleach observed at this wavelength is from the ruthenium or from the nitrotyrosine; ironically, this is a case where the very reason the ruthenium label was pursued frustrated efforts to understand the data.

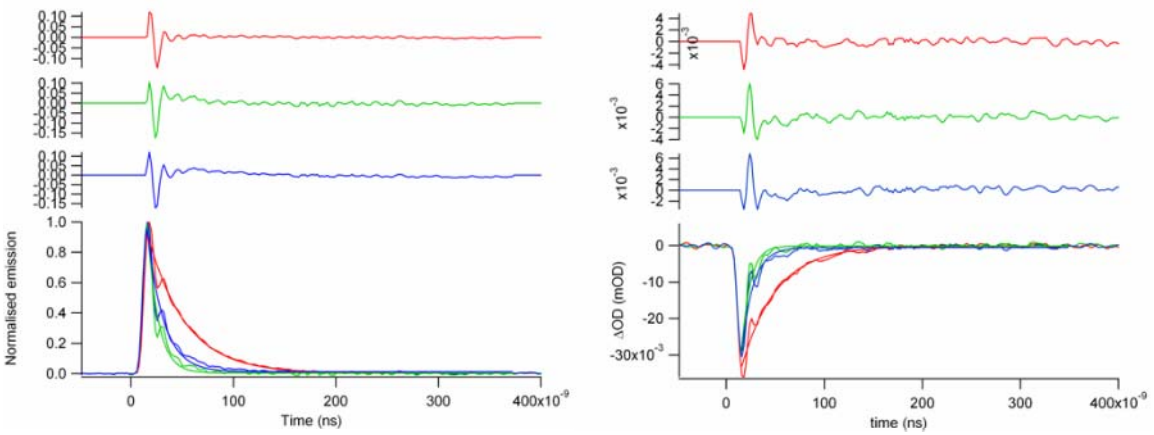

Figure 4.4. Time-resolved UV-VIS Spectroscopy of Ru124/$YNO_2$122/Az(Cu^{2+}) at pH 4.7 and 7.7. 10 μM Ru124/$YNO_2$122/Az(Cu^{2+}), 25 mM KP_i, pH 7.71 (blue), 25 mM NaOAc, pH 4.71 (green). Red trace is Ru model compound, [Ru(trpy)(tfmbpy)(im)]$(PF_6)_2$ in 25 mM KP_i, pH 7.71. **Left:** λ_{ex} = 490 nm, λ_{em} = 700 nm. Each are fit to single exponential decay. Label τ = 36 ns, pH 4.71 τ = 10 ns, pH 7.71 τ = 15 ns. **Right:** λ_{ex} = 490 nm, λ_{obs} = 510 nm. Label τ = 35 ns, pH 4.71 τ = 8 ns, pH 7.71 τ = 11 ns

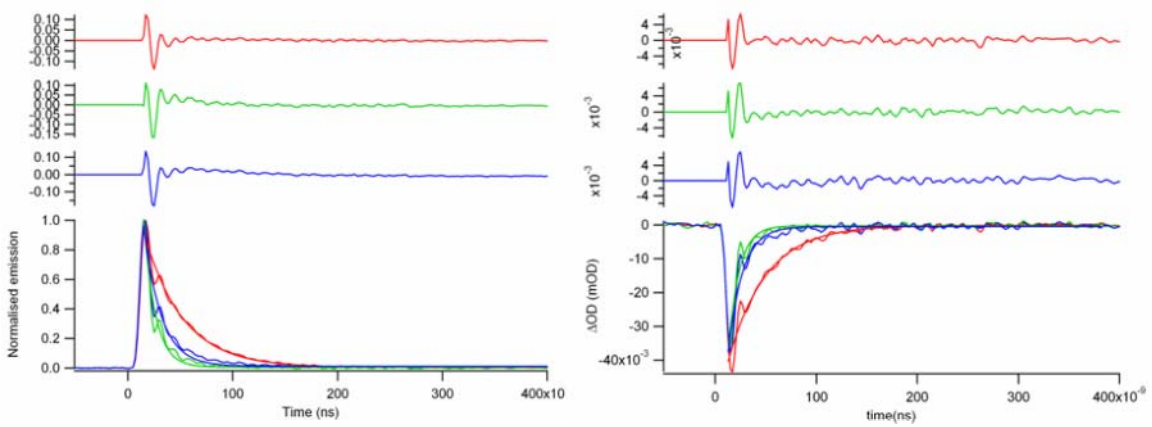

Figure 4.5. Time-resolved UV-VIS Spectroscopy of Ru124/$YNO_2$122/Az(Cu^+) at pH 4.7 and 7.7. 10 μM Ru124/$YNO_2$122/Az(Cu^{2+}), 25 mM KP_i, pH 7.71 (blue), 25 mM NaOAc, pH 4.71 (green). Red trace is Ru model compound, [Ru(trpy)(tfmbpy)(im)]$(PF_6)_2$ in 25 mM KP_i, pH 7.71. **Left:** λ_{ex} = 490 nm, λ_{em} = 700 nm. Each are fit to single exponential decay. Label τ = 36 ns, pH 4.71 τ = 11 ns, pH 7.71 τ = 16 ns. **Right:** λ_{ex} = 490 nm, λ_{obs} = 510 nm. Label τ = 37 ns, pH 4.71 τ = 11 ns, pH 7.71 τ = 14 ns

Still, the data is confusing; is the $*Ru^{2+}$ quenched by protonated or deprotonated nitrotyrosine? An argument can be made that at pH 7.71, not all the nitrotyrosine is deprotonated, and that what quenching is observed is from the protonated state. That is a possibility. Another is that the reduction potentials of both states are conducive to electron transfer. The conservative, completely correct assertion that can be made is that quenching occurs; the tyrosine analog 3-nitrotyrosine can participate in electron transfer. It is unclear what protonation state the residue is in, and there is even confusion of whether the nitrotyrosine is giving up or gaining the electron.

The Importance of Distance in Hopping

The proteins discussed in this section include Ru126/W122/Az(Cu^{2+}), Re126/W122/Az(Cu^{2+}), and Re126/F122/Az(Cu^{2+}). These proteins were prepared using the methods described in **Chapter 2**.

Ru126/W122/Az(Cu^{2+})

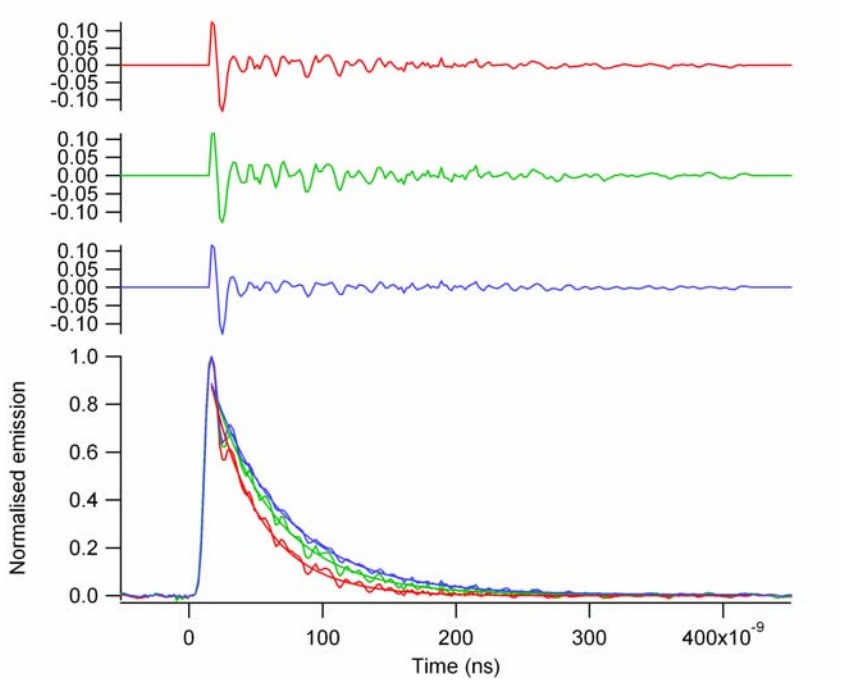

Figure 4.6. Time-resolved emission of Ru126/W122/Az(Cu^{2+}) and (Cu^{+}). 10 μM Ru126/W122/Az(Cu^{2+}), 25 mM KP_i, pH 7.14. λ_{ex} = 490 nm, λ_{em} = 700 nm. Red trace is Ru model compound, [Ru(trpy)(tfmbpy)(im)]$(PF_6)_2$ in 25 mM KP_i, pH 7.16, τ = 37 ns. Green trace is Ru126/W122/Az(Cu^{2+}), τ = 48 ns. Blue trace is Ru126/W122/Az(Cu^{+}), τ = 52 ns.

The attraction of labeling at the 126 site is that it is hoped that by placing the label farther away, the previously observed charge recombination between $W^{\bullet+}$ and Ru^{+} would be slowed enough so that $Cu^{+}/W^{\bullet+}$ electron transfer could be observed. Any pseudo π-stacking interaction between the metal label's ligand and the tryptophan would be disrupted.

The emission data of Ru126/W122/Az($Cu^{2+/+}$) indicate that attaching the label at the 126 site placed the ruthenium too far away from the tryptophan for electron transfer to occur; the electronic coupling between the two centers is too small. The lifetime of the excited state *Ru^{2+} was long, and showed no quenching (**Figure 4.6**). Quenching the *Ru^{2+} state to generate the higher-potential Ru^{3+} was once more considered as an option. The other option was to install the rhenium label at the 126 site instead, taking advantage of its higher reduction potential.

Re126/W122/Az(Cu^{2+})

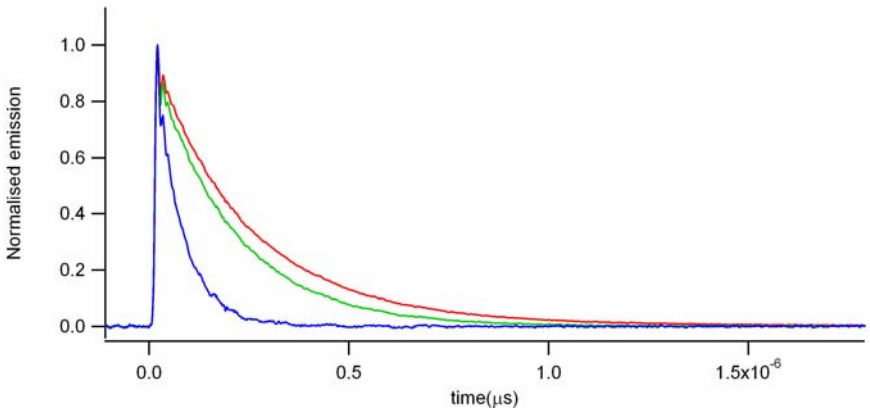

Figure 4.7. Time-resolved emission of Re126/W122/Az(Cu^{2+}) and (Cu^{+}). 10 μM Re126/W122/Az(Cu^{2+}), 25 mM KP_i, pH 7.28. λ_{ex} = 355 nm, λ_{em} = 560 nm. Red trace is Re126/W122/Az(Cu^{2+}). Green trace is Re126/W122/Az(Cu^{+}). Blue trace is Re126/W122/Az(Cu^{+}) + 10 mM $Ru(NH_3)_6Cl_3$.

The emission studies on the *Re^{+} excited state indicate that, when substituted at the 126 site, the rhenium label is simply too far away the participate in hopping the way it did in the working Re124/W122/Az(Cu^{+}) system (**Figure 4.7**). There was no quenching of the *Re^{+} in either Cu^{2+} or Cu^{+} protein. The quencher $Ru(NH_3)_6^{3+}$ had been utilized before for flash-quench experiments with the Re-modified azurin,[1] and so 10 mM

quencher was added to the sample to access the higher potential Re^{2+} state. Accessing this state drove the quick generation of Cu^{2+} within 100 ns (**Figure 4.8**).

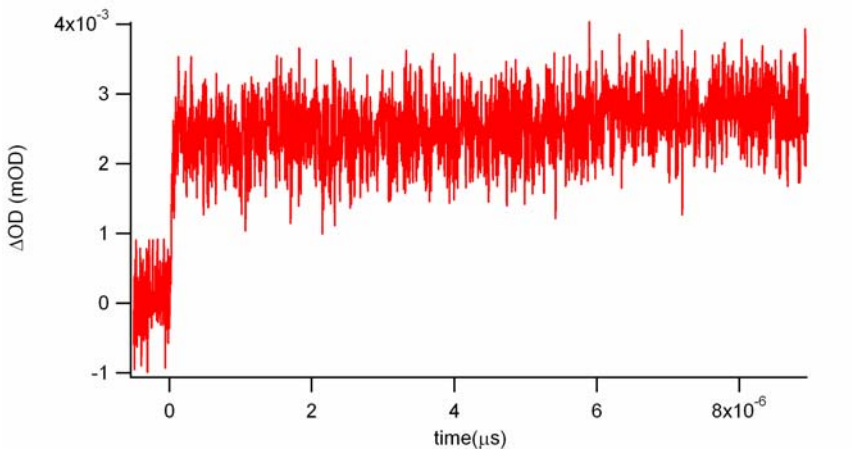

Figure 4.8. Transient absorption of Re126/W122/Az(Cu^{+}) with quencher. 10 μM Ru124/W122/Az(Cu^{+}), 10 mM $Ru(NH_3)_6Cl_3$, 25 mM KP_i, pH 7.28. λ_{ex} = 355 nm, λ_{obs} = 628 nm

The 100 ns generation of Cu^{2+} is much faster than the previously observed single-step electron transfer, which was measured to be on the order of hundreds of microseconds.[1,2] The presence of the tryptophan proved to be essential for Cu^{2+} formation, studies executed on the Re126/F122/Az(Cu^{+}) system did not reproduce the quick Cu^{2+} generation. The generation of Cu^{2+} could be accomplished through the multistep tunneling mechanism shown in **Scheme 3**. Upon excitation, the excited $*Re^{+}$ is oxidized by the quencher $Ru(NH_3)_6^{3+}$, generating the high-potential Re^{2+} state. The rhenium oxidizes the tryptophan, which in turn oxidizes the copper. The system is eventually reduced to its ground state through charge recombination with $Ru(NH_3)_6^{2+}$.

Structural characterization is needed to obtain the electron transfer distances. It is likely this system does not exhibit the same pseudo π-stacking to bring the metal label and tryptophan closer together.

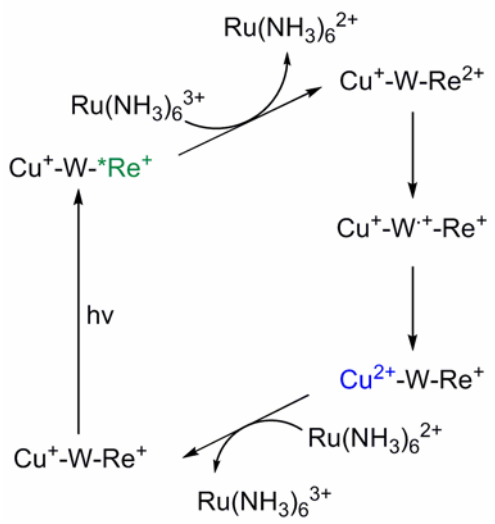

Scheme 4.3. Events after sample excitation in Re126/W122/Az(Cu^+) with $Ru(NH_6)_3^{3+}$. Colors indicate species observed spectroscopically.

4.4 CONCLUSIONS

The experiments done to perturb the working Re124/W122/Az(Cu^+) system clearly demonstrate that a balance of driving force and distance between the three redox sites is necessary to achieve observable hopping kinetics. 3-Nitrotyrosine was shown to participate in electron transfer reactions, and it is clear that further investigations need to be made to understand its behavior. Shifting the labeling site two residues away shut down the original multistep tunneling mechanism; the rhenium and tryptophan were too far apart for electron transfer to occur. However, by oxidizing the excited state rhenium to its high-potential 2+ state, a new hopping system was discovered.

4.5 EXPERIMENTALS

The metal-modified proteins were prepared as described in **Chapter 2**. Laser spectroscopy studies were carried out as described in **Chapter 2**.

4.6 REFERENCES

(1) Miller, J. E., California Institute of Technology, 2003.

(2) Miller, J. E.; Di Bilio, A. J.; Wehbi, W. A.; Green, M. T.; Museth, A. K.; Richards, J. R.; Winkler, J. R.; Gray, H. B. *BBA Bioenergetics* **2004**, *1655*, 59–63.

CHAPTER FIVE

Studying Hopping in Another Pathway of Azurin

5.1 ABSTRACT

Hopping was investigated through an established electron transfer pathway that traverses the interior of azurin. Tyrosine was installed in the 48 site of azurin with the hope that the sequestration would circumvent deprotonation of the radical cation form, thereby allowing for hopping to occur through tyrosine. Two metal-modified proteins were made for the study. Time-resolved UV-VIS spectroscopy measurements indicate that, while the substitution of tyrosine can encourage fast electron transfer between the ruthenium and the copper center, it does not actually participate in hopping.

5.2 INTRODUCTION

In the hope of generating more experimental demonstrations of multistep tunneling at different distances, a hopping system is installed along another known electron transfer pathway in azurin. The system discussed in this chapter is through a network of hydrogen and covalent bonds traversing the protein's interior, ending at the surface residue H83 (**Figure 5.1**).[1] An examination of the electron tunneling pathways between these two centers reveals that the dominant tunneling pathways utilize the backbone of residue 47, close to the wild-type W48. W48 is buried in the protein, theoretically inaccessible from the solvent. The W48 has been demonstrated to be quite important for electron transfer pathways in systems studied in azurin. A previous study

in the group using gold-modified electrodes demonstrated that W48 was important for intermolecular electron transfer.[2] Pulse radiolysis studies on azurin, which study the kinetics of the 27 Å electron transfer between a reduced anion on the disulfide bridge Cys3-Cys26 and the copper center, demonstrated that substitution of W48 with other amino acids at the site diminished electron transfer rates.[3] Substitution at this site, where so much electron transfer research revolves, with tyrosine is only natural.

In fact, it has been done before: Dr. William A. Wehbi made a Y48 mutant and labeled H83 with rhenium. He used flash-quench to observe the neutral radical by EPR.[4] It is hoped that by installing the ruthenium complex at His83, and observing the system using time-resolved spectroscopic techniques, hopping through tyrosine, uncomplicated by deprotonation, will be observed.

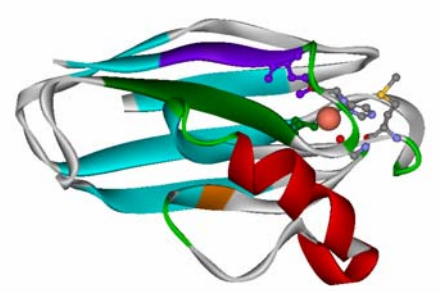

Figure 5.1. *Pseudomonas aeruginosa* azurin (PDB code: 1AZU). His83 is highlighted in orange.

5.3 RESULTS & DISCUSSION

The proteins discussed in this chapter include Ru83/Y48/Az(Cu^{2+}) and Ru83/F48/Az(Cu^{2+}). These proteins were prepared using the methods described in **Chapter 2**.

The time-resolved emission data reveal quenching of the excited state *Ru^{2+} in Ru83/Y48/Az(Cu^{2+}) (**Figure 5.2**). The Ru83/F48/Az(Cu^{2+}) does not demonstrate the

same quenching, which indicates that the tyrosine could be responsible. However, when the studies were repeated on the Ru83/Y48/Az(Cu^{+}) mutant to search for copper oxidation, the emission data belied the hypothesis (**Figure 5.3**).

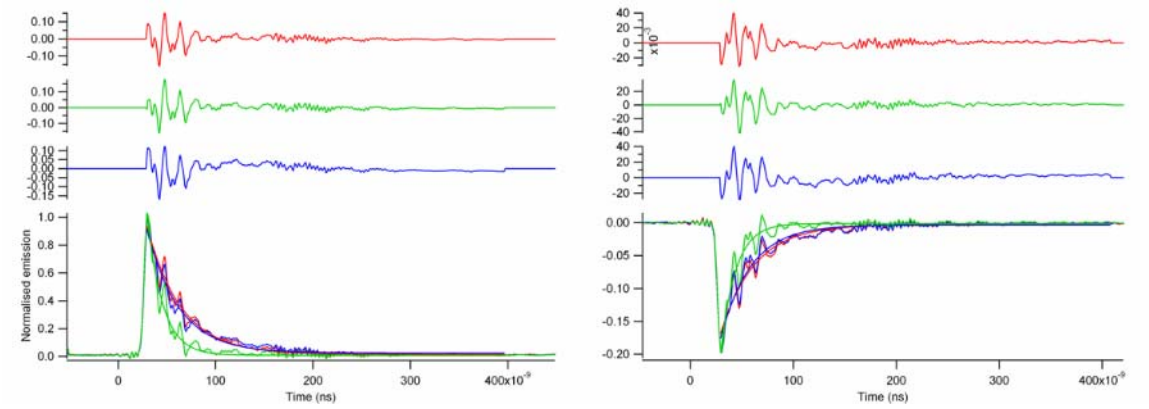

Figure 5.2. Time-resolved UV-VIS spectroscopy of Ru83/Y48/Az(Cu^{2+}). Green trace is 30 μM Ru83/Y48/Az(Cu^{2+}), 25 mM NaP_i, pH 7.4. Red trace is Ru model compound, 30 μM [Ru(trpy)(tfmbpy)(im)]$(PF_6)_2$ in 25 mM NaP_i, pH 7.4. Blue trace is 30 μM Ru83/F48/Az(Cu^{2+}) **Left:** λ_{ex} = 490 nm, λ_{em} = 700 nm. Each are fit to single exponential decay. Label τ = 35 ns, Ru83/F48/Az(Cu^{2+}) τ = 33 ns, Ru83/Y48/Az(Cu^{2+}) τ = 17 ns. **Right:** λ_{ex} = 510 nm, λ_{obs} = 480 nm. Label τ = 34 ns, Ru83/F48/Az(Cu^{2+}) τ = 30 ns, Ru83/Y48/Az(Cu^{2+}) τ = 15 ns

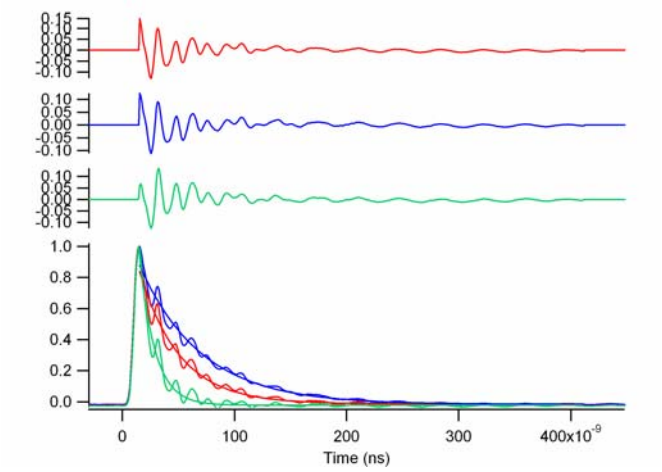

Figure 5.3. Time-resolved emission of Ru83/Y48/Az(Cu^{+}). Green trace is 30 μM Ru83/Y48/Az(Cu^{2+}), 25 mM NaP_i, pH 7.4. Red trace is Ru model compound, 25 μM [Ru(trpy)(tfmbpy)(im)]$(PF_6)_2$ in 25 mM NaP_i, pH 7.4. Blue trace is Ru83/F48/Az(Cu^{+}) λ_{ex} = 490 nm, λ_{em} = 700 nm. Each are fit to single exponential decay. Label τ = 35 ns, Ru83/Y48/Az(Cu^{2+}), τ = 17 ns, Ru83/Y48/Az(Cu^{+}), τ = 40 ns

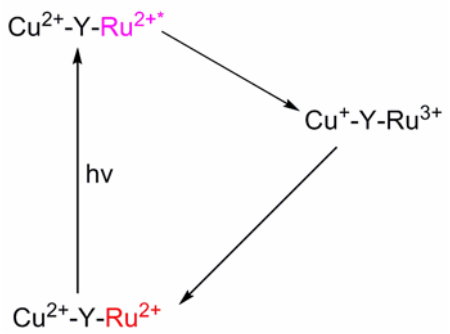

Scheme 5.1. Events after sample excitation in Ru83/Y48/Az(Cu^{2+}). Colors indicate species observed spectroscopically.

From this data, it appears that the Cu^{2+}, and *not* Y48, is participating in electron transfer with the ruthenium (**Scheme 5.1**). This is not unfamiliar behavior for a $*Ru^{2+}$-Cu^{2+} system; it was observed in the study of ruthenium-modified plastocyanins.[5] The difference in kinetics in the F48 and Y48 mutants is likely due to more efficient tunneling pathways in one mutant over the other, allowing for increased electronic coupling, and so faster electron transfer. Given that electron transfer is so efficient in these studies, it is likely that hopping does not need to be accessed for efficient electron transfer.

5.4 CONCLUSIONS

While the kinetics on the Ru83/Y48/Az(Cu^{2+}) system do not demonstrate multistep tunneling behavior, they do demonstrate that the 48 site is an important site in determining the electron transfer kinetics between Ru83 and the copper center. They also demonstrate that electron transfer between the Ru83 and copper center in azurin is already quite efficient in the system.

5.5 EXPERIMENTALS

The metal-modified proteins were prepared as described in **Chapter 2**. Laser spectroscopy studies were carried out as described in **Chapter 2**.

5.6 REFERENCES

(1) Regan, J. J. *Chem. & Biol.* **1995**, *2*, 489.
(2) Fujita, K.; Nakamura, N.; Ohno, H.; Leigh, B. S.; Niki, K.; Gray, H. B.; Richards, J. H. *J. Am. Chem. Soc.* **2004**, *126*, 13954–13961.
(3) Farver, O.; Skov, L. K.; Young, S.; Bonander, N.; Karlsson, B. G.; Vanngard, T.; Pecht, I. *J. Am. Chem. Soc.* **1997**, *119*, 5453–5454.
(4) Wehbi, W. A., California Institute of Technology, 2003.
(5) Di Bilio, A. J.; Dennison, C.; Gray, H. B.; Ramirez, B. E.; Sykes, A. G.; Winkler, J. R. *J. Am. Chem. Soc.* **1998**, *120*, 7551–7556.

CHAPTER SIX

Future Directions

6.1 SYSTEMS TO STUDY

There are many electron tunneling pathways on which to study multistep tunneling on *Pseudomonas aeruginosa* azurin. While many mutants were prepared for study, not all planned studies were accomplished. **Table 6.1** outlines mutants that were given only cursory study and their stages of preparation; it is hoped that these materials will be useful for future studies done on azurin.

Protein	Stage of Preparation	Remark
Ru107/$YNO_2$109/Cu^{2+}	Pure protein, ready for study	Cys112 arm
Re107/$YNO_2$109/Cu^{2+}	Studied once by laser spectroscopy	Cys112 arm
H107/W109/Cu^{2+}	Expressed	Cys112 arm
H107/Y109/W110/Cu^{2+}	Expressed	Double Hop
Ru107/W109/Y110/Cu^{2+}	Expressed	Double Hop
H126/W122/Zn^{2+}	Expressed	Met121 arm
H126/F122/Zn^{2+}	Expressed	Met121 arm
H83/Y48/Zn^{2+}	Expressed	
H83/F48/Zn^{2+}	Expressed	

Table 6.1. Azurin mutants which were expressed but not discussed in this dissertation

Multistep tunneling through the Cys112 arm of azurin was not at all addressed in this dissertation, which is a shame; the mutants were prepared, but there was insufficient data to draw real conclusions. However, the tentative studies on the site indicated that electron transfer occurred between Ru107 and $YNO_2$109. The 109 site was simply too

far away from the copper center to facilitate the subsequent electron transfer. It was postulated that the system would be ideally suited to study a double hop. Proteins to investigate this possibility were expressed, but never nitrated or labeled. Given the success of the Re124/W122 system, a Re107/W109 system also ought to be studied.

Along the Met121 arm, more studies need to be done to confirm the second hopping system. A Re126/W122/Zn^{2+} mutant should be prepared; it is hoped that the tryptophan radical cation's spectrum, which was masked by Re^{0} in the Re124/W122/Cu^{2+} system, can be measured in this mutant. Double hopping systems should also be investigated in this system, using 124/122 residues as hopping sites, and 126 for labeling.

6.2 THESIS CONCLUSIONS

The goal of the research done in this dissertation was to demonstrate multistep electron tunneling in a model system installed on the protein *Pseudomonas aeruginosa* azurin. This system has been successfully made and characterized. The electron transfer kinetics of system Re124/W122/Az(Cu^{+}) have been studied by different methods of spectroscopy, and all data support the same multistep tunneling model. Furthermore, the electron transfer time observed in the studies is consistent with the time calculated from theory.

This system was varied to test its robustness; the potential of both label and amino acid were perturbed. It was through these investigations that it was demonstrated that 3-nitrotyrosine could participate in electron transfer reactions, substantiating the possibility of tyrosine and its analogs being utilized as hopping intermediates in nature. It remains

unclear how the residue participates, and it is hoped that the promising initial observations will inspire future investigations of hopping through that amino acid.

When the label was installed another 5 Å away at the 126 site, electron transfer between excited state rhenium and tryptophan shut down; the centers were simply too far apart. However, once an exogenous quencher was utilized to oxidize the rhenium into its higher potential Re^{2+} state, the Re126/W122/Az(Cu^{+}) system exhibited hopping kinetics, giving the multistep tunneling program its second working system.

I hope it is clear to the reader how invigorating studies in this system are; each insight yields substantial information, which makes each experiment quite exciting to execute! There are still many unexplored possibilities in studying multistep electron tunneling on azurin and much more information on multistep tunneling to be gained. It is hoped that this report will give the reader the inspiration and methods to study them.

A P P E N D I X

MATLAB Programs and Functions Utilized in Data Analysis

The programs and functions given on the following pages were utilized in the analysis of time-resolved UV-VIS spectroscopy data from the 10 ps laser.

The function **streak_a.m** (p. 113) was used to convert streak camera image files into text files with data. It was called with the command:

```
[t,y]=streak_a;
```

Once converted, the resulting vectors were saved to a text file.

The file **max_ent.m** (p. 116) was utilized for a cursory fit to the data (when there was no concern over the instrument response). The program actually does a lot more than fitting, but for the purpose of the fits, the function was exited when asked:

```
Do you want to fit with a single MEM...
```

by hitting Ctrl-C.

The program **splice_data1.m** (p. 124) was used to splice data from different timescales together so that analysis could be performed on complete data sets with better data at faster timescales.

The function **crystal.m** (p.126) was utilized to convolve instrument response with a theoretical curve; the convolved curve would be compared to the data, and chi square

would be calculated. It calls another function **multiexp_conv.m** (p.127) that executes the convolution on a spliced data set.

streak_a.m

```
function [X,Y]=streak_a()
%
%
%           function: streak_a
%           action:  bins selected streak camera image data collected
with
%                   streak camera GPIB controller turned off.
%                           into a time vector (t) and
%                           an intensity vextor (y)
%
%           syntax:
%
%             [t,y]=streak;
%
%             remember to end with a semicolon
%             to avoid printing out the results
%             on the screen
%
%
load streak_scl
%
%deltat=[0.31329345703125; 0.9678955078125; 1.904541015625;
4.92431640625; 12.11328125; 21.474609375; 42.72265625; 102.48828125];
%
time=[A B C D E F G H];
%
filename=input('Enter the data file name: ','s');
%
fprintf(' Data in file: %24s\n',filename)
%
fid=fopen(filename,'r');
%
%
if fid < 0
   fprintf(' Error opening : %24s\n',filename)
   return
end
%
%
im=fread(fid,2,'uchar');
IM=char(im');
length=fread(fid,1,'int16');
width=fread(fid,1,'int16');
height=fread(fid,1,'int16');
xoff=fread(fid,1,'int16');
yoff=fread(fid,1,'int16');
filetype=fread(fid,1,'int16');
reserved=fread(fid,51,'int16');
icomment=fread(fid,length-52,'uchar');
comment=char(icomment');
fprintf(1,'\n%34s\n',comment(171:204))
fprintf(1,'%55s\n',comment(207:261))
fprintf(1,'%43s\n',comment(264:284))
for i=1:height-1
   tmp=fread(fid,width,'int16');
```

```
   image(i,1:width)=tmp';
end
%
%
fclose(fid);
%
%
fprintf(1,'\n\nTime Bases:\n')
fprintf(1,'  1 --> 0.2 ns\n')
fprintf(1,'  2 --> 0.5 ns\n')
fprintf(1,'  3 --> 1.0 ns\n')
fprintf(1,'  4 --> 2.0 ns\n')
fprintf(1,'  5 --> 5.0 ns\n')
fprintf(1,'  6 --> 10 ns\n')
fprintf(1,'  7 --> 20 ns\n')
fprintf(1,'  8 --> 50 ns\n')
itst=-1;
while itst<0
   timebase=input('\nEnter the number of the timebase --> ');
   if timebase >= 1 & timebase <= 8
      itst=1;
   end
end
%
%
y=sum(image);
plot(y);
axis([1 640 min(y)-((max(y)-min(y)).*0.025) max(y)+((max(y)-
min(y)).*0.025)])
xlabel('Channel Number')
ylabel('Intensity')
%
%
itst=-1;
while itst<0
   fprintf(1,'\n\nEnter columns numbers to bin in the following
format:\n')
   fprintf(1,'                      [left1 right1; left2 right2; ...
]\n\n')
   comb=input('Enter the columns to bin --->  ');
%
   [a,b]=size(comb);
   if b==2 & a>=1
      itst=1;
   end
end
%
%
j=1;
for i=1:a
   if comb(i,1) >= 1 & comb(i,1) <= 640 & comb(i,2) >= 1 & comb(i,2) <=
640 & comb(i,1) <= comb(i,2)
      COMB(j,1:2)=comb(i,1:2);
      j=j+1;
   end
end
%
```

```
%
[A,B]=size(COMB);
%
%
for i=1:A
   y=sum(image(:,COMB(i,1):COMB(i,2))');
end
%
%
plot(y)
axis([1 512 min(y)-((max(y)-min(y)).*0.025) max(y)+((max(y)-
min(y)).*0.025)])
xlabel('Channel Number')
ylabel('Intensity')
%
%
itst=-1;
while itst<0
   fprintf(1,'\n\nEnter first and last data points in the following
format:\n')
   fprintf(1,'                        [first last]\n\n')
   firlas=input('Enter the data points --->  ');
%
   [a,b]=size(firlas);
   if b==2 & a>=1
      itst=1;
   end
end
%
if firlas(1,1) <= 0 | firlas(1,1) >= firlas(1,2)
   firlas(1,1)=1;
end
%
if firlas(1,2) > 512 | firlas(1,2) <= firlas(1,1)
   firlas(1,2)=512;
end
%
Y=y(firlas(1,1):firlas(1,2))';
%X = 0:deltat(timebase):(firlas(1,2)-firlas(1,1)).*deltat(timebase);
X=time(firlas(1,1):firlas(1,2),timebase);
X=X./1000;
%
%
plot(X,Y)
axis([min(X) max(X) min(Y)-((max(Y)-min(Y)).*0.025) max(Y)+((max(Y)-
min(Y)).*0.025)])
xlabel('Time, ns')
ylabel('Intensity')
%
%
clear time A B C D E F G H
%
%
```

max_ent.m

```
%
%
%
%   script to fit two-column ascii kinetics data
%  to a distribution of rate constants using the maximum entropy method
%
%
clear all
clf
%
%
%
%        define fit function
func=['laplace_mem'];
%
fprintf('\r\r Data must be in two-column or two-row, space delimited,
ascii format:\r column(row)-1 is time; column(row)-2 is intensity\r\r')
filename=input('Enter the data file name --> ', 's');
%
%
Mm=dlmread(filename);
M=Mm(:,1:2);
[rM cM]=size(M);
if cM ~= 2
   M=M';
end
%
%
if cM ~= 2
   [aa, bb]=size(M');
   fprintf('\r\r Data are not in two-column or two-row, space
delimited, ascii format \r')
   fprintf('\r %5i Rows and %5i Columns \r', aa, bb)
   return
end
%
%
t=M(:,1);
t=t-t(1);
y_un=M(:,2);
y=y_un;
%y=y_un./max(y_un); %set max value to 1
%[t,y,wlog]=logtime(te,ye,50);
%[rt ct]=size(t);
%if ct ~= 1
%   t=t';
%end
%[ry cy]=size(y);
%if cy ~= 1
%   y=y';
%end
%[rw cw]=size(wlog);
%if cw ~= 1
%   wlog=wlog';
%end
```

```
%
%
tleng=length(t);    %length of the logarithmically space data record
%
%
fprintf('\r\r Weighting methods: (1) uniform (DEFAULT) (2) relative;
(3) Poisson\r')
weight_method=input('Select a weighting method (1,2,3) --> ');
%
%
if isempty(weight_method)
   weight_method=1;
end
%
%
sml1=sort(y);
test_y=-1;
icnt=1;
while test_y <= 0
   test_y=sml1(icnt);
   icnt=icnt+1;
end
%
%
if weight_method==1
   wt=ones(tleng,1);
elseif weight_method==2
   wt=y_un.^2;
   tty=test_y.^2;
   wt=(max(wt,tty));
   wt=sqrt(wt);
%   wt=sqrt(wt./wlog);
elseif weight_method==3
   tty=sqrt(test_y./max(y_un));
   wt=sqrt(y./max(y_un));
   wt=max(wt,tty);
%   wt=sqrt(wt./wlog);
end
%
%
clf
subplot(3,1,2)
plot(t,y)
pause(0.1)
%
%
ltest=-1;
ltest1=-1;
while ltest < 0
   while ltest1 < 0
      fprintf('\r\r 1/tmin = %12.8e ; 1./tmax = %12.8e \r\r', 1./(t(2)-
t(1)), 1./max(t))
      kmax=input(' Enter the value for the maximum rate constant in the
distribution --> ');
      kmin=input(' Enter the value for the minimum rate constant in the
distribution --> ');
      if kmax > kmin
```

```
         ltest1=1;
      else
         fprintf(' kmax must be greater than kmin !')
      end
   end
   delta=input(' Enter the value for the resolution ratio of adjacent
rate constants [k(i+1)/k(i)] --> ');
   lkspace=log10(kmin):log10(delta):log10(kmax);
   lkleng=length(lkspace);
   if (lkleng > 1) & (tleng > lkleng)
      fprintf('\r\r k-space vector has %4i elements ',lkleng)
      fprintf('\r time vector has %4i elements ',tleng)
      ltest=1;
   elseif (tleng <= lkleng)
      fprintf('\r\r # of fit parameters exceeds number of observables
')
      fprintf('\r k-space vector has %4i elements; time vector has %4i
elements ',lkleng,tleng)
   else
      fprintf('\r\r k-space vector is too short: %4i element ',lkleng)
   end
end
%
%
kspace=ones(1,lkleng);
kspace=kspace.*(10.^lkspace);
mink=min(min(kspace),1./max(t));
kspace=[mink./1e4,kspace];
kleng=length(kspace);       % length of k-space vector
A=t*kspace;
A=exp(-A);
%
%  get the lsqnonneg solution for the initial guesses
%
fprintf('\r\r Finding the lsqnonneg solution for the initial guess \r')
X0=lsqnonneg(A,y);
%
%
ycalc=A*X0;
lsqchisq=((ycalc-y)./wt)'*((ycalc-y)./wt);
%
%
subplot(3,1,1)
plot(t,y-ycalc,'b',[min(t),max(t)],[0,0],'k--')
axis([min(t) max(t) 1.05.*min(y-ycalc) 1.05.*max(y-ycalc)])
ylabel('I-I_{calc}')
subplot(3,1,2)
plot(t,y,'b',t,y,'bo',t,ycalc,'r',[min(t),max(t)],[0,0],'k--')
axis([min(t) max(t) 1.05.*min(min(min(y),min(ycalc)),0)
1.05.*max(max(y),max(ycalc))])
xlabel('time')
ylabel('Intensity')
lsqchisq=(ycalc-y)'*(ycalc-y);
tt=['  \chi^2 = ' num2str(lsqchisq)];
title(tt)
subplot(3,1,3)
bar(lkspace,X0(2:kleng))
```

```
xlabel('log(k)')
ylabel('P(k)')
pause(0.1);
%
%
lamscan=3;
while lamscan > 2
   fprintf('\r\r Do you want to fit with a single MEM regularization
parameter?')
   fprintf('\r Or scan through a range of MEM regularization
parameters? \r')
   lamscan=input(' Enter (1) for a single fit or (2) for a scan: (1 or
2) --> ');
   if (isempty(lamscan))
      lamscan=3;
   elseif (lamscan ~= 1) & (lamscan ~= 2)
      lamscan =3;
   end
end
%
%
if lamscan == 1
%
%
   fprintf('\r\r MEM regularization parameter (0 --> LSQ; inf = MEM)
\r');
   memlsq=input(' Enter a value --->  ');
   memlsq=abs(memlsq);
   old_stol=0.0001;
   old_niter=100;
   if memlsq == 0
       memlsq_1=1;
       memlsq_2=1;
       memlsq_delt=1;
   else
       memlsq_1=log(memlsq);
       memlsq_2=log(memlsq);
       memlsq_delt=1;
   end
   ip2=1;
%
%
else
%
%
   goodnum=-1;
   while goodnum < 0
   fprintf('\r\r')
      memlsq_min=input(' Enter the value for the minimum MEM
regularization parameter --> ');
      memlsq_max=input(' Enter the value for the maximum MEM
regularization parameter --> ');
      if memlsq_max > memlsq_min
         goodnum=1;
      else
         fprintf(' maximum must be greater than minimum !')
      end
```

```
   end
   memlsq_rat=input(' Enter the increment for adjacent MEM
regularization parameter [lamda(i+1)/lambda(i)] --> ');
   memlsq_1=log(memlsq_min);
   memlsq_2=log(memlsq_max);
   memlsq_delt=log(memlsq_rat);
   fprintf('\r\r')
   old_stol=input(' Enter the fitting tolerance value (CR = default =
1e-5) ---> ');
   if isempty(old_stol)
      old_stol=1e-5;
   elseif (old_stol > 1) | (old_stol < 0)
      old_stol=1e-5;
   end
%
   fprintf('\r\r')
   old_niter=input(' Enter the maximum number of iterations (CR =
default = 200) ---> ');
   if isempty(old_niter)
      old_niter=200;
   elseif (old_niter <= 1)
      old_niter=200;
   end
   %
   goodname = -1;
   while goodname < 0
      fprintf('\r\r')
      fname=input(' Enter a filename (including directory, but no
extension) for the fit results ---> ', 's');
      if ~isempty(fname)
         goodname=1;
      end
   end
   ip2=2;
%
%
end
%
%
X00=(X0.*0)+(1./(kleng-1));
X00(1,1)=0;
%%%%%%%%%%%%%%%%%%%
%
init_guess=-1;
while init_guess < 0
   fprintf('\r\rInitial guess:\r')
   init_guess=input(' Enter (1) for NNLS guess, or (2) for Maximum
entropy guess (1 or 2) ---> ');
   if isempty(init_guess)
      init_guess=-1;
   elseif (init_guess < 1) | (init_guess > 2)
      init_guess=-1;
   end
end
%
%
%
```

```
icount=0;
for iijj=memlsq_1:memlsq_delt:memlsq_2
   %
   if init_guess == 1
      pfit=X0;
   else
      pfit=X00;
   end

%
icount=icount+1;
%
%
if lamscan ~= 1
    memlsq=exp(iijj);
end
%
stol=old_stol;
niter=old_niter;
iter=0;
stest=1;
ochisq=-1;
chisq=-1;
lamda=-1;
lista=zeros(kleng,1);
alpha=zeros(kleng);
beta=zeros(kleng,1);
more_fit=1;
while more_fit==1
   fprintf('\r\r\r')
   while (stest>stol)&(iter<niter)
%
%
      [ycalc, memout pfit, chisq, alpha, beta,
lamda]=mrqmin_mem(A,memlsq,y,wt,pfit,kleng,func,lamda,alpha,beta,ochisq
);
      if (iter == 0) | (chisq < ochisq)
         if (iter ~= 0)
            stest=abs((chisq-ochisq)./chisq);
         end
         fprintf('Iteration %3i;  Chi-squared = %12.4e;  Fractional
Change = %12.4e \r',iter,chisq,stest);
         ochisq=chisq;
         subplot(3,ip2,1)
         plot(t,y-ycalc,'b',[min(t),max(t)],[0,0],'k--')
         axis([min(t) max(t) 1.05.*min(y-ycalc) 1.05.*max(y-ycalc)])
         ylabel('I-I_{calc}')
         subplot(3,ip2,2)
         plot(t,y,'b',t,ycalc,'r',[min(t),max(t)],[0,0],'k--')
         axis([min(t) max(t) 1.05.*min(min(min(y),min(ycalc)),0)
1.05.*max(max(y),max(ycalc))])
         xlabel('time')
         ylabel('Intensity')
         lsqchisq=((ycalc-y)./wt)'*((ycalc-y)./wt);
         tt=[' LSQ \chi^2 = ' num2str(lsqchisq)];
         title(tt)
         subplot(3,ip2,3)
```

```
         bar(lkspace,pfit(2:kleng))
         xlabel('log(k)')
         ylabel('P(k)')
         pause(0.1);
      end
      iter=iter+1;
%
%
   end
   if lamscan == 1
      if iter >= niter
         fprintf('\r\r Iteration count of %6i exceeded \r\r',niter)
         niter=2.*niter;
      else
         fprintf('\r\r Change in chi-squared less than %12.4e;
iterations stopped \r\r',stol)
         stol=stol./10;
      end
      fprintf(' Do you want to continue iterating ?\r\r')
      more_fit=input(' stop = 0; continue = 1 or CR: --> ');
      if isempty(more_fit)
         more_fit=1;
      end
   else
      more_fit=0;
   end
%
end
%
%
if lamscan == 1
   fprintf('\r\r')
   isave=input(' Enter a (1) to save the data, 0 or CR to quit ---> ');
   if isempty(isave)
      isave=0;
   end
   if isave == 1
      goodname = -1;
      while goodname < 0
         fprintf('\r\r')
         fname=input(' Enter a filename (including directory, but no
extension) for the fit results ---> ', 's');
         if ~isempty(fname)
            goodname=1;
         end
      end
      evalstr=[fname];
      evalstr=['save ',evalstr,' filename t y ycalc kspace lkspace
kleng A pfit chisq lsqchisq memlsq memout X0'];
      eval(evalstr);
%      save fname filename t y ycalc A pfit chisq lsqchisq memlsq
memout X0
   end
else
   pfit_out(:,icount)=pfit;
   ycalc_out(:,icount)=ycalc;
   chisq_out(icount)=chisq;
```

```
   lsqchisq_out(icount)=lsqchisq;
   memlsq_out(icount)=memlsq;
   memout_out(icount)=memout;
   subplot(3,ip2,4)
   hold on
   plot(lkspace,pfit(2:kleng),'b',lkspace,pfit(2:kleng),'bo')
   xlabel('log(k)')
   ylabel('P(k)')
   hold off
   subplot(3,ip2,5)

plot(log10(memlsq_out),lsqchisq_out,'r',log10(memlsq_out),lsqchisq_out,
'ro')
   xlabel('log(MEM regularization parameter)')
   ylabel('LSQ \chi^2')
   subplot(3,ip2,6)
   plot(log10(lsqchisq_out),log10(-
(memlsq_out.^2)./memout_out),'r',log10(lsqchisq_out),log10(-
(memlsq_out.^2)./memout_out),'ro')
   ylabel('log(1/S)')
   xlabel('log(LSQ \chi^2)')
   pause(1);
   evalstr=[fname];
   evalstr=['save ',evalstr,' filename t y ycalc_out kspace lkspace
kleng A pfit_out chisq_out lsqchisq_out memlsq_out memout_out X0'];
   eval(evalstr);
   %   save fname filename t y ycalc_out A pfit_out chisq_out
lsqchisq_out memlsq_out memout_out X0
end
   %
   %
end
%
%
%%%%%%%%%%%%%%%%%%%
```

splice_data1.m

```
%
%   script to splice together streak camera data from different time
bases
%
%
fprintf(' Data must be in two-column (time,intensity) format\n');
files=input('\n How many data sets will be spliced ? ---> ');
%
clear n
for i=1:files
%
    fprintf('\n Data set #%i:',i)
    filename=input(' enter the file name  --> ', 's');
%
    t_y=importdata(filename);
%
    eval(['time' num2str(i) '=t_y(:,1)-t_y(1,1);']);
    eval(['intensity' num2str(i) '=t_y(:,2);']);
    eval(['n(' num2str(i) ')=length(time' num2str(i) ');']);
end
%
%
[a,b]=max(n);
%
Time=zeros(a,files);
Intensity=zeros(a,files);
%
%
for i=1:files
    if n(i) < n(b)
        del=n(b)-n(i);
        eval(['Time(:,i)=[[min(time' num2str(i) ')-del:1:min(time'
num2str(i) ')-1]''; time' num2str(i) '];'])
        eval(['Intensity(:,i)=[zeros(del,1); intensity' num2str(i)
'];'])
    else
        eval(['Time(:,i)=[time' num2str(i) '];'])
        eval(['Intensity(:,i)=[intensity' num2str(i) '];'])
    end
end
%
% order the matrix in increasing time base
%
[P,Q]=sort(max(Time));
Time=Time(:,Q);
Intensity=Intensity(:,Q);
%
for i=1:files
    [a,b]=max(Intensity(:,i));
    Time(:,i)=Time(:,i)-Time(b,i);
    Intensity(:,i)=Intensity(:,i)./a;
end
%
%
[a,b]=size(Time);
```

```
%
first_pnt=floor(0.9.*a);
last_pnt=a;
%
factor=ones(files,1);
for i=2:files
    ytmp=interp1(Time(:,i),Intensity(:,i),Time(first_pnt:last_pnt,i-
1),'spline');
    ytmp=ytmp(:);

factor(i:files)=factor(i:files).*(sum(Intensity(first_pnt:last_pnt,i-
1)./ytmp)./(last_pnt-first_pnt+1));
end
%
%
Intensity=Intensity*diag(factor);
subplot(3,1,1)
semilogx(Time,Intensity)
%
Tsplice=Time(:,1);
Isplice=Intensity(:,1);
%
for i=2:files
    I=find(Time(:,i)>Time(last_pnt,i-1));
    Tsplice=[Tsplice; Time(I,i)];
    Isplice=[Isplice; Intensity(I,i)];
end
%
W = find(Tsplice>=0);
a=size(Tsplice);
Tsplice = Tsplice(W:a);
Isplice = Isplice(W:a);
subplot(3,1,2)
semilogx(Tsplice,Isplice)
%
subplot(3,1,3)
plot(Tsplice,Isplice)
```

crystal.m

```
function chi = crystal(x,R,E,t)
 %This function finds the chi square of a expression derived from
%convolution and data.

[O,Radj] = multiexp_conv(t,R,x);
%O = conv(R,T);
a = length(E);
%O1 = O(1:a);
chi = (O-E)'*(O-E);
%subplot(2,1,1);
semilogx(t,E,'b',t,O,'g')
%subplot(2,1,2);
%plot(t,O)
%plot(t,O1);
%plot(t(P1:P1+125),R(P1:P1+125),'m');
%plot(R);
```

multiexp_conv.m

```
function [O,Radj]=multiexp_conv(x,R,pram)
%
%   Syntax: [O,Radj]=multiexp_conv(x,R,pram);
%
%                   x = time vector
%                   R = response function (must have same length as x)
%
%   fitting to multi-exponential function: f(x)=alpha_0 +
%                                               alpha_1*exp(-alpha_2*x)
+
%                                               alpha_3*exp(-alpha_4*x)
+
%                                                           .
%                                                           .
%                                                           .
%
%   fit parameters: pram
%                       pram(1) = delta (response function time-shift
value)
%                       pram(2) = alpha_0
%                       pram(3) = alpha_1
%                       pram(4) = k_1
%                       pram(5) = alpha_2
%                       pram(6) = k_2
%                               .
%                               .
%                               .
%
x=x(:);
R=R(:);
pram=pram(:);
%
len=length(x);
exps=(length(pram)-2)./2;
%
if length(R) ~= len
    fprintf('Unequal lengths of time vector and response function\r');
    return
end
%
XI=x-pram(1);
Radj=interp1(x',R',XI','spline',0);
Radj=Radj./trapz(x,Radj);
Radj=Radj(:);
%
Rsums=zeros(len,exps+1);
%
for i=2:len
    %
    Rsums(i,1)=Rsums(i-1,1)+(pram(2).*0.5.*(x(i)-x(i-
1)).*(Radj(i)+Radj(i-1)));
    %
    for j=1:exps
        %
        exdx=exp(-pram(2.*(j+1)).*(x(i)-x(i-1)));
```

```
        Rsums(i,j+1)=(Rsums(i-
1,j+1).*exdx)+(pram((2.*j)+1).*0.5.*(x(i)-x(i-1)).*((Radj(i-
1).*exdx)+Radj(i)));
        %
    end
    %
end
%
%
O=sum(Rsums,2);
%
%
%subplot(2,1,1)
%semilogx(x,Radj./max(Radj),'b',x,O,'r')
%subplot(2,1,2)
%plot(x,Radj./max(Radj),'b',x,O,'r')
%
%
```